Luigi Petrucco

# A circuit for heading direction estimation in the zebrafish anterior hindbrain

March 4, 2022

This dissertation was submitted to LMU Munich in fulfillment of the requirements for a PhD at the Graduate School for Systemic Neurosciences.

CONTACT: luigi.petrucco@gmail.com

# *Abstract*

To successfully navigate their environment, animals may generate an internal representation of the environment that can be updated based on sensory cues or internally generated motor commands. Head-direction cells, neurons that fire when the animal faces a particular direction in space have been recorded in various areas of the vertebrate brain. The dynamics of heading direction circuits are well by described by *ring attractor networks*, where a ring attractor organizes the activity of the circuit and positions along the ring represent the heading direction. Although this model has found remarkable validation in the invertebrate central complex, the anatomical dissection of a ring attractor circuit has been elusive in the vertebrate brain. Here, I report experimental observations in the larval zebrafish that highlight a possible role of the interpenducular nucleus (IPN) and a connected area, the anterior hindbrain, in generating heading direction-related signals.

The internal organization of the interpeduncular nucleus is poorly understood. In the first part of this thesis, I will present anatomical reconstructions that provide crucial insights in the organization of this structure in the larval zebrafish. I will show that 1) the internal circuitry of the ventral IPN is organized in a fix number of glomeruli, domains of neuropil that receive dense and segregated dendritic and axonal arborizations and exhaustively tile the ventral IPN; and that 2) neurons in the anterior hindbrain dorsal from the interpeduncular nucleus contribute many dendritic and axonal projections to the IPN neuropil.

In the second part of the thesis, I will describe a population of *r1π neurons* in the anterior hindbrain that exhibit a highly constrained dynamics lying on a ring manifold in the phase space of the network. Intriguingly, clock- and counterclock-wise shifts along this manifold correspond to left and right movements of the fish, so that the network state can keep track of current heading direction. The dynamics of the network full-fills several criteria that define a head-direction network: 1) There is a sustained and unique bump of activity that translates across the network (*uniqueness*); 2) the activity shifts in opposite directions when the animal perform leftward and rightward movements (*integration*); 3) activation of the network is stable over tens of seconds in the absence of motion (*persistence*).

Finally, I will turn back to the anatomy of r1π neurons and show how they could connect with each other in the IPN according to their proximity in activity space, and I will conclude by proposing a mechanistic model for the organization of the ring network dynamics. Together, these data represent the first observation of a head-direction network with an anatomical organization in the vertebrate brain.

# Contents

# List of Figures

# List of Tables

# I

# ANATOMY OF THE INTERPEDUNCULAR NUCLEUS

Faced with an anatomical fact proven beyond doubt, any physiological result that stands in contradiction to it loses all its meaning. [...] So, first anatomy and then physiology; but if first physiology, then not without anatomy.
—BERNARD VON GUDDEN, *neuroanatomist and psychiatrist*

# *Introduction*

*1*

The interpenducular nucleus (IPN) is a nucleus that sits in the ventral part of the vertebrate hindbrain, whose anatomy has intrigued investigators since its first description. The tract of fibers it receives from the habenulae is *"one of the most distinguishable tracts of the human brain"*, in the words of Forel[1], and its spiralling axons has fascinated early neuroanatomists. The central position of the nucleus, and the neural systems from which it receives and to which it sends, suggest that it is highly integrative in nature, linking limbic, sensory, and other telencephalic systems to motor centers in the hindbrain. Yet, the complexity of its composition - whose *"...wealth and intricacy of detail baffle analysis"*[2] - has hindered efforts to disentangle its organization and functional roles.

In this chapter, I survey what is known about the anatomical structure of this circuit and its histochemical and ultrastuctural features, drawing from observations collected in different animal species. I will focus in particular on the internal organization of the interpeduncular region, and on the evidence that supports the notion of a glomerular organization within it. I conclude with an overview of the hypotheses around the functions that might be served by the habenulo-interpeduncular system.

[1] Forel, "Untersuchungen über die Haubenregion und ihre oberen Verknüpfungen im Gehirne des Menschen und einiger Säugethiere, mit Beiträgen zu den Methoden der Gehirnuntersuchung".

[2] Herrick, "Interpeduncular Nucleus".

## *1.1   The habenulo-interpeduncular circuit*

The habenulo-interpeduncular nucleus is one of the first circuits in the midbrain that have been identified. Its first description dates back to 1877, and was carried out by the Auguste Henri Forel in the laboratory of von Gudden[3] (see *Historical notes*). There, he described how fibers from the medial habenula, a paired nuclei located in the epithalamus (the dorsalmost part of the diencephalon), run compactly in "Meynert's bundle" (now known as fasciculus retroflexus (FR), or habenulo-interpeduncular tract) to enter, on the ventral surface of the anterior hindbrain, the interpeduncular nucleus (see Figure 1.2). The FR targets almost exclusively the IPN; therefore, the medial habenula and the interpeduncular nucleus can be considered together components of the habenulo-interpeduncular circuit.

The habenulo-interpeduncular circuit is highly conserved across vertebrates[4]. It can be recognised in the brain of fish, reptiles, birds, and mammals, suggesting that it mediates fundamental functions shared within the vertebrate clade.

[3] Forel, "Untersuchungen über die Haubenregion und ihre oberen Verknüpfungen im Gehirne des Menschen und einiger Säugethiere, mit Beiträgen zu den Methoden der Gehirnuntersuchung".

[4] Aizawa, Amo, and Okamoto, "Phylogeny and ontogeny of the habenular structure"; Stephenson-Jones et al., "Evolutionary conservation of the habenular nuclei and their circuitry controlling the dopamine and 5-hydroxytryptophan (5-HT) systems".
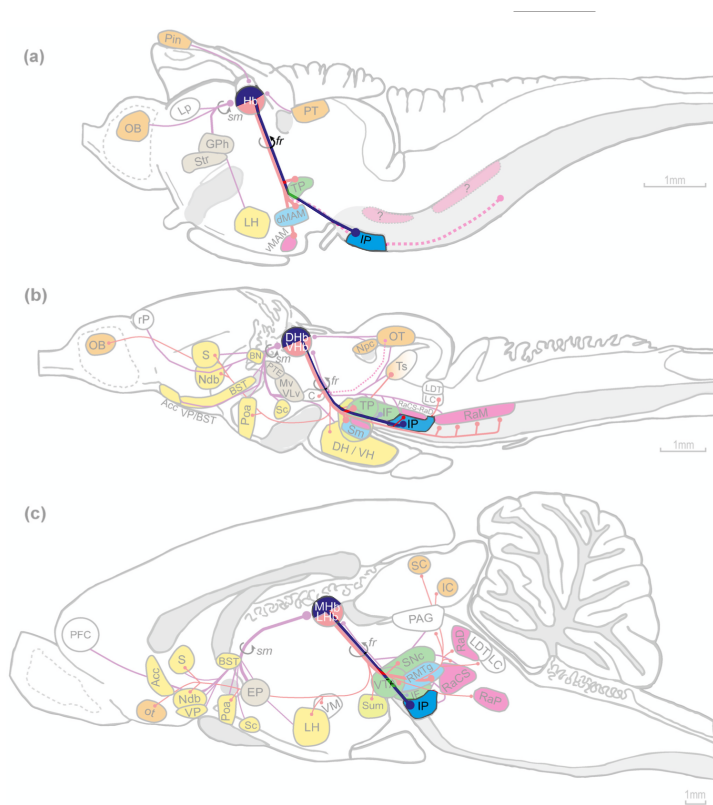
Figure 1.1: Comparative anatomy of the habenulo-interpeduncular system. *Left*, The organization of the habenulo-interpeduncular tracts (in blue) in the lamprey (*top*), the anuran (*middle*), and the mammalian (*bottom*) brain. Hb: habenula; IP: IPN. Reproduced with permission from Freudenmacher, Twickel, and Walkowiak, "The habenula as an evolutionary conserved link between basal ganglia, limbic, and sensory systems—A phylogenetic comparison based on anuran amphibians".

## 1.2   The habenula

The habenula is a paired epithalamic nucleus located in the dorsal part of the diencephalon. It is surrounded by thalamic areas and it lies very close to the mid-line, bordering dorsally and medially with the surface of the third ventricle. In mammals, it is clearly separated in a lateral and a medial part, distinguishable based on gene expression profiles and connectivity. In more basal vertebrates, the same distinctive profiles define a ventral and a dorsal habenula, that are to be considered homologues to the mammalian lateral and medial habenula, respectively[5]. In fish and amphibians, the habenula is strongly asymmetric, and its development has become a paradigm to investigate lateralization in brain circuits[6]; in birds and mammals the asymmetry is largely reduced. Only the medial habenula part[7] is involved in the habenulo-interpeduncular pathway, and I will consider only on this part of the structure for the current description.[8]

   The medial habenula is the main target of glutamatergic fibers from the medial and lateral septal nuclei, which in turn receive from the hippocampus and the subiculum[9]. In addition, it might receive dopaminergic inputs from the ventral tegmental area and noradrenergic inputs from the locus ceruleus. The axons of the medial habenula targets exclusively the interpeduncular nuclei. Although the medial habenula is mostly glutamatergic, neurons of its ventral two thirds co-release acetylcholine from their axon terminals in the IPN, and neurons in the dorsalmost third co-release and substance P.[10] This distinction seems to correspond to differences in the topographical organization of their axons: neurons from the ventral medial

[5] Namboodiri, Rodriguez-Romaguera, and Stuber, "The habenula".

[6] Bianco and S. W. Wilson, "The habenular nuclei: A conserved asymmetric relay station in the vertebrate brain"; Aizawa, Amo, and Okamoto, "Phylogeny and ontogeny of the habenular structure".

[7] ventral in fish.

[8] Bianco and S. W. Wilson, "The habenular nuclei: A conserved asymmetric relay station in the vertebrate brain".

[9] Otsu et al., "Functional Principles of Posterior Septal Inputs to the Medial Habenula"; Bianco and S. W. Wilson, "The habenular nuclei: A conserved asymmetric relay station in the vertebrate brain".

[10] Lima et al., "Afferent and efferent connections of the interpeduncular nucleus with special reference to circuits involving the habenula and raphe nuclei".

habenula target preferentially the medial part of the IPN, and neurons from the dorsal medial habenula target its lateral part. In zebrafish, cholinergic neurons are mostly observed in the right habenula, and target preferentially the ventral IPN (see *Afferents to the IPN*).

Very little is known about the *in vivo* physiology of the medial habenula in mammals, as its size and closeness to the ventricle pose significant technical challenges to elecrophysiological recordings and optogenetic manipulation[11]. In zebrafish, the left and the right habenula have been shown to be highly responsive to visual and olfactory stimuli, respectively[12].

## 1.3    The IPN

After running through the fasciculus retroflexus, axons coming from the habenula direct ventrally and converge medially in a region that is delimited ventrally by the pial surface, between the cerebellar peduncles, and terminates anteriorly with the midbrain-hindbrain boundary, at the level of the trochlear nucleus. The extent of the arborizations coming from the habenulae can be used to mark the delimitation of the interpeduncular nucleus. This region is therefore composed by an dense neuropil mesh, where the habenulo-interpeduncular afferents run and interweave with the dendrites of local interpeduncular neurons and descending fibers from the tegmentum above. The neuropil mass include groups of somas, that are organized in a column extending from the pial surface up to the floor of the fourth ventricle in fish and urodels. In mammals, sparse somas can be found in its rostral part, while they organize in compact columns in the caudal portion of the IPN[13]. Caudo-dorsally, somas from the IPN neurons and somas of the median raphe nucleus do not have any clear demarcation separating them, and it can be difficult to establish a clear boundary between those structures without considering the histochemical nature of the neurons, or their projections[14]. This ambiguity poses some challenges to the interpretation of part of the existing literature about the afferent and efferent projections of the IPN.

In fish, the IPN has a clear subdivision along the dorsoventral axis in a dorsal/anterior part, that receives fibers from the left habenula; and a ventral/caudal part, that receives fibers from the right habenula. In mammals, the internal structure of the nucleus is more debated, and multiple subdivisions have been suggested[15]. However, at least two unpaired rostral/dorsal and ventral/caudal subdivions can be clearly identified, together with two paired lateral regions[16] (Figure 1.4).

### Afferents to the IPN

*Habenular afferents to the IPN*    Fibers from the habenulae target the interpeduncular nucleus with a highly peculiar projection pattern. There, they almost immediately assume a transverse orientation (Figure 1.3) and cross the mid-line, reach the lateral edge of the nucleus, and curve back toward the mid-line, which they cross multiple times in a spiral that spans the extension of the nucleus in the frontal axis. Those axons seldom branch, and if they do, the give rise to few collaterals that keep running with a sim-

[11] Namboodiri, Rodriguez-Romaguera, and Stuber, "The habenula".

[12] Dreosti et al., "Left-Right Asymmetry Is Required for the Habenulae to Respond to Both Visual and Olfactory Stimuli"; W.-y. Chen et al., "Role of Olfactorily Responsive Neurons in the Right Dorsal Habenula–Ventral Interpeduncular Nucleus Pathway in Food-Seeking Behaviors of Larval Zebrafish".
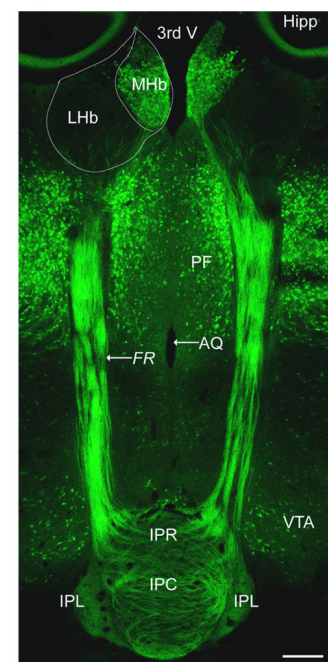


Figure 1.2: The FR running from the medial (ventral) habenula (MHb) to the central part of the IPN (IPR, IPC), in a Cbln4-mVenus mouse (bar: 200 μm). Reproduced with permission from Seigneur, Polepalli, and Südhof, "Cbln2 and Cbln4 are expressed in distinct medial habenula-interpeduncular projections and contribute to different behavioral outputs".

[13] Iwahori et al., "Terminal patterns of the tegmental afferents in the interpeduncular nucleus: a Golgi study in the mouse".

[14] Quina et al., "Specific connections of the interpeduncular subnuclei reveal distinct components of the habenulopeduncular pathway".

[15] Morley, "The Interpeduncular Nucleus".

[16] Morley, "The Interpeduncular Nucleus"; Quina et al., "Specific connections of the interpeduncular subnuclei reveal distinct components of the habenulopeduncular pathway".

ilar pattern from one side to the other of the nucleus, without arborizing extensively in any definite part of it. While traversing the nucleus, habenular axons form *en passant* synapses with cells in the IPN (see *Synapses in the IPN*).

In fish, fibers from the left habenula target the dorsal IPN, and fibers from the right habenula its ventral part. Moreover, the morphology of the axons targeting the dorsal and the ventral IPN are significantly different (see *The habenulo-interpeduncular fibers*), as is the distribution of neurons co-releasing acetilcholine, more present in the right habenula.[17]

In mammals, these projections do not seem to be lateralized. However, different regions of the habenula project to different subregions of the IPN (Figure 1.4). Neurons from the dorsal part of the medial habenula seem to target mostly the lateral lobes of the IPN, while neurons of the ventral medial habenula project to its unpaired, medial subdivisions[18].
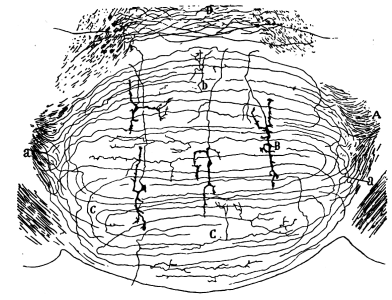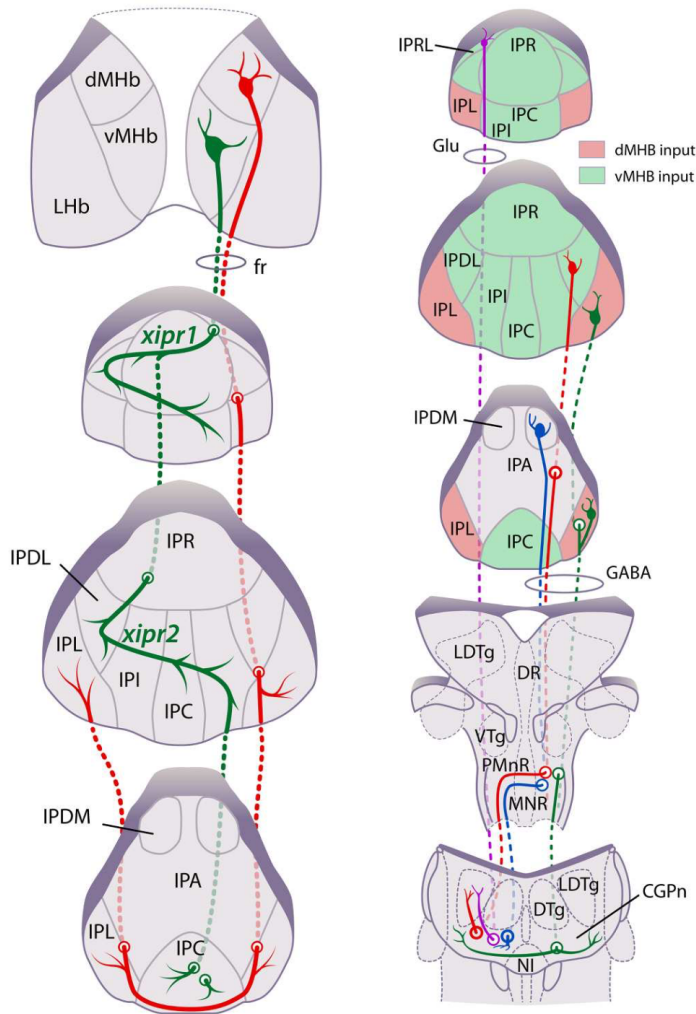


Figure 1.3: Fibers of the habenulo-interpeduncular tract in the 4 days old mouse (a, c). Reproduced from Cajal, *Histologie du systeme nerveux de l'Homme et des vertebres.*

[17] Hong et al., "Cholinergic left-right asymmetry in the habenulo-interpeduncular pathway"; Zaupa et al., "Trans-inhibition of axon terminals underlies competition in the habenulo-interpeduncular pathway".

[18] Seigneur, Polepalli, and Südhof, "Cbln2 and Cbln4 are expressed in distinct medial habenula-interpeduncular projections and contribute to different behavioral outputs"; Quina et al., "Specific connections of the interpeduncular subnuclei reveal distinct components of the habenulopeduncular pathway".



Figure 1.4: *Left*, Different afferents from the dorsal and the ventral medial habenula to the medial and lateral regions of the IPN.*Right*, posterior projections of different regions of the IPN (IPR, IPRL, IPC, IPI, IPDL: different subdivisions of the central IPN; LPN: lateral IPN; DTg and LDTg: lateral and dorsal tegmental nucleus; dMHb and vMHb: different subdivisions of the medial habenula; LHb: lateral habenula). Reproduced with permission from Quina et al., "Specific connections of the interpeduncular subnuclei reveal distinct components of the habenulopeduncular pathway".

*Tegmental afferents to the IPN*    The other main input to the IPN comes from axons coming from various areas of the dorsal tegmentum above it. Her-

rick[19] describes in the salamander *"short axons which arise from small cells of the dorsal and trigeminal tegmentum and descend directly to the interpeduncular neuropil"*, as well as *"collaterals of the thicker axons of tractus tegmentobulbaris"*. Those axons arbiruze in the IPN neuropil, of which they are an important component, and form tufted endings that form at least in part the axonic component of the glomeruli (see *Glomeruli in the IPN*). More recent observations in Golgi preparations from mouse seem to corroborate this description[20].

More precise investigations about the source of those projections using anterograde and retrograde tracing techniques identified the dorsal tegmental region as the main source of afferent to the IPN after the habenula[21]. The projection seems to terminate in the caudal part of the IPN and is topographically organized in a caudorostral pattern with no clear lateralization.

Finally, the dorsal and median raphe nuclei also seem to send projections to the IPN[22].

*Neurons of the IPN*

Most studies that have been reporting detailed observations on the morphology of interpeduncular nucleus have taken advantage of elective impregnation with the Golgi methods. Such observations have found little to no follow up in the more modern literature, that has concentrated over either the ultrastructure of its synapses, or on the broad connectivity patterns and histochemical features of the region. Therefore, many questions about the cyto-architecture of the nucleus and the morphology of its neurons remain open.

Cajal[23] observed two types of neurons in the mammalian IPN: a *large type*, with *"short, shaggy dendrites ending in very tangled expansive bouquets after a highly irregular course"*, with an axon that leaves the IPN after sending a collateral branch in the region of the cell body; and a *small type*, stellate in shape, with thin and divergent dendrites, with a thin axon that branches forming extensive arborizations inside the IPN. Recent reports[24] describe similar morphologies, with a gradient of neurons types going from medium-sized neurons (the large type) in the ventral IPN to small neurons in more dorsal regions of the nucleus.
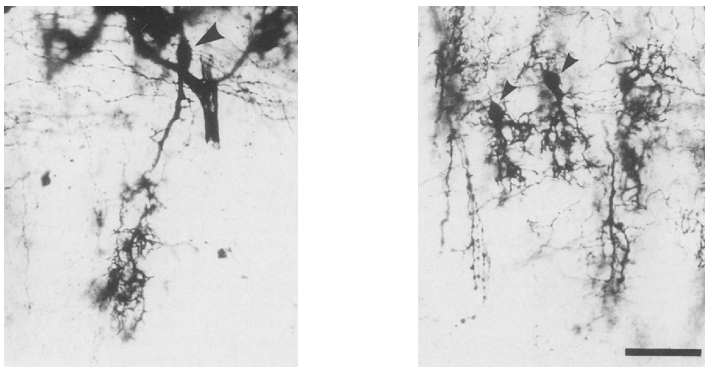


In the salamander, Herrick[25] reports that in transverse sections the dendrites of the interpeduncular neurons are generally directed ventrally, they

19 Herrick, "Interpeduncular Nucleus".

20 Iwahori et al., "Terminal patterns of the tegmental afferents in the interpeduncular nucleus: a Golgi study in the mouse".

21 Contestabile and Flumerfelt, "Afferent Connections of the Interpeduncular Nucleus and the Topographic Organization of the Habenu lo-lnterpeduncu lar Pathway: An HRP Study in the Rat"; Groenewegen et al., "Cytoarchitecture, Fiber Connections, and Some Histochemical Aspects of the Interpeduncular Nucleus in the Rat".

22 Quina et al., "Specific connections of the interpeduncular subnuclei reveal distinct components of the habenulopeduncular pathway".

23 Cajal, *Histologie du systeme nerveux de l'Homme et des vertebres.*

24 Iwahori et al., "Terminal patterns of the tegmental afferents in the interpeduncular nucleus: a Golgi study in the mouse".

Figure 1.5: Morphologies of neurons (harrowheads) in a Golgi staining of slices from the mouse IPN (bar: 100 μm). Reproduced with permission from Iwahori et al., "Terminal patterns of the tegmental afferents in the interpeduncular nucleus: a Golgi study in the mouse".

25 Herrick, "Interpeduncular Nucleus".

branch widely within the interpeduncular neuropil, and many of the branches have tufted endings in glomerular structures (see *Glomeruli in the IPN* and Figure 1.6). Those neurons produce a thin axon from the cell body or the base of the dendrite which then takes *"take tortuous courses within the interpeduncular neuropil"*, and some of them form compact tufts within the glomeruli.

### Projections of IPN neurons

Axons from the IPN neurons exit the nucleus dorsally and reach the pontine tegmentum.[26] A prominent target structure is the lateral odorsal tegmental nucleus, that receives highly lateralized GABAergic projections from the lateral (ipsilateral) part of the dorsal IPN. Interestingly, the same regions are also the target of glutamatergic projections from some rare glutamatergic cells in the rostral lateral IPN, suggesting that they might be involved in a push-pull mechanism together with the ipsilateral GABAergic projections[27]. Other targets of interpeduncular fibers are all in the tegmental region, and in addition to the dorsal tegmental nucleus (DTN) include the nucleus incertus, dorsal raphe nucleus, and the loosely defined area called central gray of the pons (Figure 1.4). Interestingly, However, the core of theDTN receives few direct inputs from the IPN, so that IPN inputs to the pontine tegmentum have almost no anatomical overlap with fibers converging there from the lateral mammillary body. This will be important when discussing the possible involvement of the interpeduncular circuit in the establishment of a heading direction system (see *Navigation and the IPN*).

Although some ascending projections to the ventral areas of the forebrain (hippocampus, medial septum, diagonal band, and mediodorsal thalamus) have been reported[28], those seem to come from the apical nucleus of the IPN, a region in close continuity with the median raphe; it is therefore likely that such fibers are not to be considered interpeduncular projections, but serotoninergic afferents from the raphe nucleus. A careful combination of anterograde and retrograde tracing[29] has concluded the IPN does not produce any ascending projections.

### Synapses in the IPN

The ultrastructure of IPN synapses has been described in detail[30]. Presynaptic boutons can be found in all parts of the non-branching axons, so that the fibers end up contacting the local dendritic arbors *en passant* in a way that could remind that of connections between parallel fibers contacts onto Purkinje cells in the molecular layer of the cerebellum. Those *en passant* between the plexus of habenular afferent axons and the dendrites of interpeduncular neurons. *En passant* synapses, termed S-synapses, constitute the large majority (90% to 95% in the rat) of synapses in the IPN. Lenn describes also crest synapses, were two axons from the habenulae form parallel contacts on the opposite sides of the same dendrites. Intriguingly, the two axons are never branches of the same cell, and they seem to always come one from the left and one from the right habenula[31].

[26] Quina et al., "Specific connections of the interpeduncular subnuclei reveal distinct components of the habenulopeduncular pathway".

[27] Quina et al., "Specific connections of the interpeduncular subnuclei reveal distinct components of the habenulopeduncular pathway".

[28] Groenewegen et al., "Cytoarchitecture, Fiber Connections, and Some Histochemical Aspects of the Interpeduncular Nucleus in the Rat".

[29] Quina et al., "Specific connections of the interpeduncular subnuclei reveal distinct components of the habenulopeduncular pathway".

[30] Nicholas J. Lenn, "Synapses in the interpeduncular nucleus: Electron microscopy of normal and habenula lesioned rats".

[31] N. J. Lenn, Wong, and Hamill, "Left-right pairing at the crest synapses of rat interpeduncular nucleus".

## Neurotransmitters of the IPN

Biochemical studies have demonstrated high concentrations of acetylcholine, choline acetyltransferase, and acetylcholinesterase in the IPN, and ACh has been found in the M-Hb neurons that project to the IPN (reviewed in Morley, "The Interpeduncular Nucleus"). In fact, the habenulo-interpeduncular circuit is considered one of the most prominent cholinergic paths in the mammalian brain. Recent functional experiments have shown that cholinergic habenular axons co-release also the excitatory neurotransmitter glutamate. Nicotinic acetylcholine receptors (nAChRs) can be found both on the somas and dendrites of IPN neurons, and on the terminals of habenular axons[32].

Another very represented neurotransmitter in the interpeduncular nucleus is GABA. IPN neurons are predominantly GABAergic [33]. Moreover, habenular terminals in the IPN express high levels of of GABA_B[34], a receptor implicated in the GABA-mediated modulation of presynaptic release. Several enzymes and receptors related to other neurotransmitters have been reported in the IPN (substance P, somatostatin, cholecystokinin, norepinephrine, serotonin, dopamine, Gonadotropin releasing hormone...)[35], but their functional role is still poorly characterized.

## Electrophysiological studies in the IPN

Complex interactions between the cholinergic/glutamatergic afferent fibers and local GABAergic activity in the IPN seem to govern the activity in this nucleus. Electrophysiological experiments in both rodents and fish have shown that cholinergic terminals from the habenula co-release both ACh and glutamate, which activate downstream neurons through separate receptors and with different kinetics[36]. Glutamate release elicit fast ionotropic receptor-mediated postsynaptic currents, while acetylcholine elicit slow inward currents, and reaches postsynaptic partners through volume transmission[37]. Another work in the larval zebrafish, Zaupa et al., "Trans-inhibition of axon terminals underlies competition in the habenulo-interpeduncular pathway", has observed presynaptic inhibition of habenular terminals mediated by GABA_B receptors and GABA released by IPN neurons. Moreover, the pre-synaptic inhibition seems to be more prominent of non-cholinergic terminals, so that the activation of cholinergic habenular terminals in the ventral IPN seem to inhibit the non-cholinergic axons of the dorsal IPN. This mechanism could be related to the competitive modulation of activity in the dorsal and the ventral IPN of the fish, which have been suggested to mediate opposite behaviors[38]. However, observations in mammals reported a peculiar mechanism of GABA-mediated pre-synaptic activation through GABA_B presynatic receptors of the habenular axons in the IPN.

Although the details of the modulation of synaptic communication in the IPN are still under investigation, it has now became clear that activity of the axonal terminals from the habenula are sculpted by local interactions in the IPN, and could be only loosely correlated with the activity in the habenular somas.

MHb-IPN synapses exhibit activity-dependent potentiation of glutamate release, through a pathway that involves GABA_B receptors on the vMHb

[32] Ables, Antolin-Fontes, and Ibañez-Tallon, "Habenular synapses and nicotine".

[33] Morley, "The Interpeduncular Nucleus"; Antolin-Fontes et al., "The habenulo-interpeduncular pathway in nicotine aversion and withdrawal"; Quina et al., "Specific connections of the interpeduncular subnuclei reveal distinct components of the habenulopeduncular pathway".

[34] Chu et al., "Distribution and kinetics of GABAB binding sites in rat central nervous system: A quantitative autoradiographic study"; Margeta-mitrovic et al., "of GABA B Receptors in the Rat Central Nervous System".

[35] Morley, "The Interpeduncular Nucleus".

[36] In fish, acetylcholine-related enzymes are expressed preferentially in the right habenula.

[37] Ren et al., "Habenula " Cholinergic" Neurons Corelease Glutamate and Acetyl-choline and Activate Postsynaptic Neurons via Distinct Transmission Modes"; Hong et al., "Cholinergic left-right asymmetry in the habenulo-interpeduncular pathway".

[38] Chou et al., "Social conflict resolution regulated by two dorsal habenular subregions in zebrafish".

terminals activated by the GABA released upn activation by IPN neurons[39].

*Glomeruli in the IPN*

Glomerular structures have been reported in the IPN since its very first observation, although they have gone almost forgotten in the most recent literature about the anatomy of the region. In his description of the IPN, Forel[40] states *"[the IPN] consists of a background substance which is extremely intensely stained by carmine and which, in cross-section, contains masses of round or ribbon-shaped, dark-appearing, more or less sharply defined small nests which, however, do not look very dissimilar to the glomeruli of the olfactory bulb of the rabbit"*[41]. Cajal[42] cites the findings from Forel's description, but he makes no further description of glomeruli in his mammalian preparations.

[39] Koppensteiner, Melani, and Ninan, "A Cooperative Mechanism Involving Ca2+-Permeable AMPA Receptors and Retrograde Activation of GABAB Receptors in Interpeduncular Nucleus Plasticity".

[40] Forel, "Untersuchungen über die Haubenregion und ihre oberen Verknüpfungen im Gehirne des Menschen und einiger Säugethiere, mit Beiträgen zu den Methoden der Gehirnuntersuchung".

[41] For a complete translation of the original text, see *Historical notes*

[42] Cajal, *Histologie du systeme nerveux de l'Homme et des vertebres.*



Figure 1.6: Diagram of the composition of the interpeduncular glomeruli Median sagittal section section at the level of the floor plate, that then runs obliquely up in the tegmentum. Two neurons of the interpeduncular nucleus are drawn with the tufted axonal terminals from tegmental afferences. Reproduced with permission from Herrick, "Interpeduncular Nucleus".

The most prominent report of glomeruli in the IPN was written by C.J. Herrick, while investigating the nervous system of Urodela using with Golgi stainings (reviewed in Herrick, "Interpeduncular Nucleus"). There, Herrick observed *"small and very numerous elongated areas of very dense neuropil"*. He continues: *"They are distributed throughout the interpeduncular neuropil, in many places densely crowded; most of them are oriented vertically and extend downward into the ventral area of specific neuropil.*

*Histological analysis of their structure is even more difficult than is that of the rest of the interpeduncular neuropil, for each of the constituent elements may present quite different appearances in Golgi sections, depending on the quality of the impregnation. These glomeruli resemble in some respects those of the olfactory bulb [...] Most of the glomerular dendrites come from cells of the interpeduncular nucleus, though some of them are branches from the transitional neurons at the ventral border of the tegmental gray [...] they are penetrated by fibers of the interpeduncular spiral"*.

Those observations by Herrick are not considered at all in the most recent literature on the IPN, although they have found remarkable validation in the electron microscopy studies published by Lenn starting from 1976[43]. Lenn describes dendritic ensheathments of multiple axonic terminals in glomerular structures approximately 20 μm in diameters. He observes that *"their distinct separation from the general neuropil in spite of a lack of glial ensheathment"*, as well as *"the complex interrelationship which*



Figure 1.7: Axonal boutons (A) surrounded by complexly branching sheet-like dendritic processes (D), highlighted in red (bar: 1 μm). Modified with permission from Nicholas J. Lenn, "Synapses in the interpeduncular nucleus: Electron microscopy of normal and habenula lesioned rats".

[43] Nicholas J. Lenn, "Synapses in the interpeduncular nucleus: Electron microscopy of normal and habenula lesioned rats"; N. J. Lenn, Wong, and Hamill, "Left-right pairing at the crest synapses of rat interpeduncular nucleus".

*existed within them between the complex elaboration of sheet-like dendritic processes and the axons forming the crest synapses which they engulfed in three dimensions"* justifies the term glomerulus to describe the structures in question in preparations from mammalian tissue. This organization has been confirmed in a study reconstructing IPN dendrites in small electron microcopy volumes[44].

The most recent paper mentioning glomeruli in the IPN is the Golgi study: Iwahori et al., "Terminal patterns of the tegmental afferents in the interpeduncular nucleus: a Golgi study in the mouse". There, authors describe tegmental afferent fibers that, after entering the IPN, branch out in what are described as glomerular arborizations, especially in the rostral IPN.
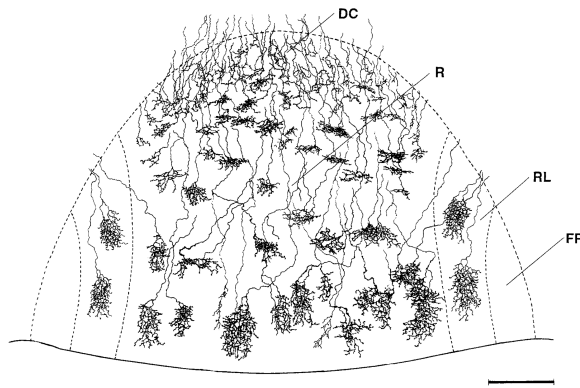
[44] Parajuli et al., "Unique synaptic topography of crest-type synapses in the interpeduncular nucleus".



Figure 1.8: Glomerular arborizations of tegmental afferents to the rostral part of the IPN, drawn from a frontal section stained with the rapid Golgi method (bar: 100 μm). Reproduced with permission from Iwahori et al., "Terminal patterns of the tegmental afferents in the interpeduncular nucleus: a Golgi study in the mouse".

In the next chapter, I will present new data that show for the first time how important is the role of the glomerular organization in the structure and function of the zebrafish IPN.

## 1.4    Functional role of the habenulo-interpeduncular circuit

### Early hypotheses

The presence of a conserved circuit such as the habenulo-interpeduncular pathway across many different animal groups suggests that it regulates some core behaviors in many species. Drawing just from neuroanatomical considerations, Herrick[45] observed that *"it is a noteworthy feature of the interpeduncular system that it is connected in parallel, as the electrician would say, with the major systems of fore-and-aft conduction of the brain stem.".* As the cerebellum, he notes, *"The interpeduncular complex is separate from this great system of activators except at its upper and lower ends.";* and like the cerebellum, it might *"act upon the motor systems as going concerns, facilitating the activity in process by reinforcement and inhibition, appropriately placed and timed.".* Writing at a time when is was not even known what could be mediating mechanisms of inhibition in the brain, he hypothesised based on anatomy alone an inhibitory role for fibers leaving the IPN[46]. He concludes, *"The intrinsic structure of the interpeduncular field seems to preclude any well-defined local representation of different functions within it. [...] The glomeruli provide apparatus for nonspecific summation and reinforcement. [...] The glomerular activities may reinforce (or inhibit) those of the spiral, or conceivably they may act independently if the habenular component*

[45] Herrick, "Interpeduncular Nucleus".

[46] An curious remark by Herrick is that *"The unusually large size of the interpeduncular nucleus of urodeles may be correlated with the fact that in the normal behavior of these animals total inhibition is a conspicuous feature."*

*is inactive.".* Decades later, these speculations seems to hold although the functional role of the interpeduncular nucleus is still largely unknown.

### Acquisition and retention of avoidance tasks

Early reports in the 60s and 70s have implicated the habenula and the interpeduncular nucleus in the acquisition and retention of avoidance tasks in rats[47]. Coherently with the overall connectivity of the nucleus, IPN lesions show consistent effects with lesions of dorsal tegmentum and septum.[48]. More recent experiments in zebrafish have shown how the genetic impairment of the (lateral) dorsal habenula (homologue to the medial habenula (MHb) in mammals) biases the fish towards freezing instead of swimming to a conditioned fear stimulus[49].

A recent study in mice, looking at the cholinergic neurons in medial habenula, found that activation of these neurons reduces the expression of fear memory. Surprisingly, these neurons mediate extinction of fear memory by GABA_B receptor-mediated excitation of their axon terminals in the interpeduncular nucleus, thereby providing an extra-amygdalar pathway for fear regulation. Thus, while relatively little is known about the functional role of medial habenula in normal behavior, it appears to perform important functions for the maintenance of appropriate affective states.

### Familiarity signaling

It has been observed that neurons in the IPN increase their activity upon repeated exposures of stimuli.[50] The silencing of IPN neurons extended the interaction with familiar stimuli, increasing their salience as if they were novel objects, while photoactivation of the same neurons mimicked familiarity, resulting in reduced exploration.

### Nicotine addiction

The MHb-IPN circuit expresses the highest density of nAChRs in the mammalian brain. Polymorphisms related to subunits $\alpha$5 and $\beta$4 have been linked to susceptibility to nicotine addiction in humans, and the effects on addiction of those subunits seem to be mediated by the habenulo-interpeduncular pathway[51]. Animals lacking the $\alpha$5 subunit have a diminished IPN activation and they continue to self-administer nicotine at doses that normally elicit aversion in wild-type animals, and the effect can be rescued by re-expression of the subunit in the medial habenula or the IPN. Selective knockdown of the gene in the medial habenula recapitulated the phenotype of the mouse mutant[52]. Optogenetic activation of IPN terminals in theDTN has proved that those fibers are mediating the expression of nicotine aversion behaviors, including nicotine-conditioned place aversion[53]. Finally, the activation of GABAergic neurons in the IPN can elicit nicotine physical withdrawal symptoms[54] in naïve and nicotine exposed mice. Finally, the expression of nicotine-insensitive variants of nAChRs lead to a reduced aversive reaction to nicotine.

[47] Thompson, "Interpeduncular nucleus and avoidance conditioning in the rat"; J. R. Wilson, Mitchell, and Van Hoesen, "Epithalamic and ventral tegmental contributions to avoidance behavior in rats".

[48] Wirtshafter, "The role of interpeduncular connections with the tegmentum in avoidance learning".

[49] Agetsuma et al., "The habenula is crucial for experience-dependent modification of fear responses in zebrafish".

[50] Molas et al., "A circuit-based mechanism underlying familiarity signaling and the preference for novelty".

[51] Fowler et al., "Habenular $\alpha$5 nicotinic receptor subunit signalling controls nicotine intake"; Frahm et al., "Aversion to Nicotine Is Regulated by the Balanced Activity of $\beta$4 and $\alpha$5 Nicotinic Receptor Subunits in the Medial Habenula".

[52] Fowler et al., "Habenular $\alpha$5 nicotinic receptor subunit signalling controls nicotine intake".

[53] Wolfman et al., "Nicotine aversion is mediated by GABAergic interpeduncular nucleus inputs to laterodorsal tegmentum".

[54] Zhao-Shea et al., "Activation of GABAergic neurons in the interpeduncular nucleus triggers physical nicotine withdrawal symptoms".

## Social behavior

In zebrafish, it has been shown that different parts of the habenulo-interpeduncular tracts had opposite effects over the probability of a fish to win a fight.[55]. The likely-hood to win was decreased by silencing the (fish) dorsal IPN-projecting lateral subnucleus of the dorsal habenula and increased by silencing the ventral IPN-projecting medial subnucleus of the dorsal habenula, and activity in the two parts of the network was consistently increased or decreased in winning or losing animals.

## Differential roles for ventral and dorsal medial habenula projections

It has been proposed that two parallel pathways run from the MHb to the IPN. Impairing the expression of the neurexins cerebellin 2, expressed in the dorsal medial habenula, and cerebellin 4, expressed in the ventral medial habenula, had selective effects on behavior.[56] The former pathway (from dorsal medial habenula) impaired spatial learning in a water T-maze and the acquisition of avoidance behaviors. The second pathway (from ventral medial habenula) mediated the increase anxiety levels measured by open field and elevated plus maze tests that has been confirmed in other works[57].

The existence of two parallel pathways within the medial habenula is also suggested by the observation of differential projections to the ventral and the dorsal medial habenula coming from the triangular septum and the bed nucleus of the anterior commissure, respectively.[58] Impairing selectively the triangular septum-ventral medial habenula produced an effect on the expression of anxiety behaviors, while impairing the bed nucleus of the anterior commissure-dorsal medial habenula projections impaired fear and avoidance learning behaviors.

## Navigation and the IPN

One minor line of research around the function of the IPN investigated its potential involvement in circuits related to head direction representation and navigation, and will be of particular interest in the second part of the thesis. The IPN might be connected with the regions in theDTN, the most basal structures where heading direction cells can be found in mammals[59](but see[60]).

It has been reported that lesions to the habenula and to the IPN[61] can impair the performance of rats in tests that assess navigation abilities like the Morris water maze or food-carrying navigation tasks. Crucially, after IPN ablations the impairment was not affecting beacon navigation[62], suggesting that the IPN is implicated in the generation and stabilization of a heading direction signal, but its deficit can be rescued in a task where visual cues are used instead of a cognitive map to direct navigation.

Consistently with this hypothesis, electrolytic or neurotoxic lesions in the IPN altered the dynamics of head direction cells in the anterior dorsal thalamus, increasing the drift of their directional selectivity in darkness.[63]. However, we note that some (not extensive) recording of neurons in the IPN has been performed, and it has shown that IPN neurons seem to carry

[55] Chou et al., "Social conflict resolution regulated by two dorsal habenular subregions in zebrafish".

[56] Seigneur, Polepalli, and Südhof, "Cbln2 and Cbln4 are expressed in distinct medial habenula-interpeduncular projections and contribute to different behavioral outputs".

[57] Pang et al., "Habenula cholinergic neurons regulate anxiety during nicotine withdrawal via nicotinic acetylcholine receptors".

[58] Yamaguchi et al., "Distinct roles of segregated transmission of the septo-habenular pathway in anxiety and fear".

[59] J. S. Taube, R. U. Muller, and Ranck, "Head-direction cells recorded from the postsubiculum in freely moving rats. I. Description and quantitative analysis".

[60] Quina et al., "Specific connections of the interpeduncular subnuclei reveal distinct components of the habenulopeduncular pathway".

[61] Lecourtier, Neijt, and Kelly, "Habenula lesions cause impaired cognitive performance in rats: Implications for schizophrenia"; Thornton and Davies, "A water-maze discrimination learning deficit in the rat following lesion of the habenula"; Clark and Jeffrey S. Taube, "Deficits in Landmark Navigation and Path Integration After Lesions of the Interpeduncular Nucleus".

[62] Clark and Jeffrey S. Taube, "Deficits in Landmark Navigation and Path Integration After Lesions of the Interpeduncular Nucleus".

[63] Clark, Sarma, and Jeffrey S. Taube, "Head direction cell instability in the anterior dorsal thalamus after lesions of the interpeduncular nucleus".

only information about running speed, and no turning or head orientation signals[64].

Data in the fish also point in the direction of a role for the IPN in directional motion and orientation. A previous article from our lab investigated whole-brain responses to a directional stimuli with various degree of motion strength, and found reliable activation of the IPN that correlated with the strength of stimulus directional motion and fish turning rate.[65] Moreover, in an operant learning paradigm, it has been shown that habenular projections to the (dorsal) IPN are necessary in the acquisition of the association between a self-generated left or right turn, and a reward, but not in the association of an external stimulus and the reward.[66] This result proves that the habenulo-interpeduncular pathway is implicated in the encoding of egocentric directional information, which could be a step toward the generation of a representation of space in an allocentric frame of reference.

[64] Sharp, Turner-Williams, and Tuttle, "Movement-related correlates of single cell activity in the interpeduncular nucleus and habenula of the rat during a pellet-chasing task".

[65] Dragomir, Štih, and Portugues, "Evidence accumulation during a sensorimotor decision task revealed by whole-brain imaging".

[66] Cherng et al., "The Dorsal Lateral Habenula-Interpeduncular Nucleus Pathway Is Essential for Left-Right-Dependent Decision Making in Zebrafish".

# *2*

# *Results and discussion*

In the first chapter I have summarized what is known about the IPN of vertebrates. In the larval zebrafish the precise organization of this structure, the composition of its neuropil, and the morphology of it neurons have been only partially described. Here, I will outline some observations that we have been performing through confocal imaging and electron microscopy that reveal previously unknown details about the organization of the fish IPN, and of a related structure, the anterior hindbrain.

## 2.1  Anatomical relations of the larval zebrafish IPN

In the 7 days post fertilization (dpf) fish larvae, the IPN region sits right at the centre of the brain.
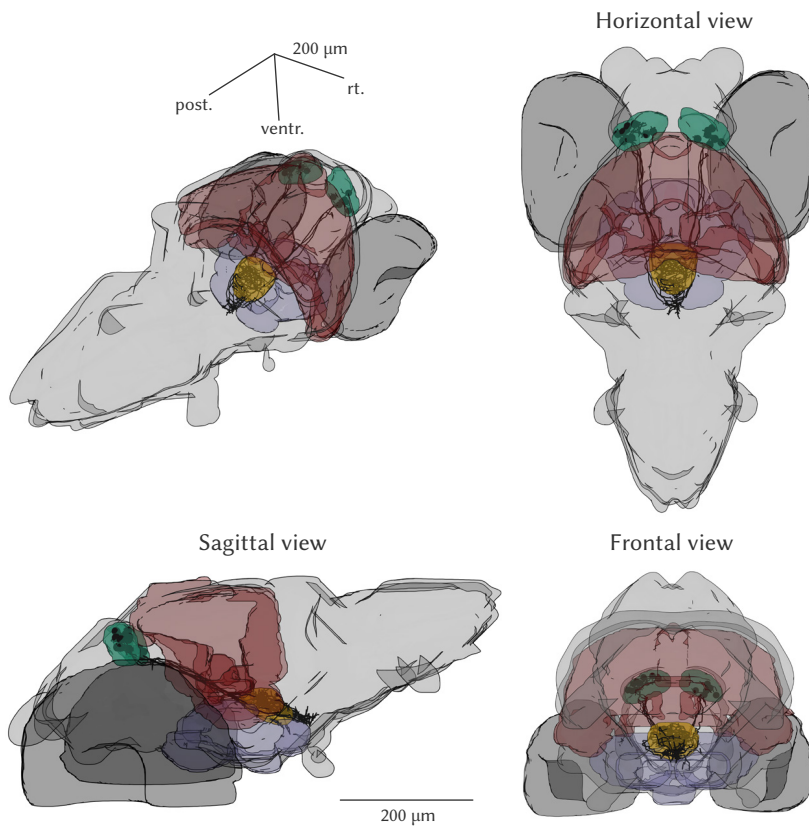


Figure 2.1: Anatomical relations of the IPN. In yellow, the IPN, in turquoise, the habenula. In light blue, the hypothalamus, evaginated ventrally in the larval brain. In maroon, the midbrain, that delimits anteriorly the IPN. In dark gray, the morphologies of habenulo-interpeduncular neurons, from the database published in Kunst et al., "A Cellular-Resolution Atlas of the Larval Zebrafish Brain".

It is delimited anteriorly by the midbrain/hindbrain boundary, and ventrally by the pial surface of the brain that separates it from the hypothalamus (which in the larval zebrafish brain is evaginated ventro-posteriorly

under the midbrain and the hindbrain).

The dorsal and lateral borders of the IPN are more arbitrarily defined, and they are made to coincide with the extension of the course of the habenulo-interpeduncular projections. This can be appreciated in Figure 2.2, that show habenular axons reconstructed from the SBEM dataset in a 5 dpf fish, with the mesh delimiting the IPN that will be used in the illustrations of this chapter.

### Histology of the IPN

The internal organization of the IPN region can be observed at high resolution in Figure 2.3, that shows sections from confocal acquisition of the interpeduncular region in different transgenic fish lines, co-registered in the same anatomical space.

The *Tg(16715:Gal4)* line, that labels habenular neurons (in pink), clearly shows how the boundaries of the region can be defined based on the habenulo-interpeduncular projections. The holes that they leave in the central part of the IPN corresponds to the location of the somas that can be seen from the *Tg(H2b:GCaMP6s)* line expression, where the fluorophore is expressed in all cell nuclei. From this line, we can observe a *core* of cells in the central part of the IPN. This core, of densely packed cell somas, planar in shape, separates a dIPN from a ventral IPN (vIPN). we refer to the area of neuropil around this central core as the intermediate IPN (iIPN).
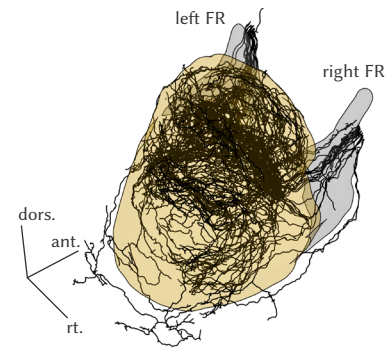


Figure 2.2: Axons delimiting the IPN region.
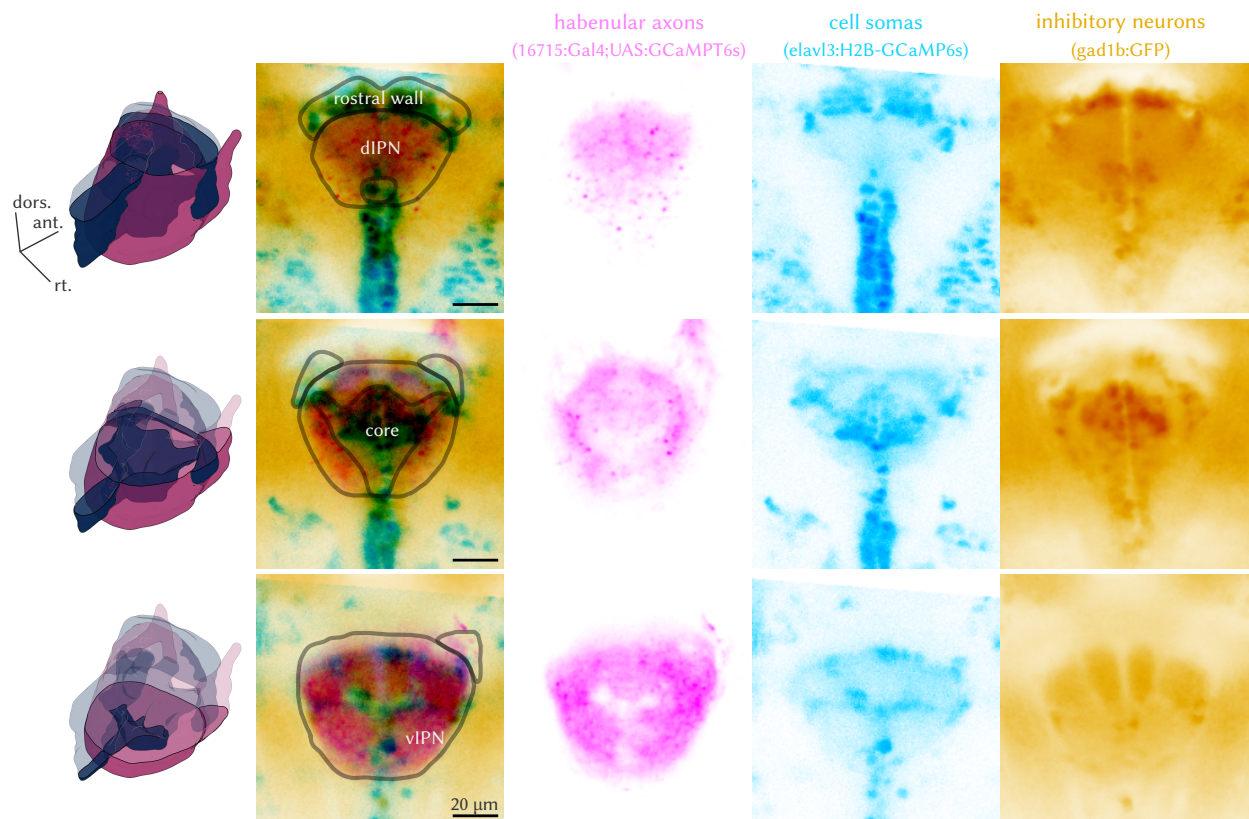


Figure 2.3: (*Left*) Cartoon of the position of the sections shown on the right. (*Right*) Slices from confocal stacks of three different transgenic lines co-registered in the same anatomical space.

The cell bodies are not entirely surrounded by neuropil: some thin stripes

of somas extend rostrally, up to a rostral *wall* of cell bodies that delimits the dIPN anteriorly; some vertical columns of somas extend downward until the ventral edge of the nucleus, in a typically triangular shape in horizontal section; and another crest of cells extends upward and caudally coming out from the dIPN, joining posteriorly, without a clear demarcation, to the dorsal raphe nucleus above it. These continuities make any precise definition of what constitutes a *IPN neuron* somewhat difficult, as several neurons can be counted or not depending on the precise location of the boundaries of the region.

The continuity of somas inside and outside the nucleus suggests that there might be a continuity also in the diversity of their functions. Moreover, many neurons that are up to 100 μm far from the IPN have both their axons and dendrites in the IPN, and could be functionally considered IPN interneurons even if their soma is very far from this region, as we will see in *Anterior hindbrain projections to the IPN*. The expression pattern of the *Tg(gad1b:GFP)* line, where GFP is expressed by a large fraction of GABAergic cells, suggest that most of the IPN neurons, expecially the neurons of the core, are GABAergic. Moreover, in the ventral sections of the gad1b:GFP stack (bottom row), we can observe some densities that tile the volume of the IPN, more evident in its rostral part. Those structures, which might correspond to the glomeruli previously observed in the IPN (*Glomeruli in the IPN*) will be described in a later section (*Glomeruli in the IPN neuropil*).

## 2.2 The habenulo-interpeduncular fibers

In fish, the habenulo-interpeduncular tract, or FR, is a strongly lateralized projection tract. Fibers from the left habenula target mostly the dIPN, and fibers from the right habenula mostly the vIPN (Figure 2.5).

We characterized the habenulo-interpeduncular tract in the SBEM dataset. First, we localized in the stack by looking for a compact bundle of fibers running together from the location of the habenula in the direction of the IPN (only the left habenula is included in the SBEM stack, but the right tract could be located by searching for fibers in a position symmetric to the fibers of the left FR tract).

after locating the tract, we counted the number of axons in the left and right bundle, approximately midway between the IPN and habenula. we could count 683 to 702 axons in the left FR and 555 to 581 axons in the right FR (the two numbers refer to two different counts that were done at slightly different rostro-caudal positions). Consistently with the higher number of axons counted there, the section of the left FR was larger than the right FR.

We then reconstructed fibers in the right FR and in the left FR. we could follow 19 axons from the right FR and 21 axons from the left FR for long enough to describe their projection pattern. table 2.1 reports the target area for all the axons we reconstructed.



Figure 2.4: Localization of neuron somas (dark areas) inside the IPN. The central core separates the dorsal from the ventral IPN.
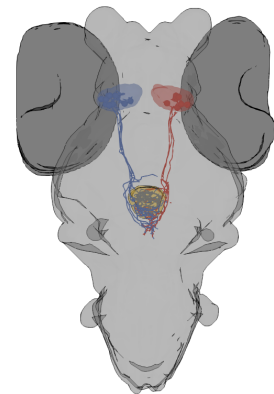


Figure 2.5: Projections of the left (blue) and the right (red) habenula.

| FR side | axons n. | dIPN | iIPN | vIPN | caudal |
|---------|----------|------|------|------|--------|
| Left | 21 | 14 (66.7%) | 1 (4.8%) | 6 (28.6%) | - |
| Right | 19 | - | - | 17 (89.5%) | 2 (10.5%) |

Table 2.1: Targets of habenulo-interpeduncular neurons.

In accordance with previous observations[1], we found that from the left FR, the majority of axons targeted the dIPN, while all the IPN-projecting axons from the right FR targeted the vIPN (Figure 2.6). A significant fraction of axons from the left FR innervated the vIPN, while none of the seeded axons from the right FR targeted the dIPN. One axon from the left IPN remained confined to the iIPN, while two axons from the right habenula did not entered the IPN and ended up in a more caudal area, presumably the median raphe nucleus.

[1] Bianco, Carl, et al., "Brain asymmetry is encoded at the level of axon terminal morphology".
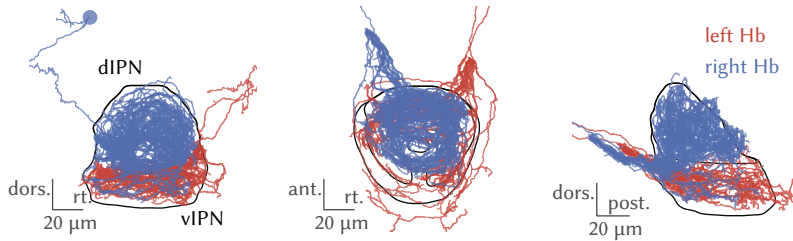


Figure 2.6: Habenulo-interpeduncular projections from SBEM reconstructions, colored by the side of the source neuron.

Unfortunately, the occurrence of artefacts in the EM dataset hindered the reconstruction of axons in the left half of the the ventral-caudal IPN, leaving some of those skeletons abruptly interrupted.

Habenular axons that reach the IPN do not arborize in a particular area in it; instead, while they remain precisely segregated in either the dorsal or the ventral part of the nucleus, where project diffusely. Although similar in the loose organization of their projections, the morphology of habenular axons projecting to the vIPN and the dIPN of zebrafish are very distinct, as previously described[2]. In the dIPN, axons branch extensively to form a mesh of fibers that wrap the entire neuropil; in the vIPN, each axon splits in a few branching points, and then spirals both clockwise or anti-clockwise in almost circular patterns around the entirevIPN (Figure 2.7).

[2] Bianco, Carl, et al., "Brain asymmetry is encoded at the level of axon terminal morphology".
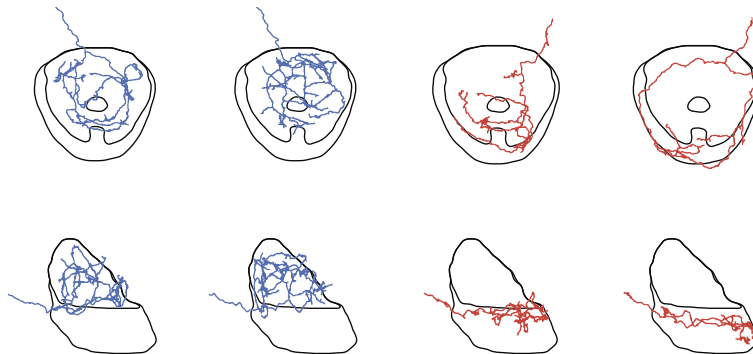


Figure 2.7: Individual plots of habenulo-interpeduncular axons from SBEM reconstructions, colored by the side of the source neuron.

## 2.3   Morphologies of interpeduncular neurons

Morphologies of IPN neurons of the larval zebrafish are very scarcely described in the literature. Some reconstructions have been obtained from single cell electroporations[3], but the low number of cells, their diversity and the incompleteness of the reconstructions (they often lacked an axon) did not permit a systematic description of their features.

[3] Bianco, Carl, et al., "Brain asymmetry is encoded at the level of axon terminal morphology".

To understand better the organization of this structure, we used the SBEM dataset to reconstruct individual neurons. First, we identified in the SBEM data all somas of cells in the IPN, leveraging the knowledge we have gained from the confocal experiments to find the boundaries of the region. In this count, we found approx. 120 cell bodies within a region roughly corresponding to the IPN mesh[4]. we prepared as candidates for reconstruction 170 somas, including also some from the wall of cells that delimits rostrally the dorsal IPN. Then, we randomly chose 90 of those cells for manual reconstruction (see SBEM *data skeletonization* for a description of the reconstruction procedure), and we included 78 neurons for which the reconstruction was satisfactorily complete in the analysis below (see *Morphological clustering*).

Figure 2.8 presents a broad overview of all the reconstructed skeletons. To better understand the morphological profiles that were recurring across cells, we obtained a distance matrix quantifying the similarity of the dendrites of IPN cells [5]. Then, we defined different morphological clusters using a hierarchical clustering procedure. After clustering the similarity of dendritic trees, we computed an additional clustering step on the similarity of axons within some of the most prominent clusters that exhibited the highest axon variability (see *Morphological clustering*).

[4] Number for a 5 dpf larvae

[5] For this calculation, neurons with a dendrite in the right side of the brain were mirrored to the left side.
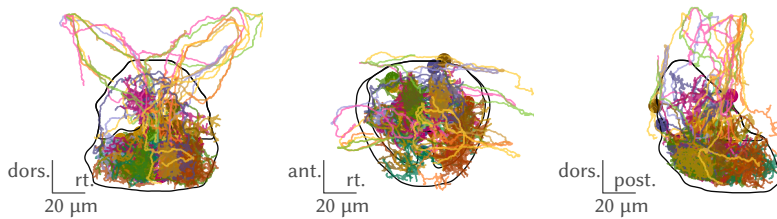


Figure 2.8: Reconstructed cells from the SBEM dataset. Each neuron is shown in a different color, with the axon in a lighter hue. For clarity, only one third of the neurons are displayed.

## *Dendrites of IPN neurons*

All of the reconstructed cells have a dendritic tree that is entirely contained within the IPN region that can be defined by the FR axons. Moreover, a large majority of neurons in the IPN extend a dendritic tree in the ventral IPN; only 7 out of 78 neurons had a dendrite in the dorsal IPN. Interestingly, all the observed cells in this group have a dendrite in the left side of the dIPN, where the afferent fibres from the habenula are entering the nucleus (see *Taxonomy of IPN neurons morphologies*, Cluster 1), although this might come from a bias in the seeding, as the somas were close to the mid-line with a bias on the left.
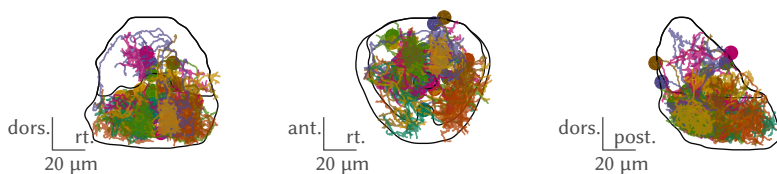


Figure 2.9: Dendrites of the cells presented in Figure 2.8.

When looking at individual clusters (Figure 2.11, Figure 2.12), one can notice several differences in the broad morphology of the dendrites. Some neurons (*e.g.* clusters 3, 7, and 9) have broad dendrites with sparse branching that can span a large portion of the ventral IPN. A consistent cluster of cells in this category has a dendritic tree that covers exactly either the left or the right half of the IPN. Some other clusters presented a very localized dendritic tree (*e.g.* clusters 4, 5, 6, and 10), entirely contained in a small volume of the IPN where they arborize extensively. Interestingly, the boundaries within which those arborizations were contained were highly consistent across neurons of the same cluster (*e.g.* clusters 4, 5, 6, and 10; see *Glomeruli in the IPN neuropil*).

### Axons of IPN neurons

Earlier reports[6] on the morphology of neurons in the larvae IPN reported that they mostly lacked an axon. we believe this observation came from technical limitations of the employed techniques, as in our sbem reconstructions we could detect an axon in at least 78 cells (out of 90 reconstructed cells). In many cases this axon was incomplete, lacking terminal arborizations and synaptic contacts. Sometimes this was clearly due to artefacts in the sbem dataset that made it impossible to reconstruct the thin axonal process, in some cases this was not the case, and the axonal process really seems to end abruptly after a fairly long course, without arborizing.[7] Therefore, all observations over axon course and targeted regions that we report below can be partial and incomplete.

In most cells, the axon course is directed outside the IPN, even for neurons that subsequently target a region inside the IPN. Axons tipically leave the IPN running upward, close to the mid-line, in two major tracts, one anterior and one posterior. Then, they increasingly bend laterally and ventrally, until they close a loop and completely invert their course, running again toward the mid-line. Some neurons (*IPN projection neurons*) target regions outside the IPN, typically in areas located dorso-caudally from the IPN; while some others (*IPN interneurons*) enter again in the IPN. This looping course is intriguing, as it is unclear why axons targeting different portions of the IPN should extend for such a long tract outside the nucleus, running for a total distance of up to ten times the distance between the soma and the ultimate axonal arborization area.

[6] Bianco, Carl, et al., "Brain asymmetry is encoded at the level of axon terminal morphology".

[7] This could be the sign that axons are still growing out it the 5 dpf larvae, although no evidence of a growth cone could be observed.
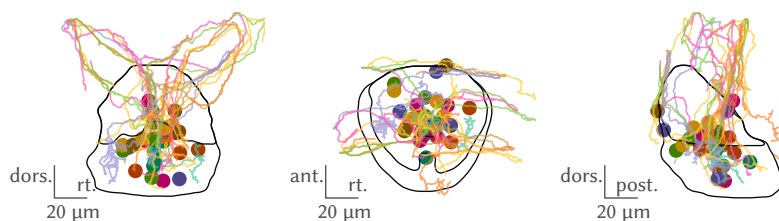


Figure 2.10: Axons of the cells presented in Figure 2.8.

*Taxonomy of IPN neurons morphologies*

Here we provide a description of each of the observed clusters, illustrated in Figures 2.11 and 2.12.

**Cluster 1.** Cluster 1 is the only cluster with cells with a dendritic tree in the dorsal IPN. All those cells had a soma in the dIPN, close to the midline, with a slight bias on the left side. Their axons extended dorsally and leftward, but were mostly short and not branching.

**Cluster 2.** Cluster 2 contains projection cells that have a compact, highly branching dendritic arbor in the rostral vIPN, either on the left or the right side, and an axons that extended ipsilaterally in the lateral direction to innervate a region lateral from the IPN. One neuron's axon follows the IPN axons loop and crossed the mid-line before targeting the lateral region on the contralateral side.

**Cluster 3.** The dendrites of cluster 3 cells extends on either the left or the right side of the upper intermediate IPN (just above the soma core). Their axons entered the axons loop or extended laterally.

**Cluster 4.** Cluster 4 cells have a dendritic tree that branches extensively in a confined patch in the caudal, ventral IPN, either on the left or the right. All their axons enter the dorsal loop we described above (*Axons of IPN neurons*); the most complete ones follow it until crossing the mid-line, and in some cases entering again in the ventral IPN and arborize there.

**Cluster 5.** Cluster 5 cells' dendrite is highly branching and strictly confined in a small region in the rostral part of the ventral IPN, either on the left or the right side. Their axons first leave the IPN laterally and very rostrally, and then invert their course, re-entering the IPN, crossing the mid-line, and arborizing extensively in a confined area of the contralateral ventral IPN.

**Cluster 6.** Cluster 6 cells have confined, highly branching dendrites in a region of the ventral IPN located between the dendrites of cluster 5 and cluster 4. Remarkably, the dendrites are precisely confined to the area where the axonal arborization of Cluster 5 cells are located. In most cases the axon branches dorso-caudally after leaving the loop; sometimes it re-enters the vIPN, and in one remarkable case it targeted the same area in the rostral IPN where the dendrites of Cluster 5 cells are found.

**Cluster 7.** Cells in cluster 7 have very wide dendrites, spanning most of either the left or the right side of the ventral IPN, while never crossing the mid-line and only sparsely branching. Their axons enter the dorsal fibers loop and, in some cases, remained dorsal and ipsilateral, branching dorso-caudally from the IPN.

**Cluster 9.** The dendrite of cluster 9 cells is large and with only few ramifications, and covers bilaterally the ventral part of the intermediate IPN, on the ventral side of the central cell core. Their axons entered the loop, and in one cell where it was particularly well reconstructed it re-entered the cell, innervating a region largely overlapping with the region span by the dendrite.

**Cluster 10.** Cells in cluster 10 have dendrites with the same features of cells in cluster 5, from which they were separated based on their axonal features. Their axon in most cases entered the axonal loop more caudally then the axons of cluster 5 cells, crossed the mid-line, and branched closed
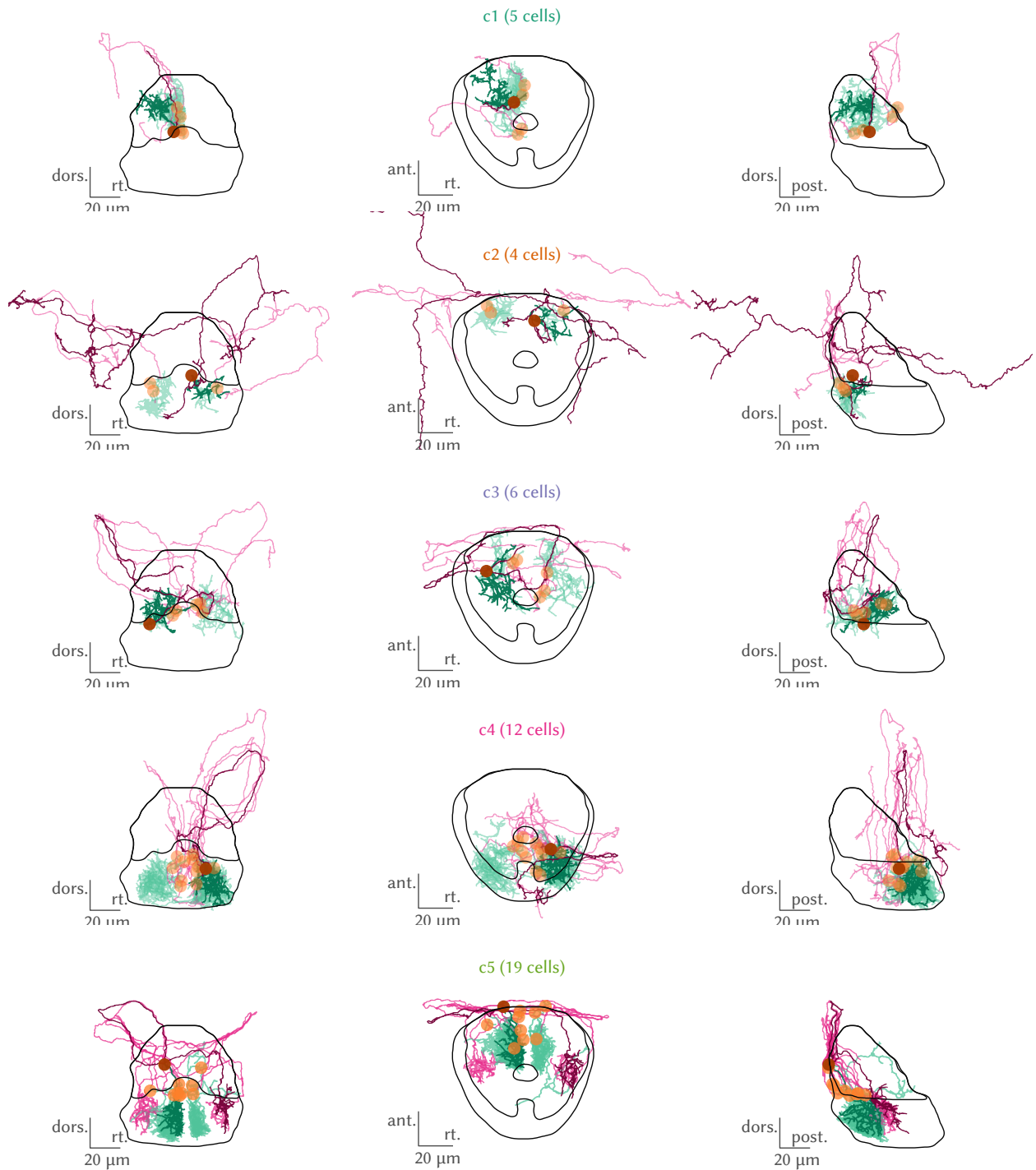
Figure 2.11: IPN neurons morphological clusters, 1 to 5. Green: dendrite; magenta: axon; yellow: cell soma. All neurons from the cluster are shown in transparency, with a representative neuron highlighted from each cluster.

c6 (23 cells)

c7 (15 cells)

c8 (4 cells)

c9 (11 cells)

c10 (9 cells)
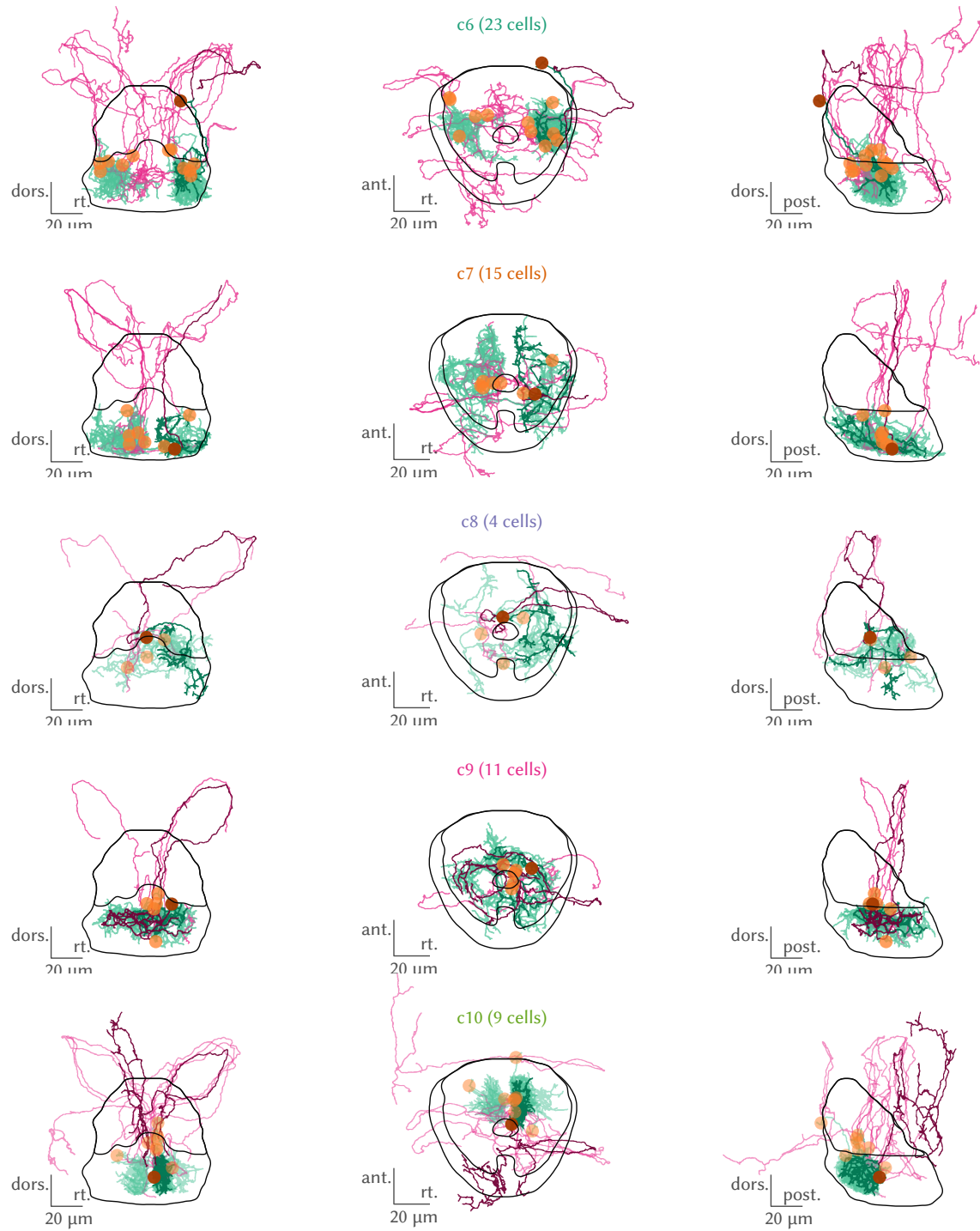
Figure 2.12: IPN neurons morphological clusters, 6 to 10. Legend as in Figure 2.11.

to the mid-line, contralaterally and dorso-ventrally from the IPN.

### Glomeruli in the IPN neuropil

The dendrites of neurons in clusters 4, 5, 6, and 10 are remarkable because they are very dense and highly compartmentalized.
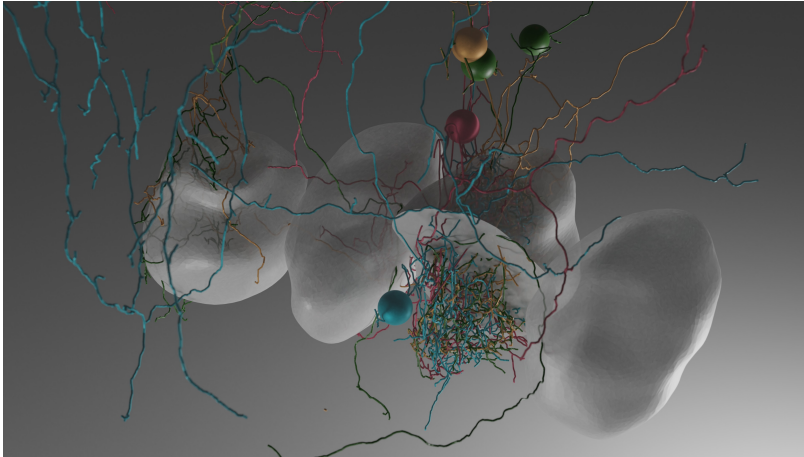


Figure 2.13: Rendering of neurons of IPN glomerulus 1. Neurons (dendrites only) are represened in different colors, and the gray highlighted areas represent the two medial and the two lateral glomeruli.

The dendrites of all the neurons of each of those clusters arborize extensively, but all the branching happens in a very confined volume of the IPN, so the cells end up occupying an almost identical region of the brain, delimiting very precisely its borders with the end of their projections. Their organization is highly reminiscent of the structures described in Herrick, "Interpeduncular Nucleus" as *glomeruli*, and we keep this denomination to refer to them.

From the localization of the dendrites we could define six glomeruli in the ventral IPN, three for each side. Interestingly, the position of the soma was highly correlated with the dendritic tree glomerulus of the same cell, as can be seen in Figure 2.14. Together, the six glomeruli tile the entirety of the ventral IPN.[8] To refer to the different glomeruli we number them from 1 (rostral-most) to 3 (caudal-most), as illustrated in Figure 2.14.

[8] No glomerular organization with this degreee of compartimentalization could be observed so far in the dorsal IPN.

Figure 2.14: *Left*, Glomerular neurons of the IPN color-coded by the glomerulus they project to. *Right*, Numbering scheme for the IPN glomeruli.



The glomeruli can also be observed from confocal imaging. The gad1b:GFP line shown in Figure 2.3 presents some brighter fluorescent areas in the ventral IPN, especially in the rostral part, and the localization of the signal actually corresponds to the distribution of the clusters we defined from the

SBEM data. Moreover, immuno-staining against the gabaergic cells marker GAD67 can be used to highlight even more strongly the presence of six glomeruli in the ventral IPN (Figure 2.15).

For shortness, we will refer to cells with a dendrite contained within a particular glomerulus as dG{N}, where {N} is the glomerulus number. In the same way we will specify the location of the cell's axon with aG{N}{side}, were now {side} is the side of the target glomerulus relative to the dendritic tree - i(psi) or c(ontra). Therefore, cells of cluster 5 and cluster 10 are dG1 neurons, cells of cluster 6 dG2 neurons, and cells of cluster 4 dG3 neurons. More precisely, cells of cluster 5 are dG1-aG2c neurons, with an axon in the contralateral G2.

Axon projections of IPN neurons were often targeting glomeruli in the IPN. When this was the case, the target glumerulus was in most cases contralateral, and it was never the same as the source one, nor the same number (*e.g.*, axons from neurons with dendrites in G1 would never target G1, either ipsi- nor contralaterally). Sometimes the branching of the axon was not as precisely confined as the branching of the dendrites; for example, aG1 axons from dG2 neurons would often seem to span to some degree glomeruli 1 on both sides of the IPN.

### Calcium activity in the IPN glomeruli

The observation of glomeruli at the anatomical level resonates with the notion that, as we have seen in the previous chapter, calcium activity in the IPN neuropil can be highly compartmentalized, even if the habenular axons that target the area do not show any specific compartimentalization. This has be seen in previous reports[9], and in recent experiments performed in the lab[10].

For example, Figure 2.16 presents pixelbased direction selectivity maps obtained by imaging different cell types in the IPN neuropil while showing to the fish a stimulus drifting in eight different directions. In a GABAergic line, the anterior glomeruli 1 and 2 are clearly visible. Interestingly, the activity is very strongly correlated across pairs of glomeruli (G1 and contralateral G2). Given the sparse expression observed in the line, we believe that the signal comes from one or a few cells only, and that the high correlation we observe is the result of the raise in calcium in both dendrites and axons when the neurons are active.
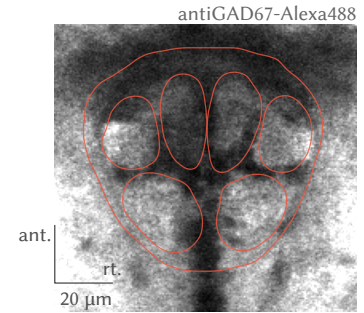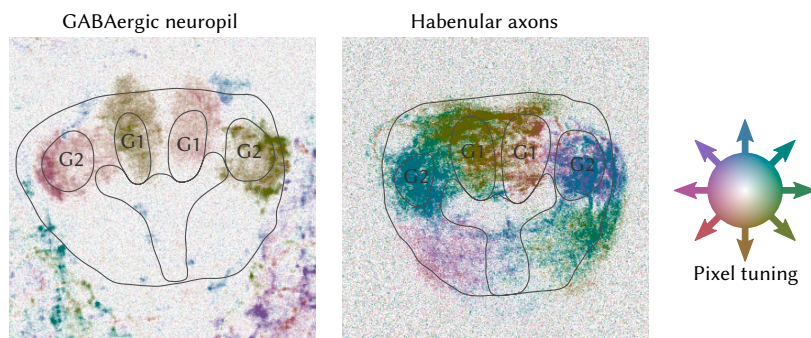


Figure 2.15: Anti-GAD67 immunostaining reveals the IPN glomeruli (data acquired by You Kure Wu).

[9] W.-y. Chen et al., "Role of Olfactorily Responsive Neurons in the Right Dorsal Habenula–Ventral Interpeduncular Nucleus Pathway in Food-Seeking Behaviors of Larval Zebrafish"; Dragomir, Štih, and Portugues, "Evidence accumulation during a sensorimotor decision task revealed by whole-brain imaging".

[10] Štih, "Signatures of motion processing and decisions in the larval zebrafsh brain".



Figure 2.16: Tuning to directional motion in the vIPN glomeruli, imaged in ( Tg(gad1b:Gal4;UAS:GCaMP6s)) (expressing GCaMP6s in GABAergic neurons, *left*), and in ( Tg(15:Gal4;UAS:GCaMP6s)) (expressing GCaMP6s in all habenular axons, *center*). Pixels are color-coded by a regression-based estimation of their tuning to a stimulus directional motion, with hue mapping the preferred tuning angle and brightness the tuning strength (*right*). From Štih, "Signatures of motion processing and decisions in the larval zebrafsh brain", data acquired by Hagar Lavian.

Intriguingly, calcium signals from the axons of the habenulo-interpeduncular tract show highly compartimentalized maps of directional selectivity. In Figure 2.16, we can see how different areas of habenular axonal neuropil had very similarly directional selectivity, and how those areas roughly correspond to different glomeruli of the IPN. This happens despite the fact that there is nothing in the axon morphology that would correspond to glomerular demarcations, as each habenular axon spirals across the entire IPN (see Figure 2.7). Therefore, we hypothesised that the local organization of the axon activity in the IPN could be the result of axo-axonic modulation of the habenulo-interpeduncular fibers by the glomerular cells.

*Axo-axonic synapses in the IPN*

To understand better the internal connectivity of the IPN, and to see whether it is possible that the activity of the glomerular neurons can influence the activity of the habenulo-interpeduncular axons, we asked annotators to find postsynaptic partners for two neurons, a left and a right dG1-aG2c neuron. Annotators marked 217 and 269 synaptic contacts for the left and the right neuron, respectively. Almost all the synaptic contacts were found to be located in the branching part of the axon (Figure 2.17).
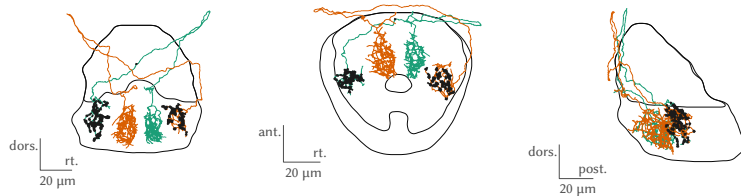
Figure 2.17: Two glomerular dG1-aG2c neurons on the two sides of the IPN were annotated for synapses (in black).



Without prior biasing inputs, the annotators observed that some of the contacts were axo-axonic contacts, an example of which can be appreciated in Figure 2.18. Axo-axonic contacts seem to account for a significantly large proportion of the total number of synapses, as the tracing results reported below confirmed several post-synaptic processes to be axons.

To understand to which post-synaptic partners those belonged to, we seeded 15 post-synaptic partners for a new round of reconstructions. There results were the following:

- 4/16 postsynaptic partners were either putative or confirmed habenular axons. Putative habenular axons were segments running on the horizontal plane in the ventral IPN; confirmed habenular axons could be traced fully back to the fasciculus retroflexus.

- 5/16 postsynaptic partners were other interpeduncular glomerular cells. Most of those partners where prominent dG2 cells, although in one case, the target of the focal neuron was the axon of a aG1 neuron.

- 5/16 postsynaptic partners were cells whose soma was located very dorsally from the IPN, up to 100 μm above the IPN.
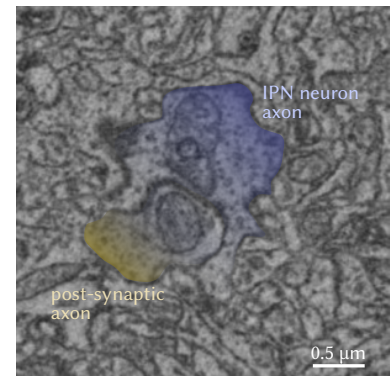


Figure 2.18: Axo-axonic synapse in the IPN. The pre-synaptic neuron, in blue, is one of the two neurons presented in Figure 2.17.

- 2/16 postsynaptic partners were axons that could not be traced back to a cell but whose morphology reminded the aG2c projections of cells of cluster 5.

These observations confirmed the hypothesis that axons of glomerular neurons can make synaptic contacts with habenulo-interpeduncular fibres, and could play a role in the modulation of their activity.

## 2.4    Anterior hindbrain projections to the IPN

The postsynaptic partners that we identified outside the IPN have an intriguing morphology. Their soma is located 20 μm to 100 μm above the IPN, at the same level on the rostro-caudal axis, in an area that the Mapzebrain atlas labels as the *superior dorsal medulla oblungata (stripe 2)*[11]. Neurons in this area have been referred in the larval zebrafish literature as anterior hindbrain neurons[12], and we will keep here this denomination. In a later section (*Possible analogy between the DTN and the zebrafish aHB*) we will speculate about what are the possible analog regions in the mammalian brain.

After the first observation of IPN-projecting anterior hindbrain neurons, we investigate whether we could reconstruct more neurons of this kind. we could easily identify up to 100 neurons with a morphology similar to that of the first tracedaHB neurons, suggesting that they constitute a significant fraction of the anterior hindbrain neuronal population. we seeded for a full reconstruction 42 of those neurons.

Among the reconstructed cells, we could observe 24 satisfactorily reconstructed neurons targeting either the dorsal and the ventral IPN with their somas and dendrite; Figure 2.19 shows all those cells with their soma in the anterior hindbrain and their dendrites in the IPN. Interestingly, the groups of ventral IPN- and dorsal IPN-targeting neurons were entirely non-overlapping: neurons with a dendrite in the dIPN never projected to the vIPN, and vice-versa.

[11] Kunst et al., "A Cellular-Resolution Atlas of the Larval Zebrafish Brain".

[12] X. Chen, Mu, et al., "Brainwide Organization of Neuronal Activity and Convergent Sensorimotor Transformations in Larval Zebrafish"; Dunn et al., "Brain-wide mapping of neural activity controlling zebrafish exploratory locomotion"; Dragomir, Štih, and Portugues, "Evidence accumulation during a sensorimotor decision task revealed by whole-brain imaging"; Bahl and Engert, "Neural circuits for evidence accumulation and decision making in larval zebrafish."



Figure 2.19: Reconstructed neurons with the soma in the anterior hindbrain and the dendrite in the IPN. Most of them have an axon that goes back to the IPN, while a fraction targets a dorso-rostral region.

### Morphologies of anterior hindbrain neurons

All anterior hindbrain neurons produce a single thick extension downward toward the IPN, which runs downward (soma located at very different heights, so the lengths of such extension could significantly vary) and bifurcates in a dendrite and an axon 10 μm to 40 μm above the IPN.[13] The dendrites proceed downward and target one of the ipsilateral glomeruli, branching extensively in it as dG1-2-3 cells of the IPN do. In most cases the axons, after branching out, run in bundles together with the axons of interpeduncular neurons

[13] Dendrites and axons can be reliably recognised by their thickness and the distribution of pre- and post-synaptic terminals

until entering the IPN, where they target one of the glomeruli, mostly contralaterally. A subset of the reconstructed cells had an axon that extended caudally and dorsally from the IPN.

### Clusters of anterior hindbrain neurons morphologies

We decided to cluster the reconstructed anterior hindbrain neurons using a procedure similar to the one followed for interpeduncular neurons. we obtained two clusters for the dorsal IPN and two clusters for the ventral IPN, reported in Figure 2.20.

**Cluster 1.** In cluster 1, dendrites and axons entirely overlap with the processes of dG1-aG2c interpeduncular neurons of cluster 5 in Figure 2.11. The dendritic process arborizes in the first glomerulus ipsilaterally to the cell position; the axon is almost always targeting the contralateral glomerulus 2, apart from one cell that extends laterally outside the IPN.

**Cluster 2.** Cluster 2 neurons are dG2-aG1c cells, similar to one cell observed in Cluster 6 of Figure 2.12. The dendritic process arborize in the second glomerulus ipsilaterally to the cell position, while the axon targets the contralateral glomerulus 1. In some cases the axon starts branching already at the level of the ipsilateral glomerulus 1, and it is therefore possible that cells of this cluster innervate the glomeruli 1 of both sides of the IPN.

**Cluster 3.** Cluster 3 contains neurons with a dendrite in the ipsilateral dorsal IPN and an axon projecting outside the IPN. interestingly, the dendrite is planar, and extends almost entirely over a sagittal plane, with very little extension over the frontal axis. This was particularly visible in the cells with the most medial dendrite. The axon would extend caudally and ipsilaterally, arborizing in a region rostro-caudal from the IPN.

**Cluster 4.** Cluster 4 contains neurons with a dendrite in the ipsilateral dorsal IPN and an axon targeting the contralateral, dorsal IPN. The dendrite was remarkably planar, like in the cells of cluster 3. Intriguingly, the location of the axon arborization was highly correlated with the position of the dendrite over the frontal axis, with cells with a more medial dendrite having a more lateral axon, and vice-versa.

The morphology of cells in cluster 4 might be highly relevant to the organization of their activity. Therefore, we will discuss them again in further detail in a later chapted (see *aHB neurons arborize in the dorsal IPN*).

## 2.5    Conclusions

### Glomeruli are central to the organisation of the IPN microcircuitry

Glomeruli seem to be a paramount element around which the structure and function of the IPN is organised. By focusing on the definition of the IPN based on its habenular afferents, studies on the IPN in the larval zebrafish have previously overlooked those structures. When looking at functional responses already reported in the literature[14], we could observe an activity compartmentalisation compatible with the imaging results we present in Figure 2.16.

Connectivity in the glomeruli is highly recurrent. This can be clearly

[14] Dragomir, Štih, and Portugues, "Evidence accumulation during a sensorimotor decision task revealed by whole-brain imaging"; W.-y. Chen et al., "Role of Olfactorily Responsive Neurons in the Right Dorsal Habenula–Ventral Interpeduncular Nucleus Pathway in Food-Seeking Behaviors of Larval Zebrafish".
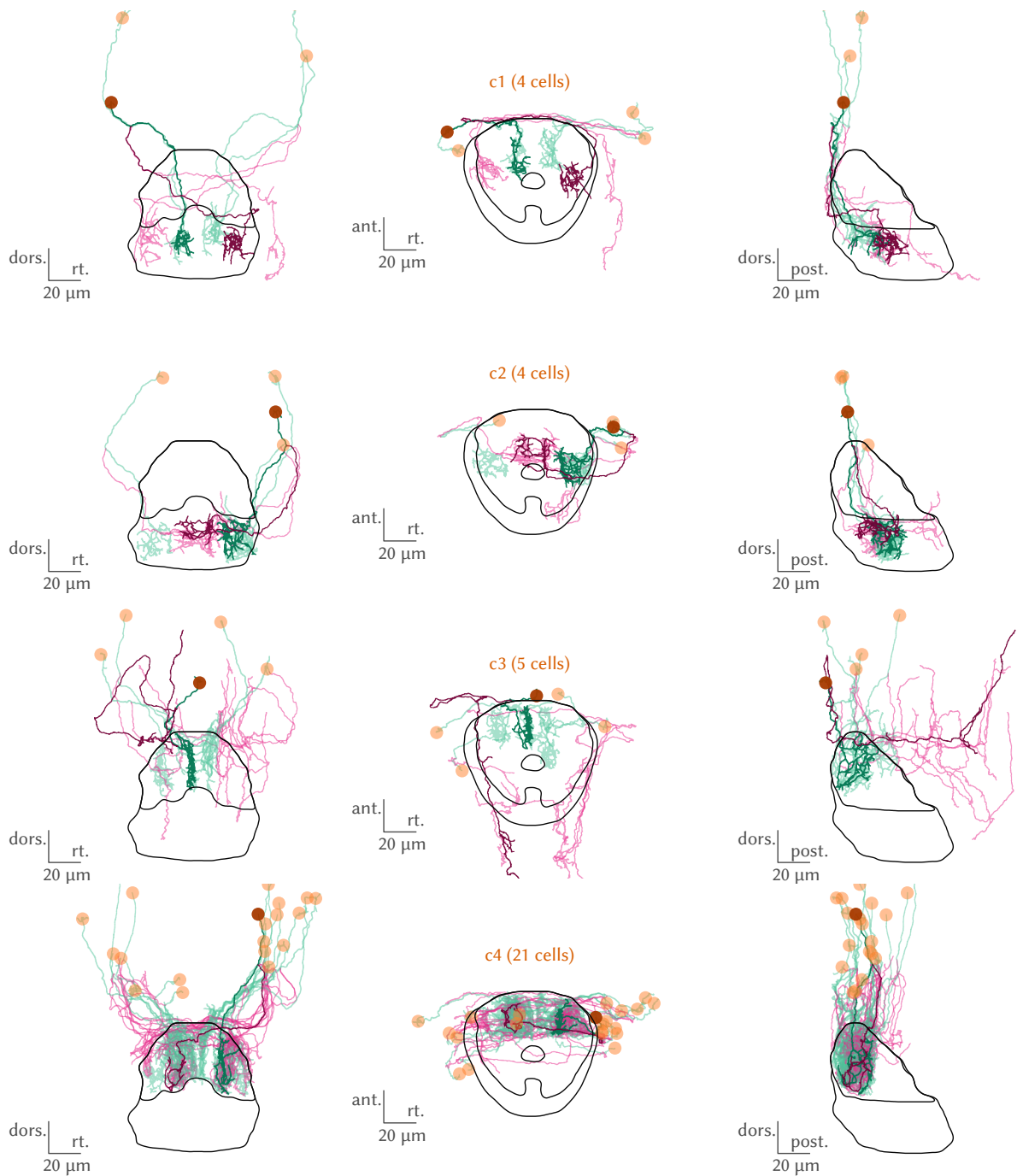
Figure 2.20: Green: dendrite; magenta: axon; yellow: cell soma. All neurons from the cluster are shown in transparency, with a representative neuron highlighted from each cluster.

appreciated in Figure 2.21, where a dG1-aG2c and a dG2-aG1c neurons are highlighted.

To understand whether this connectivity motif is shared across all glomeruli, we pooled together information about the axonal terminals of all neurons having the dendrite in a glomerulus, regardless of the position of their soma (IPN or anterior hindbrain), looking at whether they were targeting another glomerulus, somas in the central core, or regions outside the IPN. Figure 2.22 show the results. Interestingly, while a large fraction of dG1 and dG2 neurons were targeting with their axon another glomerulus, this seemed not to be the case for dG3 neurons, that were invariably targeting regions outside the IPN or the central core. This would suggest that the glomerular compartmentalization is not "radially symmetrical", and there is a rostro-ventral gradient in the degree of inter-connectivity of the glomeruli. However, even if the reconstructions of IPN neurons were randomly seeded, we cannot rule out that this result just come from an incomplete sampling of dG3 neurons, whose number was limited. More dense reconstructions of the IPN neuropil will be required to confirm or reject this observation.

### aHB neurons are functionally integrated within the IPN

Our morphological data prove that the aHB contains a large number of neurons that can be functionally considered a part of the IPN, as their connectivity completely overlaps the connectivity of glomerular interneurons of the IPN. we conclude that glomerular neurons could be found in the IPN soma core, in the rostral wall, and in the aHB above the IPN, but they all exhibited similar integration within the rest of the IPN microcircuitry. Furthermore, in the dorsal IPN the dendrites ofaHB neurons were much more represented than the dendrites of IPN neurons.

Those observations suggest that the functional boundaries of what we define as IPN is much broader than currently appreciated, because even interpeduncular interneurons (neurons that receive and project to interpeduncular neuropil) can have their soma considerably distant from the IPN. Importantly, in the aHB somas of glomerular neurons could be found intermingled with somas of neurons that did not target the IPN with their projections, making it difficult to disentangle, based on soma location only, which neurons belong to the IPN circuitry.

Those considerations are crucial for in the interpretation of functional imaging data obtained from the soma of neurons observed through whole brain recordings[15], as it proves that activity of neurons located very distant from the IPN has to be recognised as coming from synaptic interactions that happens entirely within this nucleus.[16] Moreover, we expect that within a very confined volume of the anterior hindbrain one can find a large diversity of neuronal responses, as neurons with similarly located somas can participate in completely different circuits. This can be problematic when pooling results from arbitrarily defined brain volumes over multiple fish.

### Limitations, open questions and future directions

Most of the observations of this chapter have been based on non-dense skeletonizations performed on a single 5 dpf animal. Although the histo-
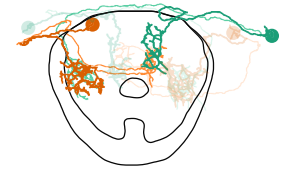


Figure 2.21: Recurrent connections in the IPN glomeruli 1/2. Two neurons making reciprocal connections in G1 and G2 are shown, and two symmetrical neurons are hinted.
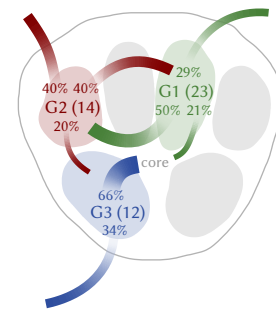


Figure 2.22: Connectivity summary for the observed glomerular neurons. In brackets, number of cells with the dendrite in each glomerulus. Percentages refer to the proportion of axons that were arborizing in each target region, among all the axons with a clear arborization (not interrupted).

[15] X. Chen, Mu, et al., "Brainwide Organization of Neuronal Activity and Convergent Sensorimotor Transformations in Larval Zebrafish"; Bahl and Engert, "Neural circuits for evidence accumulation and decision making in larval zebrafish."; Dragomir, Štih, and Portugues, "Evidence accumulation during a sensorimotor decision task revealed by whole-brain imaging".

[16] The region that contains the somas of those neurons is entirely devoid of axons. The only processes that can be observed close to the somas are the extensions that run ventrally before splitting in axon and dendrite. Therefore, we can safely exclude axo-somatic synapses in this context.

logical features of the area were largely matching the organisation found in older animals (see for example Figure 2.3, illustrating confocal images from a 7 dpf animal), we need to be aware of the possibility that later in development the reorganization of the tissue and the migration of cells might produce a different configuration of somas localization and projection courses.

Another key piece of missing evidence is the neurotransmitter type for neurons that are part of this circuit. The known literature in other vertebrates as well as the expression pattern of the gad1b gene in the larval zebrafish ensure that a good fraction of the glomerular neurons are GABAergic. However, we cannot rule out that some glomerular neurons are excitatory in nature, or use neurotransmitters that are not GABA or glutamate.

The identification of precise target areas from neurons of the IPN has proved challenging. The most consistent projection patterns across cluster were from IPN interneurons, projecting back to the IPN. The only clear area that was receiving fibers from manyIPN or anterior hindbrain neurons was the caudo-dorsal region delimited by axons fibers of cluster 3 of anterior hindbrain neurons (targeted sporadically also byIPN neurons of different clusters). The identity of this region, as well as the morphology of postsynaptic partners located there is still under investigation.[17]

Another open question is the presence of afferent fibers other than the habenular axons. Even in a random seeding of axons in the IPN, we could identify only habenular axons and glomerular neurons as afferents to the interpeduncular region. Given the presence of interesting activation profiles in the imaging data, which seem to be patterned independently of the organization of habenular fibers, we can speculate whether different inputs related to sensory stimuli (Figure 2.16) or motor behavior are conveyed to different glomeruli or different parts of the IPN.

[17] The projections look largely similar to the results obtained with anterograde tracing in adult zebrafish in Agetsuma et al., "The habenula is crucial for experience-dependent modification of fear responses in zebrafish". There, the postsynaptic region was identified as the *griseum centrale*, defined by them as *"the periventricular structure that most likely includes the regions corresponding to mammalian peri-aqueductal gra, dorsal tegmental nucleus and nucleus incertus"*.

Finally, the reconstructions reported here are not been obtained in an entirely random sampling of the interpeduncular region. After the first tracing of IPN neurons, our reconstructions have been been partially biased, as cells has been seeded for reconstructions based on the consistency of their projection pattern with previously observed morphologies. This has proven fundamental for the anterior hindbrain reconstructions, where an entirely unbiased seeding would have lead to the reconstructions of many cells with projection patterns entirely unrelated to the interpeduncular microcircuitry, but it might have biased the reconstruction of morphologies occurring in neurons whose fibers run in specific regions that were highly targeted during the seeding.

In the future, the improvement of techniques for automatic segmentation of electron microscopy data will hopefully allow for a dense reconstruction of fibers in the IPN, and a version of a trained automatic segmentation neural network is already been developed (Svara et al, in review). Those tools will finally unravel the entirety of the diversity of neuronal morphologies in the IPN, and address in much more details the crucial connectivity questions like the nature of afferent fibers and postsynaptic partners of IPN neurons. Automatic segmentation tools will significantly facilitate the identification

of synapses, and will eventually provide us with a complete connectivity
matrix of this circuit.

# Materials and methods

## 3.1 Zebrafish husbandry

All procedures related to animal handling were conducted following protocols approved by the Technische Universität München and the Regierung von Oberbayern. Adult zebrafish (*Danio rerio*) from Tüpfel long fin (TL) strain were kept at 27.5 °C to 28 °C on a 14/10 light cycle, and hosted in a fish facility that provided full recirculation of water with carbon-, bio- and UV filtering and a daily exchange of 12% of water. Water pH was kept at 7.0 to 7.5 and conductivity at 750 µSv to 800 µSv. Fish were hosted in 3.5 L tanks in groups of 10 to 17 animals. Adults were fed with Gemma micron 300 (Skretting) and live food (*Artemia salina*) twice per day and the larvae were fed with Sera micron Nature (Sera) and ST-1 (Aquaschwarz) three times a day.

### Breeding

All experiments were conducted on 6 dpf to 9 dpf larvae of yet undetermined sex. The week before the experiment, one male and one female or three male and three female animals were left breeding overnight in a Sloping Breeding Tank or breeding tank (Tecniplast). The day after, eggs were collected in the morning, rinsed with water from the facility water system, and then kept in groups of 20 to 40 in 90 cm Petri dishes filled with 0.3× Danieau's solution (17.4 mM NaCl, 0.21 mM KCl, 0.12 mM MgSO$_4$, 0.18 mM Ca(NO$_3$)$_2$, 1.5 mM HEPES, reagents from Sigma-Aldrich) until hatching and in water from the fish facility afterwards. Larvae were kept in an incubator that maintained temperature at 28.5 °C and a 14/10 hour light/dark cycle, and their solution was changed daily. At 4 dpf to 5 dpf, animals were lightly anesthetized with Tricaine mesylate (Sigma-Aldrich) and screened for fluorescence under an epifluorescence microscope. Animals positive for GCaMP6s/GFP/mCherry fluorescence were selected for the imaging experiments.

## 3.2 Confocal experiments

For confocal experiments, larvae were embedded in 1.5% agarose and anesthetized with tricaine. High resolution stacks of the ipn were acquired from 7 dpf larvae of different transgenic lines (*Tg(16715:Gal4)*, *Tg(H2b:GCaMP6s)* ×*Tg(16715:Gal4)*, and *Tg(gad1b:GFP)* ×*Tg(16715:Gal4)*) were acquired using a 20× water immersion objective (NA = 1.0) with a voxel resolution of 0.5 µm × 0.5 µm × 0.5 µm (LSM 880, Carl Zeiss). The stacks were registered

to one another using `dipy`[1] on the channel with the *Tg(16715:Gal4)* signal. A segmentation of the IPN subregions was then painted manually on the volume using `napari`.

[1] Garyfallidis et al., "Dipy, a library for the analysis of diffusion MRI data".

### 3.3    Electron microscopy experiments

#### Serial block-face electron microscopy dataset acquisition

Details of the SBEM dataset acquisition will be published elsewhere (Svara et al., in preparation). Briefly, a 5 dpf larval *Tg(elavl3:GCaMP5G)a4598* transgenic zebrafish was fixed with extracellular space preservation and stained as described previously[2]. The sample was embedded in an epoxy mixture containing 2.5% Carbon Black[3]. The brain was imaged at a resolution of $14\,nm \times 14\,nm$ and sections were cut at a thickness of 25 nm. The long (y) axis of each image tile was scanned by gradually moving the stage, while the short axis (x) was scanned with the electron beam. The shape of the tile pattern was determined based on a 4 μm voxel size X-Ray microCT scan (SCANCO Medical AG, Brütisellen) of the embedded sample.

[2] Svara et al., "Volume EM Reconstruction of Spinal Cord Reveals Wiring Specificity in Speed-Related Motor Circuits"; Briggman, Helmstaedter, and Denk, "Wiring specificity in the direction-selectivity circuit of the retina".
[3] Nguyen et al., "Conductive resins improve charging and resolution of acquired images in electron microscopic volume imaging".

#### SBEM data skeletonization

The first reconstructions of cells in the aHB with processes in the IPN were observed by seeding for reconstruction dendrites or axons in the IPN and reaching from there somas in the aHB, in the context of a (still unpublished) broader reconstruction effort. The IPN location in the SBEM stack was firstly inferred by the recognizable organization of the neuropil and cell somata in the rhombomere 1 ventral region. Then, it was confirmed by the tracing of axons that could be reconstructed back to the habenulae through a long bundle of fibers unambiguously identifiable as the fasciculus retroflexus by its course (unpublished data). After those first observations, additional cells with the soma in the aHB were seeded based on the similarity of their processes with already reconstructed cells.

Skeletonization was performed manually by a team of annotators at ariadne.ai ag (Buchrain). Annotators were instructed to flag difficult locations without extending the skeleton at those locations, and to stop tracing after a total time of 2 h was reached. At that point, or when a cell was completed, a quality check was performed by an expert annotator. Difficult locations were then decided by the expert, and sent back to the annotator team for additional tracing if necessary. This procedure was iterated until all cells were fully traced. The skeletons were then annotated to distinguish the dendrite and the axon by their morphological features (processes thickness and presence of presynaptic boutons) independently by Ariadne expert annotators or the authors, with convergent results. All further analyses and quantification of the reconstructions were performed using Python.

#### Morphological clustering

To cluster the morphology of IPN and aHB neurons, first we used a modified version of the NBLAST algorithm[4] to obtain a distance matrix for all cells. For every pair of neurons, we took for every one of their node the

[4] Costa et al., "NBLAST: Rapid, Sensitive Comparison of Neuronal Structure and Construction of Neuron Family Databases".

minimum distance to a node of the other neuron. Then, we computed the median across all nodes. As this distance matrix will be asymmetric, we then considered only the minimum between the two distances obtained for each pair.

After having obtained a distance matrix, we employed the `scipy`[5] `linkage()` function implementating the Ward's method for hierarchical clustering to obtain the aggregation tree (Figure 3.1). Then, we plotted the clusters resulting from different choices of a threshold, and we selected a threshold that was separating the categories that were the most distinct upon visual inspection. This procedure was applied on the dendrites of IPN neurons, followed by a second step on the axons to split a large cluster with very consistent dendritic morphology (the aggregation of cluster 5 and 10 in Figure 2.11); and on the dendrites of aHB neurons.

## 3.4 Anatomical registrations

To work with the anatomical spaces and their annotations, we used the BrainGlobe `bg-atlasapi` package[6] and either the larval zebrafish brain reference MapZeBrain[7], or a custom lab reference of the aHB and IPN region that will be published together with the data, created by morphing together stacks from different lines using either `dipy`[8] or Computational Morphometry Toolkit (`CMTK`)[9]. To visualize functional data in the references, an average anatomy computed after centering all stacks with the centering point described in (*Lightsheet imaging data preprocessing*), and then a manual affine registration was performed to the IPN reference. A similar procedure was used to map the electron microscopy data. From the skeletons, a density stack was computed in which the shape and features of the IPN were prominently visible. An affine matrix transformation was found to match this stack on the IPN reference, and used for transforming the neuron's coordinates. The masks delimiting the IPN and the dIPN were drawn in the IPN reference atlas looking at the localization of habenular axons afferents to the region.

Visualizations were created using `matplotlib`[10] and `brainrender`[11].
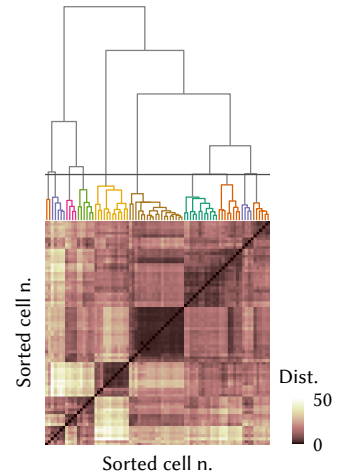


Figure 3.1: Hierarchical clustering of IPN morphologies.

[5] Virtanen et al., "SciPy 1.0: fundamental algorithms for scientific computing in Python".

[6] Claudi, Petrucco, et al., "BrainGlobe Atlas API: a common interface for neuroanatomical atlases".

[7] Kunst et al., "A Cellular-Resolution Atlas of the Larval Zebrafish Brain".

[8] Garyfallidis et al., "Dipy, a library for the analysis of diffusion MRI data".

[9] Rohlfing and Maurer, "Nonrigid image registration in shared-memory multiprocessor environments with application to brains, breasts, and bees".

[10] Hunter, "Matplotlib: A 2D graphics environment".

[11] Claudi, Tyson, et al., "Visualizing anatomically registered data with brainrender".

# II

# A HINDBRAIN CIRCUIT THAT REPRESENTS HEADING DIRECTION

> The test of the truth of a scientific law or principle is its predictive value, and the prediction is an act of faith. There is always a factor of faith in every scientific generalisation and indeed in every fact - faith in the order of nature, faith in the reliability of the observations, and faith in the trustworthiness of the record...
>
> —C.J. HERRICK, *neuroanatomist*

# *Introduction*

4

In the second part of the thesis, I will discuss the possible involvement of the fish IPN in the generation of heading representations in the larval zebrafish brain. In this first chapter, I summarize the general properties that are required for a network to represent head orientation, and I discuss theoretical models that have been proposed to recapitulate the essential features of a head-direction representation network. Finally, I briefly introduce the main examples that have been reported so far of networks encoding animal orientation in animals (the rodent heading direction circuit, and the fly central complex), focusing on the features most relevant to the discussion of the results that will be reported in the next chapter.

## 4.1   Navigating gradients and navigating maps

Many organism, from small bacteria to large mammals, have evolved the capability of move through their environment in order to search for resources, flee predators, or find optimal homeostatic conditions. In order to do so, they need to be equipped with suitable navigation strategies to move in the direction that increase - or decrease - the availability of nutrients, the distance from predators, the optimality of temperature, etc. To navigate, organisms might use different strategies. In the simplest case, taxis, they can simply follow a gradient of some external feature of the environment (light, for example, or odors) that has a value for the organism's fitness, to reach points in space where that feature is the highest or the lowest. Alternatively, the animal's brain may represent a map of the environment and the animal's position within it.[1] This cognitive map may then be used by the animal to plan efficiently its movements, and to tie together the neuronal representations of different locations with a topology that correspond to the topology of their arrangement in the real world.

[1] T. Zhang et al., "Endotaxis: A Universal Algorithm for Mapping, Goal-Learning, and Navigation".

## 4.2   Circuits for heading direction

The first block required to build and update a cognitive map of the external environment is a representation of the animal orientation with respect to the external space.[2] Inputs related to changes in the animal location in the environment (efference copies from motor neurons, acceleration-related vestibular inputs, and visual inputs related to optic flow) are all framed in egocentric coordinates (with respect to the animal). For them to come together and inform a representation of the animal location in the environment in allocentric coordinates (with respect to an external fixed point in

[2] Jeffrey S. Taube, "The head direction signal: Origins and sensory-motor integration"; Hulse and Jayaraman, "Mechanisms Underlying the Neural Computation of Head Direction".

space), they need to be linked together through a constant integration of the animal orientation with respect to the environment, which then can be used to also keep track of absolute coordinate changes.

There are four criteria that a network has to satisfy to be considered bearing heading direction representations[3]:

- It has to provide a non-ambiguous read-out of the orientation of the animal with respect to the surrounding environment
- Its activity has to persist in the absence of motion of the animal
- The orientation estimate should be updated based on integration of the angular velocity of the animal/head
- It should be able to integrate external visual cues to anchor the representation and correct drifts.

Networks that satisfy those criteria have successfully been observed in several mammals (rodents, primates, and bats[4]) and insects.[5]

The classical cells involved in this circuit are head-direction neurons (HDNs), neurons that are tuned to a direction of motion of the animal. When the animal is directed toward a particular direction in the environment, the neuron will be highly active, and its firing rate will decrease proportionally to the angular distance of the animal orientation and the preferred angle. The firing of HDNs can be characterized in terms of amplitude of their direction-dependent modulation, and width of their tuning to a specific direction (Figure 4.1).
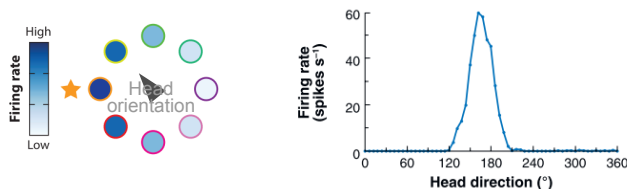


However, neurons related to the representation of direction can also have more complex tuning that still allow to decode the orientation of the animal when the responses are analyzed at the population level[6].

## 4.3    The ring attractor network model

Neural networks fulfilling the computational requirements of the head direction system -uniqueness, persistence, integration- have been proposed to account for the experimental evidence related to head direction neurons.[7] This class of models have been named ring attractor networks. The name evokes the main feature of these models, which is the presence in their $N$-dimensional phase space ($N$ is number of neurons of the network) of a set of stable attractor points organized in a 1-dimensional topological ring. In such networks, each point on the attractor ring represents a direction that can be read out from it, and activity is stable until a - either sensory or motor - input impinges on the network and shifts its activation along the ring.

[3] Green and Maimon, "Building a heading signal from anatomically defined neuron types in the Drosophila central complex"; Hulse and Jayaraman, "Mechanisms Underlying the Neural Computation of Head Direction".

[4] J. S. Taube, R. U. Muller, and Ranck, "Head-direction cells recorded from the postsubiculum in freely moving rats. I. Description and quantitative analysis"; A. Rubin, Yartsev, and Ulanovsky, "Encoding of head direction by hippocampal place cells in bats"; Robertson et al., "Head direction cells in the primate pre-subiculum".
[5] Seelig and Jayaraman, "Neural dynamics for landmark orientation and angular path integration"; Beetz et al., "Flight-induced compass representation in the monarch butterfly heading network".

Figure 4.1: *Left*, Firing rate of a head-direction cell as the animal faces different directions in space. *Right*, The same cell, with firing rate plotted over orientation of the animal. Adapted from Jeffrey S. Taube, "The head direction signal: Origins and sensory-motor integration".

[6] Chaudhuri et al., "The intrinsic attractor manifold and population dynamics of a canonical cognitive circuit across waking and sleep".

[7] K. Zhang, "Representation of spatial orientation by the intrinsic dynamics of the head-direction cell ensemble: A theory"; Angelaki and Laurens, "The head direction cell network: Attractor dynamics, integration within the navigation system, and three-dimensional properties".

Finally, the basin of attraction around the ring ensures that the activation is unique, and persistent.

### Classes of ring attractor models

Two main classes of biophysically plausible ring attractor networks have been proposed[8].

*In models of the first type,*    neurons are arranged in a ring and form strong excitatory connections with their neighbours, and connections with decreasing excitation strength with more distant neurons (Figure 4.2). Moreover, they send excitatory connections with inhibitory neurons that in turn send inhibitory connections to the whole network. Under proper balance of excitatory and inhibitory weights, this network topology allows for the creation of a bump of activity in one position of the ring, that gets self-sustained through the local recurrent excitatory connections (providing persistence); and for the suppression of all the activity that is not localized in the self-sustained bump, thanks to the widespread inhibition.

This model just account for the stabilization and uniqueness of a bump of activity. In order to encode heading direction, it has to incorporate a mechanism to update the position of the bump by using information about angular velocity. To do so, so called *rotation cells* can be added to the model, that receive inputs from both the excitatory ring neurons and angular velocity neurons, and have an asymmetric connectivity, projecting either to neurons on the left, or neurons on the right (Figure 4.3). In this way, when they are activated by the convergence of inputs from the sustained bump and angular velocity signals from outside the network, they produce a clockwise or counterclockwise rotation of the activity bump.

When such network is implemented, then orientation of the animal can be decoded just by looking at the activation of neurons along the ring: each of those cells will have a tuning to one particular orientation in space, and will be activated every time the integration of clockwise and counterclockwise shifts corresponding to left and right turns of the animal lead to the estimation of that specific direction as the animal facing direction.

Finally, landmark inputs can easily be included in the model as cells that send excitatory inputs to one particular location along the ring, hence forcing, when active, the localization of the bump in that position.

*In models of the second type,*    neurons are arranged in a ring, but local recurrent excitatory connections are not required. Instead, either biophysical intrinsic mechanisms or widespread excitatory inputs provide a constant source of activation to all neurons (Figure 4.4). In addition, excitatory neurons provide also driving inputs to inhibitory rotation cells that are connected - with an offset - with cells on the opposite side of the the ring.

## 4.4    Head direction signals in mammals

In mammals, head direction cells have been first reported in the rat postsubiculum. These neurons were recorded while the animal was free to move

[8] Hulse and Jayaraman, "Mechanisms Underlying the Neural Computation of Head Direction".



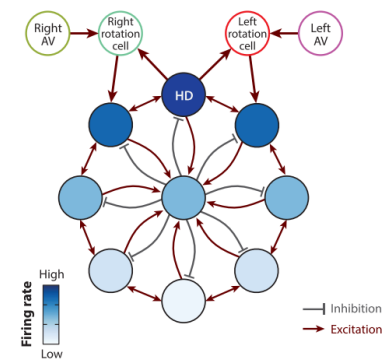Figure 4.2: Connectivity in a ring attractor network of the first type (AV: angular velocity). All the schemes of this chapter are adapted with permission from Hulse and Jayaraman, "Mechanisms Underlying the Neural Computation of Head Direction".
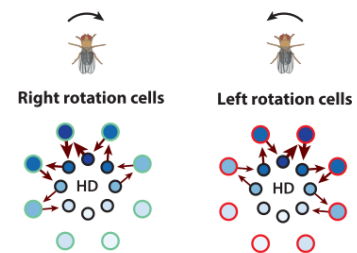


Figure 4.3: Activity rotation in a ring attractor network.
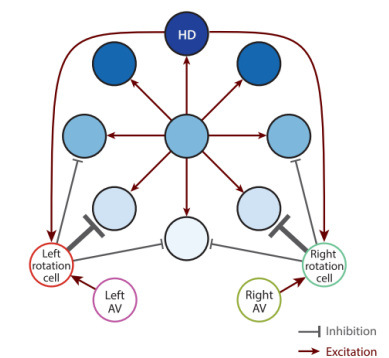


Figure 4.4: Connectivity in a ring attractor network of the second type (AV: angular velocity).

in an arena, and the firing rate of the cells was remarkably tuned to the direction that the animal was facing (Figure 4.5). Since then, many experiments have reported the presence of head-direction cells in many limbic structures within the classic Papez circuit, including the anterior dorsal thalamic nucleus, the mammillary bodies, and the retrosplenial and enthorinal cortex (see Jeffrey S. Taube, "The head direction signal: Origins and sensory-motor integration" for a review). The region where cells in different areas can differ in terms of their tuning width or amplitude, or they can carry mix representation that also include variations in firing rate depending on angular velocity of the animal, or direction of turning. However, in all areas one can observe neurons tuned to all heading directions, suggesting a large degree of redundancy in the head-direction network. Importantly, no topographical organization has ever been reported for head-direction cells in the vertebrate brain.
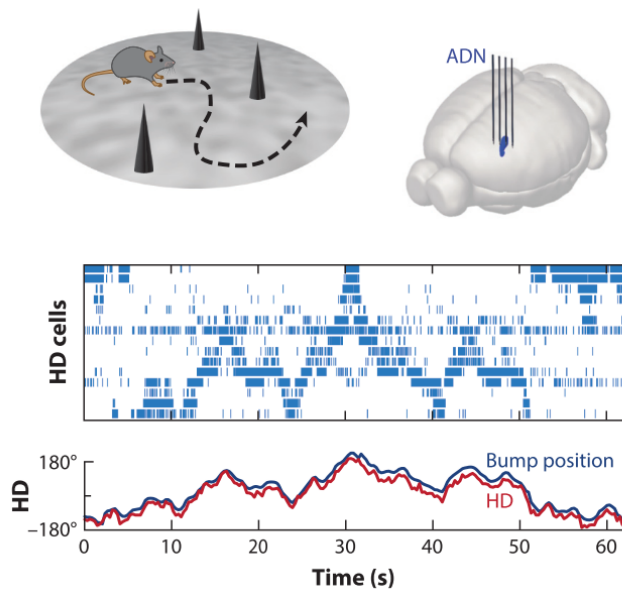


Figure 4.5: As the animal move through the environment (*top, left*), tetrode recordings *top, right* in different brain areas reveal the presence of HDNs; each cell is active when the animal is facing a particular direction, so that the orientation of the animal can be read out from the localization of the activity across the network (*bottom*). ADN: anterior dorsal thalamic nucleus. Adapted from Hulse and Jayaraman, "Mechanisms Underlying the Neural Computation of Head Direction".

*Subcortical generation of head-direction signals*

In rodents, the area where the representation of head orientation is the most prominent is the anterior dorsal thalamus, where up to 60% of neurons are HDN neurons.[9] Upstream of this structure, there are several subcortical structures that seem to contain HDNs (Figure 4.6). Lesion studies and careful analyses of the latencies of head-direction signals in different areas of the vertebrate brain have lead to the hypothesis that the head direction signal is established though a hierarchy of reciprocally connected areas that process angular velocity cues to refine a consistent heading representation[10] (Figure 4.6).

Vestibular inputs and motor efferences both seem to be contributing to the establishment of angular velocity signals in the dorsal tegmental nucleus (DTN). On one hand, lesions of the vestibular system can produce severe impairments of the head direction circuit.[11] On the other, active and passive movements result have different effects on angular velocity cells and HDNs, with passive motion often resulting in decreased or suppressed firing in

[9] Jeffrey S. Taube, "Head direction cells recorded in the anterior thalamic nuclei of freely moving rats".

[10] Jeffrey S. Taube, "The head direction signal: Origins and sensory-motor integration".

[11] Stackman and Jeffrey S. Taube, "Firing properties of head direction cells in the rat anterior thalamic nucleus: Dependence on vestibular input".

HDNs[12]. The integration of self-motion with vestibular inputs could happen already at the level of the vestibular nuclei[13].

## The DTN

Vestibular and motor signals can come together (either converging, or after convergence in vestibular nuclei) in the DTN, that has important connections with vestibular nuclei. In turn, the DTN is bidirectionally connected with the lateral mammillary nucleus, which is one of the main afferents to the anterior dorsal thalamus. Therefore, it seems that the DTN→lateral mammillary nucleus→dorsal thalamus might be the main route through which head direction circuits enter the telencephalon from subcortical areas. Coherent with this view, HDNs have been observed in the DTN, and, as one progressively move in the downstream areas, HDNs become more common and more sharply tuned, hinting that the head direction representation is inherited and refined in those structures, and potentially also integrated with other signals such as visual landmarks[14].

The DTN is a paired GABAergic nucleus located in the anterior hindbrain (it originates from the first rhombomere[15]). The DTN is located dorsally from the IPN, and represents one of the main areas after the habenula that targets and receive fibers from the IPN. HDNs have been observed in the DTN, although they have very broad tuning and they represent only 10% of cells in the nucleus, whose cells are predominantly coding for angular velocity[16]. It is indeed based on its connections with the DTN that a role for the IPN in the in the head direction network has been postulated. In fact, as described in *Navigation and the IPN*, lesions in the IPN and habenula do affect the stability of HDNs found in the thalamic and limbic parts of the circuit[17].

## Head-direction cells form a ring attractor

Although the architecture and connectivity of the mammalian head direction circuit remains poorly understood, several lines of evidence suggest that the network dynamics can be best explained by postulating an attractor network that implements it. The activity of HDNs when the network is disengaged from sensory inputs (either during sleep, or after vestibular regions) remain consistent with the idea of a bump of activity travelling through the network, even if it has lost any relation with the actual orientation of the animal.[18] Although indirect, this evidence suggests that the network is structured in a way that ensure a robust dynamics despite the absence of strong driving inputs. The absence of recurrent excitatory connections between mammillary neurons, as well as the GABAergic nature of the DTN neurons lead to the hypothesis that the mammalian head-direction network might function as a ring attractor of the second type.[19]

In presenting our results later, we will hypothesise that the areas of the anterior hindbrain that we observed as anatomically related to the IPN in larval zebrafish might have some relation with the DTN dorsal tegmental nucleus of mammals (see *Possible analogy between the DTN and the zebrafish aHB*).

[12] Sharp, Tinkelman, and Cho, "Angular velocity and head direction signals recorded from the dorsal tegmental nucleus of gudden in the rat: Implications for path integration in the head direction cell circuit."

[13] Cullen and Jeffrey S. Taube, "Our sense of direction: Progress, controversies and challenges".
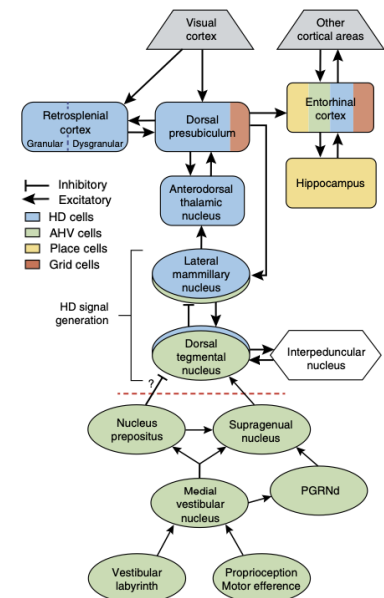
Figure 4.6: Connectivity of head-direction related areas in the mammalian brain.

[14] Jeffrey S. Taube, "The head direction signal: Origins and sensory-motor integration".

[15] Puelles, "Comments on the limits and internal structure of the mammalian midbrain".

[16] Sharp, Tinkelman, and Cho, "Angular velocity and head direction signals recorded from the dorsal tegmental nucleus of gudden in the rat: Implications for path integration in the head direction cell circuit."

[17] Thornton and Davies, "A water-maze discrimination learning deficit in the rat following lesion of the habenula"; Clark and Jeffrey S. Taube, "Deficits in Landmark Navigation and Path Integration After Lesions of the Interpeduncular Nucleus".

[18] Clark and Jeffrey S. Taube, "Vestibular and attractor network basis of the head direction cell signal in subcortical circuits"; Chaudhuri et al., "The intrinsic attractor manifold and population dynamics of a canonical cognitive circuit across waking and sleep".

[19] Hulse and Jayaraman, "Mechanisms Underlying the Neural Computation of Head Direction".

## 4.5    *The* Drosophila *heading direction circuit*

In insects, representations of heading direction can be found in a region of the brain termed the central complex. In particular, activity tuned to heading direction has been observed in a toroidal neuropil structure called the ellipsoid body[20]. The ellipsoid body is covered by the processes of cells, termed EPG neurons. In head-restrained flies moving in a virtual reality arena, activity in the processes of EPG neurons in the ellipsoid body was found to be constantly sustained in one part of the toroid, tiled by the processes of a few EPG cells (Figure 4.7). This activity was propagating clockwise and counterclockwise depending on the left and right turns of the animal. Interestingly, this region had previously been implicated in navigation, as experiments have shown that in insects that perform sophisticated navigation behaviors, the central complex bears representations of the polarization of sun light that can be used by the animal as a compass.[21] In *Drosophila*, where the system has been probed with a variety of different experiments, activity in the ellipsoid body has been shown to integrate visual flow and self-motion cues to drive the bump of activity coherently with the animal orientation.
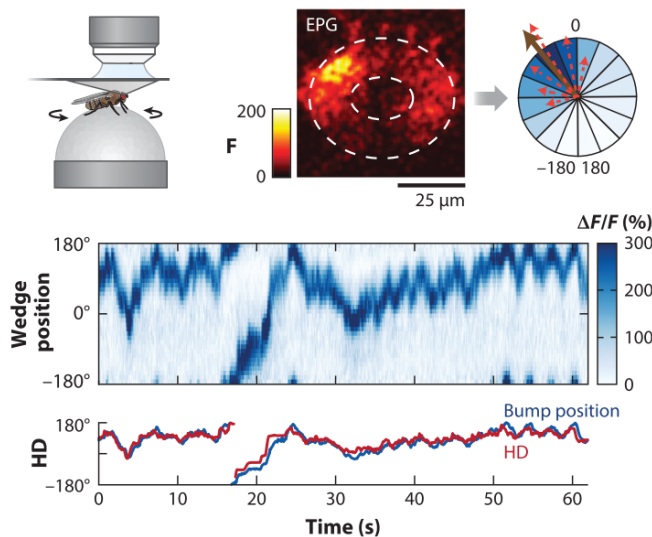
[20] Seelig and Jayaraman, "Neural dynamics for landmark orientation and angular path integration".
Note that the ellipsoid body is only toroidal in flies (diptera), it is an open (non-circular) structure in all other arthropods.

[21] Heinze and Homberg, "Maplike Representation of"; Heinze and Reppert, "Sun compass integration of skylight cues in migratory monarch butterflies".



Figure 4.7: When recording signals in the central complex of a head-tethered fly moving in a virtual reality arena (*top, left*) a bump of activity can be observed propagating across the ring of the ellipsoid body (*top, right*). The position of the activity bump in the ring can be used to read out the (fictive) orientation of the animal in the virtual arena.

### *Generation of heading representations in the fly*

The small dimension of the *Drosophila* head direction system, together with the availability of powerful genetic tools and vast anatomical knowledge from genetic sparse expression dense electron microscopy reconstructions[22], have informed plausible biophysical models that explain with an increasing level of detail the neuronal mechanisms behind the generation of heading representations in the central complex (Figure 4.8). Here I summarize the main principles of organization of the network, as outlined in recent reviews.[23]

EPG cells, whose "dendrites"[24] tile the toroidal ellipsoid body, send an axon that duplicates the heading signal in a glomerulus in a neighbour

[22] Wolff and G. M. Rubin, "Neuroarchitecture of the Drosophila central complex: A catalog of nodulus and asymmetrical body neurons and a revision of the protocerebral bridge catalog"; Hulse, Haberkern, et al., "A connectome of the drosophila central complex reveals network motifs suitable for flexible navigation and context-dependent action selection".

[23] Green and Maimon, "Building a heading signal from anatomically defined neuron types in the Drosophila central complex"; Hulse and Jayaraman, "Mechanisms Underlying the Neural Computation of Head Direction".

[24] In invertebrates, the same processes can host pre- and post-synaptic terminals.

paired structure, the protocerebral bridge (Figure 4.8). The signal is du-
plicated in both the left and the right protocerebral bridge. Sustained ac-
tivity in the dendrites of EPG cells could come from multiple sources. The
first is the presence of both pre and post-synaptic terminals in the ellip-
soid body EPG processes (see note above), which can generate recurrent
activation. Moreover, a neuron type known as PEG, has constituent cells
with dendrites in the protocerebral bridge and axons in the ellipsoid body,
and could therefore act to create a recurrent ellipsoid body-protocerebral
bridge-ellipsoid body loop that ensures the persistence of the local bump
of activity. Finally, intrinsic cellular dynamics and tonic inputs from the
legs could provide additional mechanisms for maintaining tonic activation
of EPG neurons.
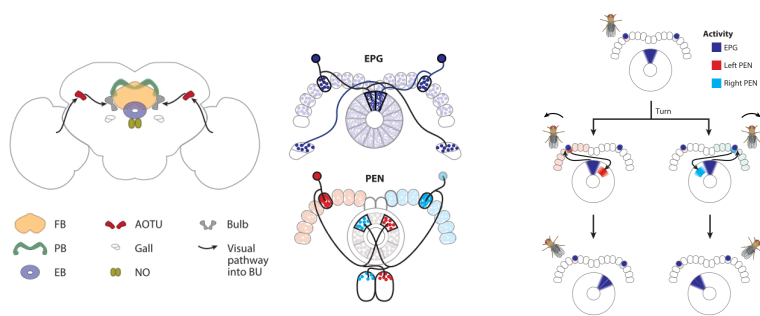


Figure 4.8: *Left*, Organization of the
central complex in the fly brain. *Center*,
Connectivity of EPG and PEN neurons.
*Right*, PENs neurons can act as rotation
cells. Adapted from Jeffrey S. Taube,
"The head direction signal: Origins and
sensory-motor integration".

Signals that are carried to the protocerebral bridge impinge on the den-
drites of a second group of neurons, termed PEN neurons (Figure 4.8). PEN
neurons receive inputs from the EPG cells, and target back the ellipsoid
body, with an offset with respect to the tile that was originally tiled by the
EPG cell (clockwise offset for left PENs, and conter-clockwise offset for right
PENs). In this way, left and right-PENs can act as rotation cells, since their
activity is differentially modulated when the fly is performing left and right
turns.

Inhibitory mechanisms are needed to provide the localization of activity
and ensure uniqueness of the bump position. First, inhibitory population
named Δ7 interneurons in the protocerebral bridge send axons to glomeruli
in the protocerebral bridge with an offset with respect to the glomerulus
where their have the dendrite in. This could provide lateral inhibition to the
neuropil at 180 phase difference with the ongoing bump position. Second,
widespread, global inhibition can come from GABAergic ring cells with an
axon that target the entire torus of the ellipsoid body.

Ring neurons might also play a role in the use of landmarks to inform
heading representations (Figure 4.9). Visual ring neurons that have a small
receptive field in the animal field of view seem to also send projections to
the whole ellipsoid body ring. Anti-hebbian Plasticity at the level of their
synaptic terminals could lead to an negative association between the acti-
vation of the neuron with a localized visual cue and the localization of ac-
tivity in one part of the ring. In this way, that subsequent activation of the
(inhibitory) ring neuron from the visual input can then provide sculpted
inhibition to the network side in antiphase with the preferential, learned
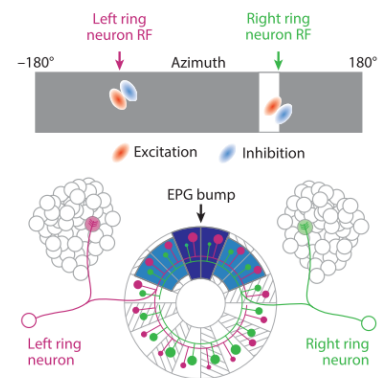


Figure 4.9: *Top*, Receptive field of two
represented ring neurons. *Bottom*, Ring
neuron connectivity with the ellipsoid
body, with synaptic strength (circles
radius) anti-correlated with distance from
the bump when visual stimulus is in the
receptive field.

bump position, and drive the bump toward the associated location.

### *A ring attractor in the* Drosophila *central complex*

Thanks to the amenability of the system to genetic targeting and activity manipulation, attractor dynamics in the fly central complex have been observed in a much more direct way when compared to the vertebrate circuit. Optogenetic manipulation has been used to externally drive activity in the network, proving the existence of a winner-take-all process that ensure uniqueness of the activation bump - interestingly, with a constant amount of excitation required to create a new bump, regardless of the distance from the ongoing activity localization. Overall, the connectivity principles revealed so far in the insect head-direction network seem compatible with the first class of ring attractor networks described, with recurrent, local excitation and widespread inhibition keeping down activity in the rest of the network.

### *From head-direction signals to allocentric travelling direction representations*

in *Drosophila*, recent experiments have shown how the heading direction signals can be used together with optic flow information to generate a representation of the travel vector in an allocentric frame of reference in a structure of the central complex, the fan-shaped body.[25] Similarly to what happens in the protocerebral bridge and ellipsoid body, in the fan shaped body we can find a bump of activity that propagates across a line depending on the heading direction of the animal. However, the bump of activity in the fan-shaped body has an offset with respect to the ellipsoid body representation, that depends on the main direction of perceived optic flow (in an experiment where the animal is tethered and the optic flow is decoupled from the animal's motion). This offset is 0 when the optic flow simulates a forward translation, and decreases/increases up to $-180°/180°$ with shifts in the optic flow angle up to $-180°/180°$ (optic flow simulating a backward translation).

The generation of this signal is a computational process that involves the calculation of a vector sum. A key insight of this work is the demonstration that a sinusoidal bump of activity, as the one found in the fan-shaped body, seems to be ideally suited to perform vector operations. Just by summing convergent inputs from two sinusoidal representations for heading and optic flow the circuit can obtain a vector whose amplitude and phase correspond to the amplitude and phase of the sum of the two correspondent vectors, a principle that might underlie vector operations in other areas and in the brain of different animals. Indeed, we will speculate in the next chapter that the circuit we describe in the larval zebrafish has features that suggest it might rely on similar mechanisms to integrate heading direction information with other vector representations (see *A heading-direction network in the fish aHB*).

[25] Lyu, Abbott, and Maimon, "Building an allocentric travelling direction signal via vector computation".

## 4.6    Spatial cognition in teleost fish

To the observations of head-direction cells in mammals and insects in neuronal recordings from the animal brain, correspond the reporting of behaviors that rely on an internal sense of direction for both mammals and insects. This leaves open a fundamental question: do zebrafish show any sign of behaviorally relying on a representation of external space, and not just attraction or repulsion from environmental attractants and repellers? And do zebrafish larvae also use such representations?

In natural environments, teleost fishes can display sophisticated spatial navigation and orientation skills. Some can perform migratory behaviors over wide geographical scales, and can use multisensory cues to orient and navigate to their territory.[26] In an experimental setting, fish, including zebrafish, can learn spatial memory tasks where they use distant landmarks in a room to navigate to a specific site of a rectangular or plus-maze for a reward (such as the presence of a conspecific).[27] Interestingly, they can also learn a more advanced task where instead of directing toward a specific location, they have to always turn left or right in the plus maze, a task that seems to require an intact IPN.[28]

Zebrafish larvae display a significantly limited range of behaviors,[29] and a paradigm that proves the usage of spatial-related representations in the zebrafish larve has not been described yet. However, there is some support for the idea that, even in the absence of explicit spatial information, the swimming larvae keep track of the current direction of swimming. A virtual phototaxis assay has been described, where the light is switched off when the fish crosses an arbitrary boundary of the arena.[30] When the larvae pass the boundary and the light is switched off, they are then able to turn back to the area that keeps the light on with a bout that is correctly oriented toward the (invisible) boundary, suggesting that they somehow store information about their current orientation with respect to the virtual boundary.

In the next chapter, we will raise the intriguing hypothesis that heading-direction neurons could exist also in the larval zebrafish, and that the circuits involved in their generation might be conserved across vertebrates.

[26] Rodríguez et al., "Spatial cognition in teleost fish: Strategies and mechanisms".

[27] Baratti, Potrich, and Sovrano, "The Environmental Geometry in Spatial Learning by Zebrafish (Danio rerio)"; Vargas et al., "Encoding of geometric and featural spatial information by goldfish (Carassius auratus)".
[28] Cherng et al., "The Dorsal Lateral Habenula-Interpeduncular Nucleus Pathway Is Essential for Left-Right-Dependent Decision Making in Zebrafish".
[29] Orger and De Polavieja, "Zebrafish Behavior: Opportunities and Challenges".

[30] X. Chen and Engert, "Navigational strategies underlying phototaxis in larval zebrafish".

# 5

## Results and discussion

ORIENTATION IN THE ENVIRONMENT is represented by head direction cells, neurons that are active any time the animal faces a particular direction in space. Head direction cells were originally described in the postsubicular cortex, but have since been observed in several other cortical and subcortical areas[1]. The lowest region of the brain where head-direction related signals have been found is the DTN[2], a paired, GABAergic nucleus located in the brainstem that originates from rhombomere 1[3].

In the larval zebrafish, two prominent groups of GABAergic nuclei can be observed in the aHB at the level of the first rhombomere at 7 dpf. Although representations of optic flow and directional swimming behavior have been described in the fish aHB[4], the function of this brain region in the larval zebrafish is still poorly understood.

Here, I report some observations on the activity of a population of GABAergic cells in the larval zebrafish aHB that indicate their involvement in the heading direction system. Past directional motion is encoded in the position of a bump of activity that translates across the population, as predicted by ring attractor models of head direction networks[5]. Overall, the dynamics of the circuit is largely compatible with the requirements that a circuit needs to fulfill to represent heading direction. Finally I will show, using electron microscopy, that neurons in the aHB form highly organized reciprocal connections in the dorsal IPN, and I will propose a connectivity scheme that might underlie the implementation of a ring attractor network. These data represent the first demonstration of an anatomically organized heading direction circuit in a vertebrate brain.

### 5.1 A population of cells with ring attractor dynamics in the fish aHB

Starting from the observation that neurons in the aHB project fibers in the IPN, we decided to perform volumetric lightsheet imaging in 7 dpf to 9 dpf zebrafish larvae expressing GCaMP6s in GABAergic neurons in the aHB (Figure 5.1). The GABAergic line we used shows prominent expression in the dorsal part of the IPN, suggesting that the population of aHB neurons that express GCaMP are indeed the ones that project to the IPN from this region (see *aHB neurons arborize in the dorsal IPN*).

Larvae were head-restrained but free to move their tail, and were imaged either in darkness or while presented with a visual stimulus in either closed or open-loop (see *Visual stimuli*).

[1] Jeffrey S. Taube, "The head direction signal: Origins and sensory-motor integration".

[2] Sharp, Tinkelman, and Cho, "Angular velocity and head direction signals recorded from the dorsal tegmental nucleus of gudden in the rat: Implications for path integration in the head direction cell circuit."

[3] Puelles, "Comments on the limits and internal structure of the mammalian midbrain".

[4] X. Chen, Mu, et al., "Brainwide Organization of Neuronal Activity and Convergent Sensorimotor Transformations in Larval Zebrafish"; Dragomir, Štih, and Portugues, "Evidence accumulation during a sensorimotor decision task revealed by whole-brain imaging"; Bahl and Engert, "Neural circuits for evidence accumulation and decision making in larval zebrafish."

[5] Skaggs et al., "A model of the neural basis of the rat's sense of direction."; K. Zhang, "Representation of spatial orientation by the intrinsic dynamics of the head-direction cell ensemble: A theory".
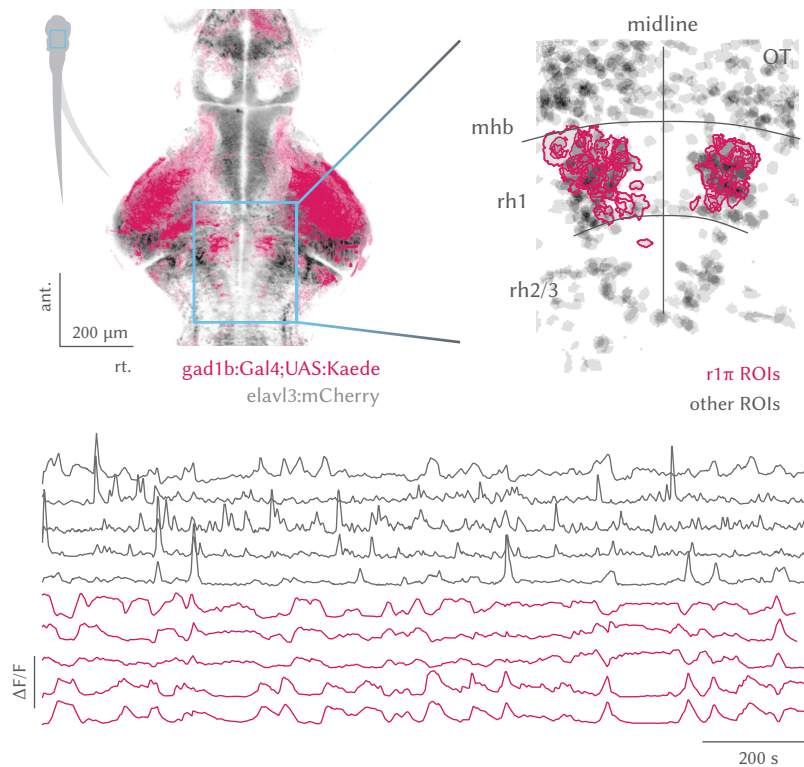
Figure 5.1: *Top, left*, Expression pattern of the *Tg(gad1b:Gal4)* line over a brain reference. *Top, right*, Example view from an imaging experiment. r1π ROIs are highlighted in pink over the shades of all ROIs from the experiment (OT: *optic tectum*, mhb: *midbrain/hindbrain boundary*, rh: *rhombomere*). *Bottom*, Example traces from one experiment.

We observed a population of 50-100 neurons (median = 74, Q1 = 48, Q3 = 115, n = 31 fish) with a peculiar dynamics. Their activity was biphasic, with sustained activation lasting tens of seconds or minutes. Moreover, activity in pairs of neurons was strongly anti-correlated (Figure 5.1).

When looking at the raw imaging data, a sustained bump of activity could be observed, propagating either clockwise or counterclockwise across the network in a horizontal plane (Figure 5.2, Movie 1 showing a sped-up example recording).



Movie 1: https://doi.org/10.6084/m9.figshare.17871875
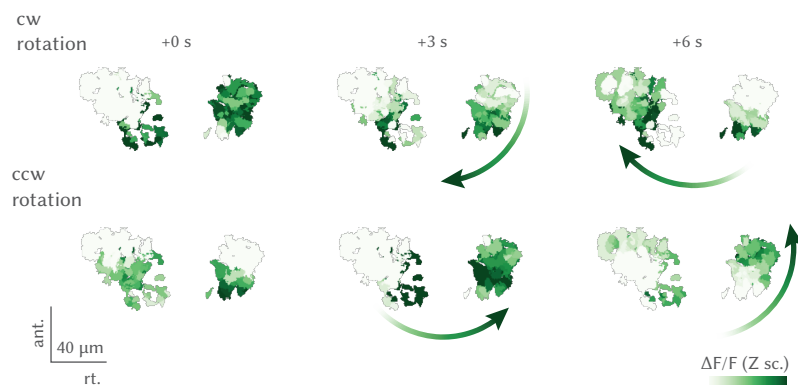


Figure 5.2: Circular propagation of activity. Intensity of fluorescence for all ROIs in the course of a *top*, clock-wise and *bottom*, counterclockwise propagation event. The arrow shows the direction of activity propagation.

These GABAergic neurons could be parsed out from the imaging data by filtering ROIs based on their anticorrelation (see *Detecting r1π neurons*). When looking at their anatomical distribution, they were consistently located in rhombomere 1 across fish (Figure 5.3). For this reason, the oppo-

nent nature of their activity, and their anatomical configuration (see later), we decided to name them *π-neurons of the first rhombomere*, **r1π**.
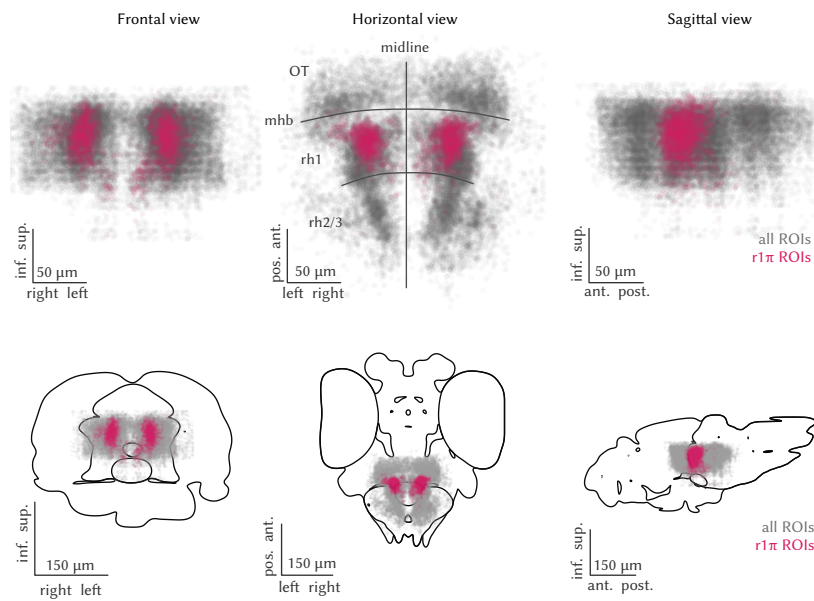


Figure 5.3:
*Top*, Horizontal and sagittal views for the r1π neurons in the imaging experiments registered in a common anatomical space (pink), visualized together with all the ROIs extracted from the same experiments (gray). OT: optic tectum, mhb: midbrain/hindbrain boundary, rh: rhombomere. *Bottom*, The same views for coordinates, now registered on the mapzebrain atlas.

## Rotatory dynamics in phase space

In order to further characterize the dynamics of the network, we performed principal component analysis (PCA) to observe the population dynamics in a space with reduced dimensionality. We observed that the first two PC captured over 80% of the variance (median = 0.800, Q1 = 0.770, Q3 = 0.836, n = 31 fish) (Figure 5.4). When projected over those first two components, the network trajectory was constrained to a circle over the whole duration of the experiment, which lasted tens of minutes (Figure 5.4). For their location in rhombomere 1, the fact that they have an anticorrelated partner at a πangle on the PC space, and based on their morphological features described in a later section of the paper, we call those cells **r1π neurons**.
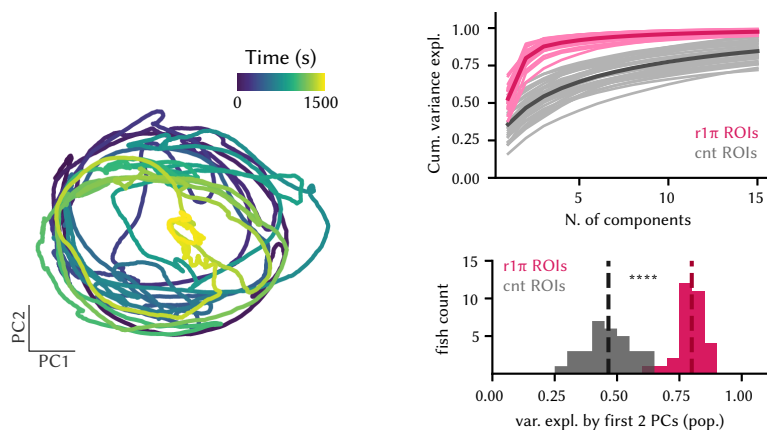


Figure 5.4: *Left*, Trajectory in 2D PCs phase space of the network, color-coded by time. *Right, top*, Cumulative relative variance explained by the first 15 principal components from PCA decomposition over population for r1π neurons (purple) and a population of randomly drawn neurons from the same imaging experiments matching in number the r1π neurons. *Right, bottom*, Variance explained by the first two PCs.

*Anatomical organization of r1π neurons*

To address how the activity of r1π neurons and their anatomical location was related, we performed a different PCA analysis. This time, we looked for a change of axes to reduce the *N*-dimensional array corresponding to activity in *N* time points of each neuron to a reduced number of dimensions over which to project the activity pattern of each neuron. As it was the case in the first PC decomposition, the first two principal components were capturing a high fraction of the variance. (variance explained: median = 0.858, Q1 = 0.827, Q3 = 0.868, n = 31 fish) (Figure 5.5).

When projected over the first two principal components, r1π neurons were organized in a circle. This was the case consistently for many animals. This representation is consistent with the observed pattern of activity: neurons that are neighbors in this projection are similar to each other in their activation pattern; neurons on the opposite sides of the circle are neurons that are anti-correlated with each other.
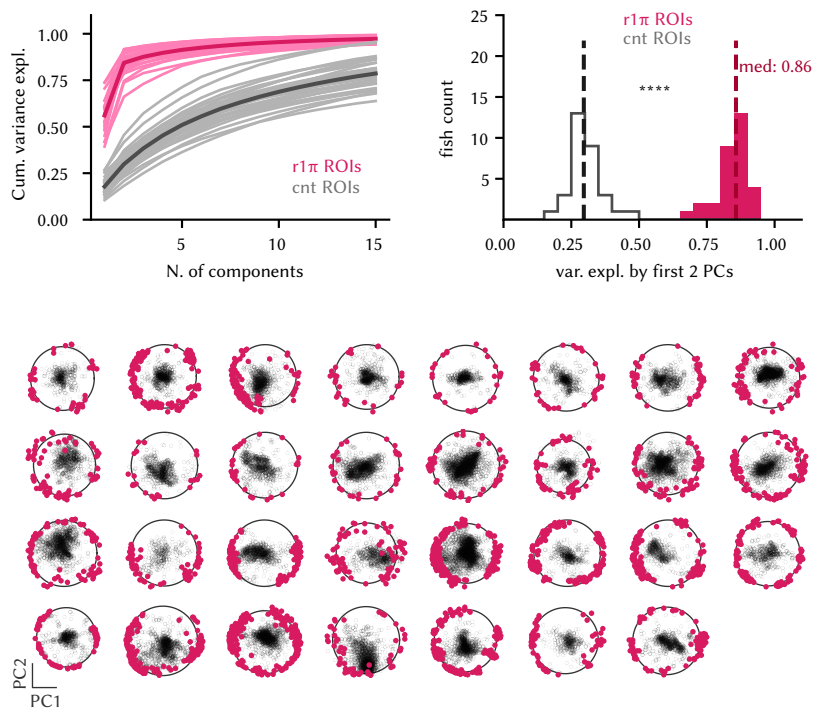


Figure 5.5: *Top*, Cumulative relative variance explained by the first 15 principal components from PCA decomposition over population for r1π neurons and a population of randomly drawn neurons from the same experiments, and variance explained by the first two PCs. *Bottom*, Projections over first two principal components calculated over the r1π neurons (in pink) of all neurons (in gray) for each fish, for all fish in the dataset.

Since we have observed activity propagating across the network, we can predict that anatomical organization of ROIs correlate with their position in the circle. This was indeed the case: the neuron's angle on the circle $\alpha$, correlated with the neuron's anatomical location (Fisher-Lee circular correlation $\rho_t$: median = 0.549, Q1 = 0.298, Q3 = 0.696, n = 31 fish) (Figure 5.6, *top*).

To visualize this correspondence across fish, we devised a procedure to register PC projections across fish (see *Rotated principal component calculation*). After this rotation, the correspondence between angle in PC space (rPC after the registration) is very evident (Figure 5.6, *bottom*). The only exception to this remarkable organization was in the caudal part of the re-
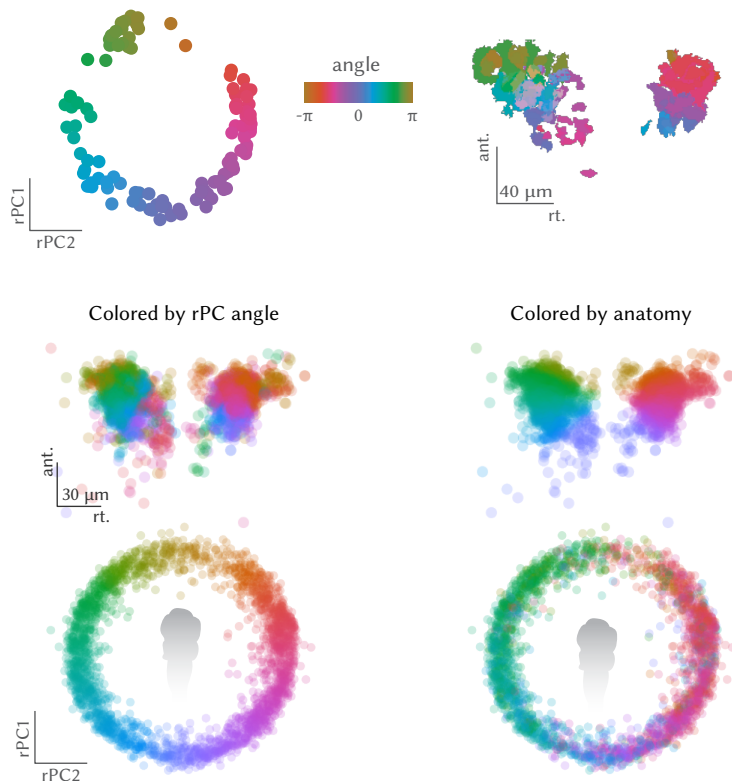
Figure 5.6: *Top, left*, Projection over the first 2 rotated principal components (rPCs) in time of all neurons for a fish color-coded by their angle, α.*Top, left Left*, Projection over the first 2 rPCs in time of all the r1π neurons, color-coded by angle around the circle (for rPC calculation, see *Rotated principal component calculation*, and Figure 6.4). *Right*, Anatomical distribution of the same neurons, color-coded by angle in rPC space.

gion, where sometimes ROIs were more correlated with the activity in the contralateral side (note the colors of the caudal ROIs in Figure 5.6, *bottom, left*).

We conclude that the circular dynamics we had previously observed in phase space can be seen to correspond to an anatomical circle.

## *Defining a phase for the r1π network*

In order to describe the position of the bump of activity within the network at any instance in time, we defined an instantaneous network phase $\phi(t)$ as the average over neurons of their angle $\alpha$ defined above, weighted by their activity at time $t$ (Figure 6.7 and Movie 2). For a full description of the procedure, see *Network phase calculation*. We anchored $\phi$ by setting it to be 0 when the posterior part of the r1π was active, and to increase with clockwise rotations of activity in the horizontal plane (see *Rotated principal component calculation*).

This network phase $\phi(t)$ roughly corresponded to the angle of the network state over time in the circular space (Figure 5.7).

At this point, we used the computed angle $\alpha$, for each neuron to sort the traces for all neurons. In this plot, we can observe a bump of activity gradually translating across the network (Figure 5.8 and Figure 5.9). This visualization show an activity pattern very similar to what can be observed in the ellipsoid body of *Drosophila*, after the wedges have been linearized (see Figure 4.7). The computed phase of the network tracks at each time point the position of the peak of activation across the network.

Movie 2: https://doi.org/10.6084/m9.figshare.17871941
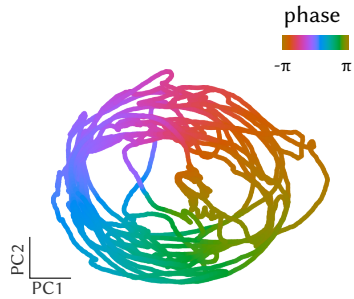
Figure 5.7: Trajectory of the network in PCA-reduced phase space, color-coded by the network phase.
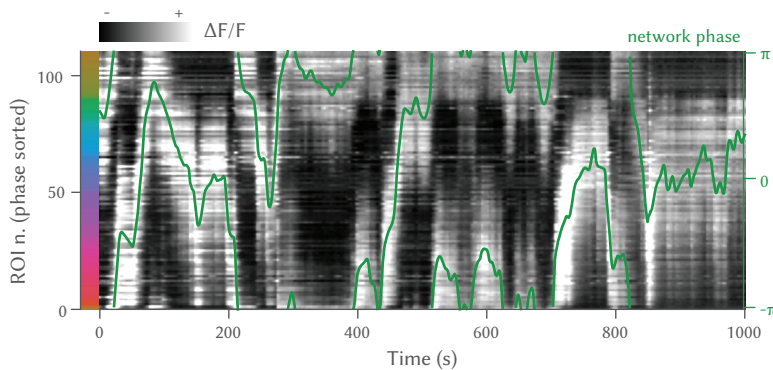


Figure 5.8: Traces of r1π neurons, sorted by angle in PC space for the neurons, and phase of the network (green line).

*Average profile of network activation and phase tuning curves*

To further characterize how individual neurons contributed to the network activity, we computed the average over time of the network activity profile (see *Calculation of average activity profile*, Figure 6.9), to get an idea of how wide was the excitation bump that was translating across the network. To compute this average, we devised a phase-zeroing procedure combined with an interpolation over putative missing neurons of the network (see *Calculation of average activity profile*).

We observed that the average activity profile was close to a sine wave, with a full width at half maximum (FWHM) of approximately $\pi$ (mean = 2.910 ± 0.115 rad, n = 31 fish) over the circle of neurons (Figure 5.10). This was not an artefact of the interpolation procedure used, as the observation was consistent even without resampling activity around the circle (Figure 6.9, right).

When looking at the tuning curves of individual neurons over network phase, they had an approximately sinusoidal shape, with FWHM of ≈ $\pi$ (Figure 5.11). As expected, neurons in different anatomical positions had tuning curves whose peaks were at different phase values. This profile is consistent with the average profile of activation across the network that is shown in Figure 5.10

## 5.2 *The aHB r1π network integrates heading direction*

We next investigated what was driving changes in the phase of the network. We observed that phase was stable in epochs when the fish was not moving, and was changing the most during sequences of left or right swims (Figure 5.12).

When looking at trajectory in the phase space, sequences of left- or right-
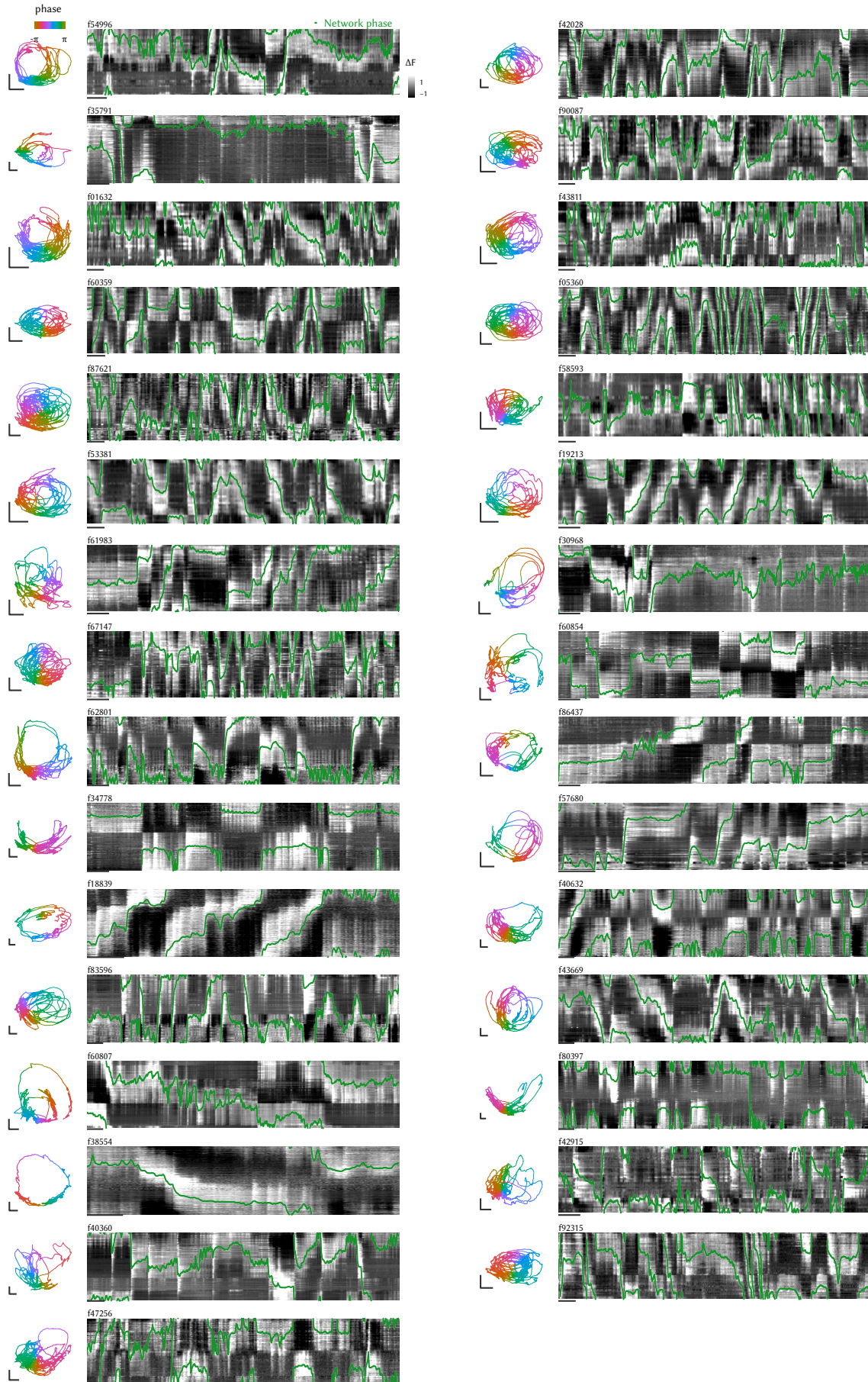
Figure 5.9: Summary plot for all fish. Raw data showing for each fish of the dataset the trajectory of the network in PC space over the entire duration of the experiment color-coded by network phase (panel on the left), and the raw traces of r1π neurons sorted by neuron angle $\alpha$ and network phase in green. The scale bar in the phase space has length of 5, and the bar below the traces indicates 100 s.
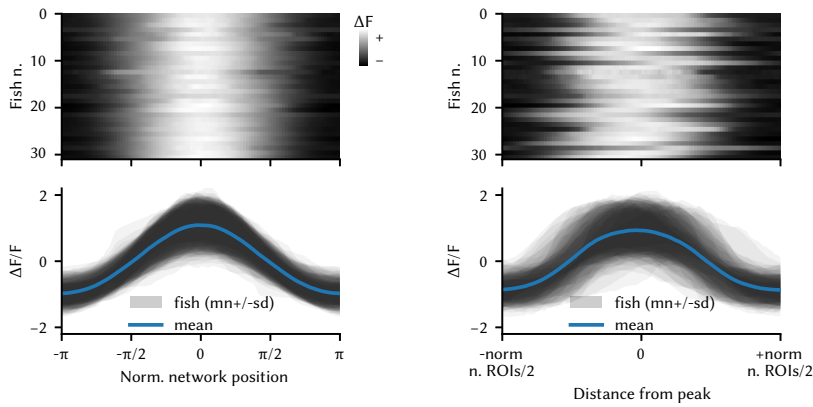
Figure 5.10: Network activity profile. *Left*, Average activation profile for all fish in the dataset (n = 31 fish). *Top*, Matrix showing the average activation profile for all fish in the dataset and *bottom*, mean ±std over time for each fish (shaded areas) and population average (blue). *Right*, Same plots, computed by phase-zeroing in the traces matrix without interpolation (see *Calculation of average activity profile*).
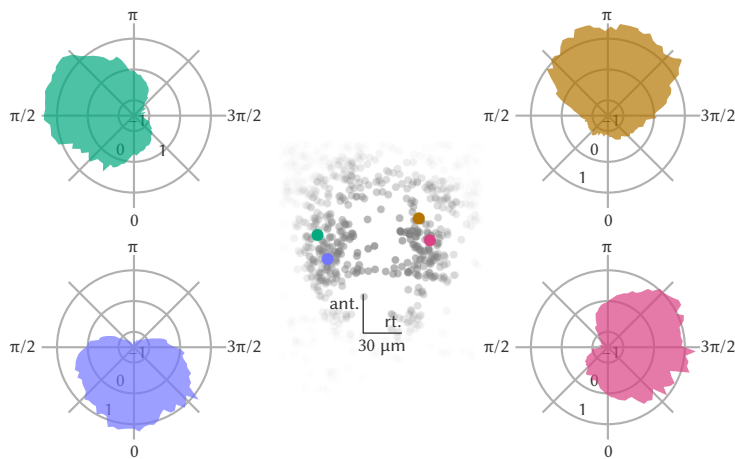


Figure 5.11: Polar plots showing tuning curves of individual neuron activations as a function of network phase from one fish. Each panel shows the curve for a neuron, color coded by their angle $\alpha$. The anatomical locations of the four neurons are represented in the central inset.
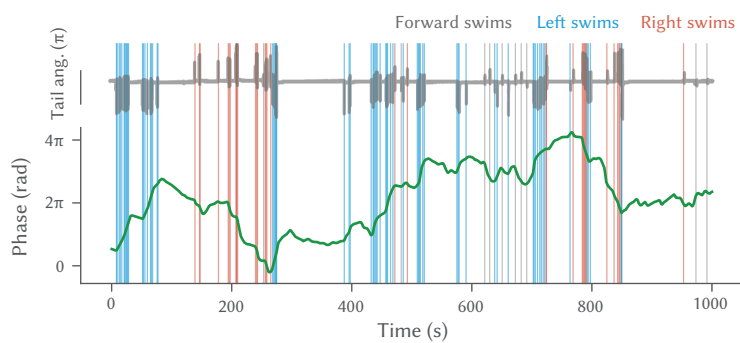


Figure 5.12: Network phase and motor activity. *Top*, Tail angle over time (gray line). Vertical lines mark the occurrence of swims. *Bottom*, Unwrapped network phase (green line) over time.

turns were accompanied by clockwise or counterclockwise rotations along the circular manifold. Crucially, this was happening irrespective of the starting phase position (Figure 5.13).
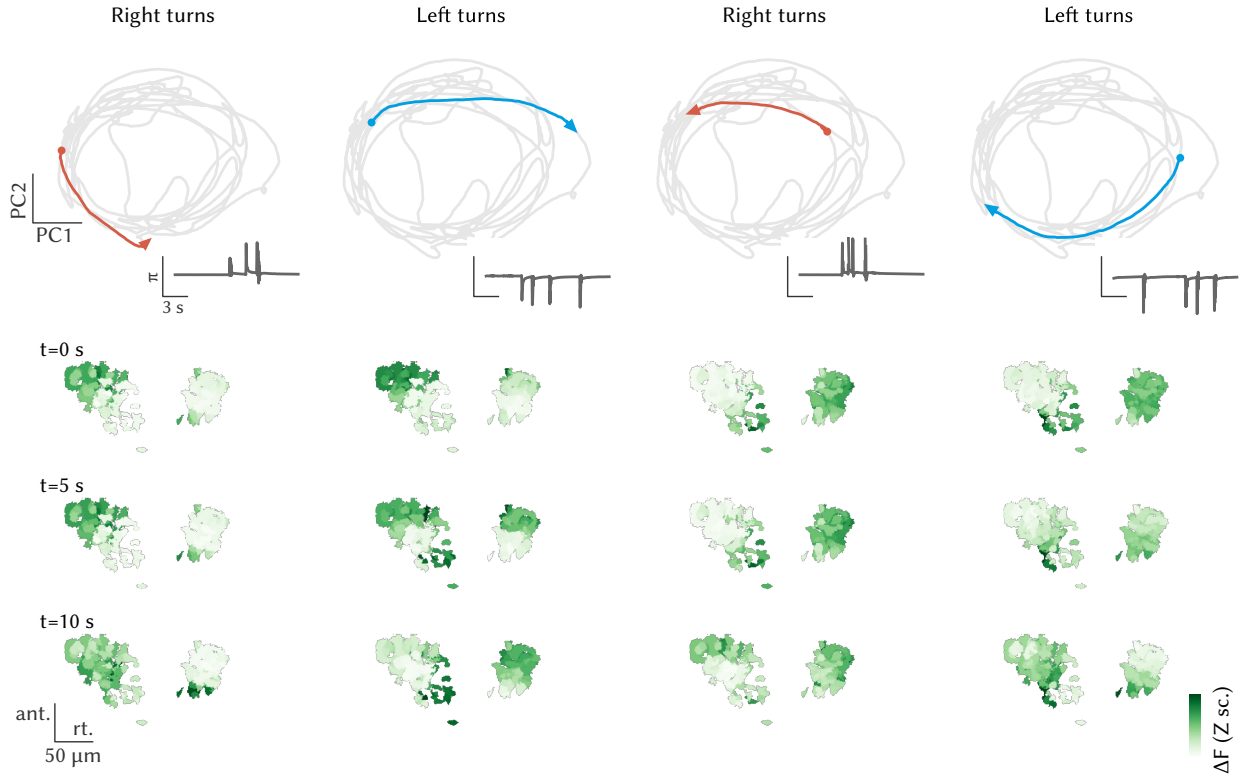


Figure 5.13: *Left*, Network trajectory during sequences of left and right swims. *Top*, Trajectory in phase space during a sequence of left swims (see tail angle in the insert). *Bottom*, State of activation of the network before and after the sequence. *Center-left*, The same plots for a sequence of right swims. *Center-right, right*, The same plots for two sequences of left and right swims that occurred when the network was at a different state.

As we have shown in Figure 5.7, such rotations along the circular manifold in rPC space correspond to increments and decrements of the network phase that we defined above. Therefore, to quantify the amount of rotation that is triggered by each swim, we computed a swim-triggered change in phase. First, we can notice that the bout-triggered change in phase is consistently increasing or decreasing after left and right swims (Figure 5.14). Left swims (that is to say, counterclockwise rotations of the fish) would produce clockwise rotations in the network, and right swims (clockwise rotations of the fish) would produce counterclockwise rotations in the network. There-
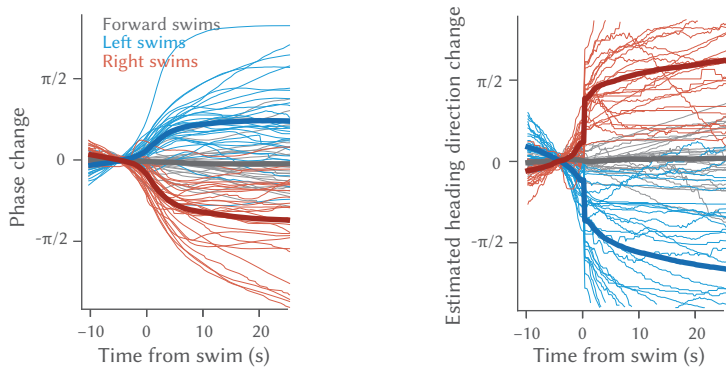


Figure 5.14: *Left*, Swim-triggered average change in network phase for all fish (thin lines, n = 31 fish) and their average (thick lines). *Right*, changes in (estimated) heading direction, triggered on the same swims.

fore, as in the *Drosophila* ellipsoid body, the direction of rotation of the bump in the anatomical space is opposite to the direction of rotation of the animal. As predicted by this model, forward swims did not produce any consistent change in the network phase.

Oscillatory activity with left/right bistability in (a more caudal region of) the larval zebrafish hindbrain has been reported to increase probability of left and right swims and guide the direction of turning of the fish. It was therefore important to control whether the actual phase of the network (and not at its bout-triggered changes) had or not any correlation with the direction of the fish swim. We found that there was no effect of the network phase over the direction of the generated swims: the probability for the network phase to be in any state between $-\pi$ and $\pi$ when a swim occurred was flat for left, right, and forward swims (Figure 5.15). This indicates that the absolute/instantaneous network phase does not correlate with specific behavioral outputs, and suggest that the neuronal activity in the network does not directly drive any directional behavior.
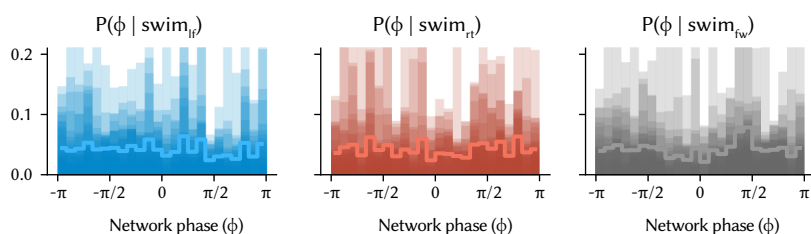


Figure 5.15: Probability of network phase given that a forward, left, or right swim occurred (shaded areas: individual fish; line: population average, n = 31 fish). The distribution is flat, suggesting that the network phase is not instructive with respect to the direction of swimming.

Another crucial observation can be made on the swim-triggered changes in network phase (Figure 5.14). The amount of angular change elicited by a single swim after 10 s was approximately $\pi/4$ (median = 0.828 rad, Q1 = 0.492, Q3 = 1.28, n = 31 fish). This value is comparable in size to the angle turned by a swim performed by a freely swimming fish[6]. Moreover, continuous turning in one direction resulted in several rotations around the network (Figure 5.16). This observation corroborates the idea that the network dynamics indeed lies on a topologically circular manifold, and confirm that it is ideally suited to integrate directional motion to compute a representation of heading direction, for which a $2\pi$ angular motion would result in an identical faced direction.

[6] Huang et al., "Spinal projection neurons control turning behaviors in zebrafish".
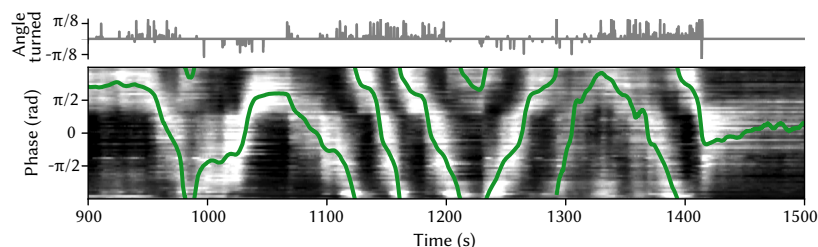


Figure 5.16: Example of clockwise and clockwise shifts traversing multiple times the entire network during sequences of repeated directional swims.

We therefore hypothesized that the network could work as a heading direction integrator, shifting the position of its activity with every turn and keeping track of the heading direction of the animal in allocentric coordinates.

*Estimating heading direction from r1π neurons activity*

To understand to which degree the network could produce an estimate of heading direction over time, we reconstructed a fictive heading direction for the head-embedded fish integrating the angle turned by each swim over time (see *Estimated heading calculation and correlation with phase*, Figure 6.10). This reconstructed heading direction and the network phase were significantly anticorrelated over a period of minutes (Figure 5.17).
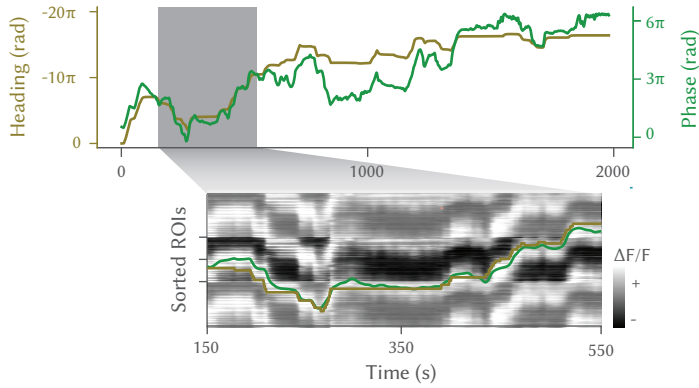


Figure 5.17: *Top*, Network phase (green line) and estimated fish heading (golden line) for the entire duration of an experiment. Note that the axes are different, and have opposite signs. *Bottom*, The enlargement shows the same traces, overlaid on the traces from the r1π neurons, tiled to match the phase unwrapping.

Although some errors accumulated over time (due to drifts or long sequences of very vigorous motion events and struggles) around each time point the phase in the network could be used to read out an estimate of the current heading direction (Figure 5.17, enlargement). In fact, the two were significantly anticorrelated (correlation r: median = −0.723, Q1 = −0.863, Q3 = −0.564, n = 31 fish) (Figure 5.18).
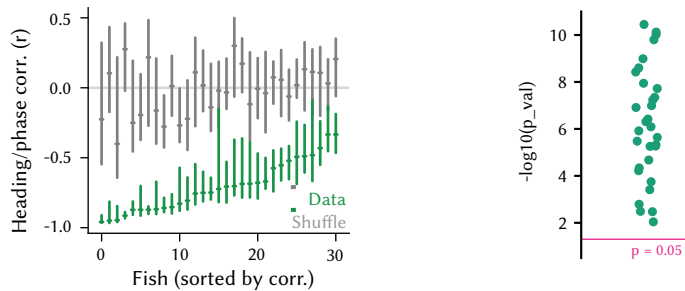


Figure 5.18: *Left*, Correlation of heading and network phase for all fish in the dataset, compared with a shuffle of the same data. Bars report median and first and third quartile for the data (green) and a shuffle (gray). *Right*, Distribution of p values from the comparison of correlation of phase and heading in chunks of 5 min in the data and a shuffle (Wilcoxon test, < 0.01 for all fish). n = 31 fish.

## 5.3 The aHB ring attractor network is not affected by visual inputs

Next, we asked whether sensory inputs are required for the observed heading direction integration. As our preparation was head restrained (Figure 5.19, Figure 6.1), we could ascertain that vestibular sensory inputs were not required, even though these are known to contribute to the mammalian heading direction system[7].

In our experiments, we observed the integration of heading direction in both complete darkness and in open-loop (without visual reafference) (Fig-

[7] Yoder and Jeffrey S. Taube, "The vestibular contribution to the head direction signal and navigation".
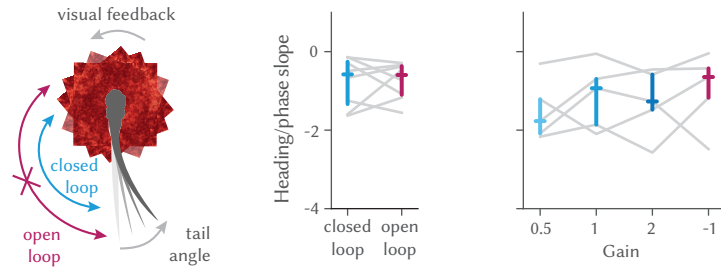
ure 5.19), indicating that visual feedback is not required for a stable heading direction representation.

Furthermore, we tested closed-loop experiments with a range of gains that provided different amounts of visual feedback. In these experiments, we observed no relationship between the representation of heading direction and the experimental gain (Figure 5.19, right). This shows that visual feedback not only is not required, but that it does not contribute to the activity we describe. These observations suggest that efference copies are the main drivers of the activity we observe.

### Neurons of rhombomeres 2/3 might provide efference copy inputs

Interestingly, the activity of left and right GABAergic clusters in rhombomeres 2 and 3, immediately caudal to the r1$\pi$ neurons, show a remarkable degree of correlation with leftward and rightward swims, respectively (Figure 5.21). This population did not overlap almost at all the population of r1$\pi$ neurons, whose correlation with motor activity was much smaller because of their intrinsically slower dynamics (Figure 5.20). We speculate that those caudal neurons might be part of a network that provide motor efference-related inputs to the r1$\pi$ network.
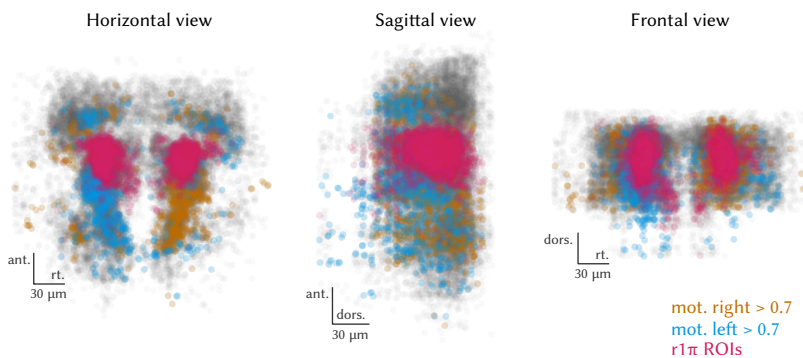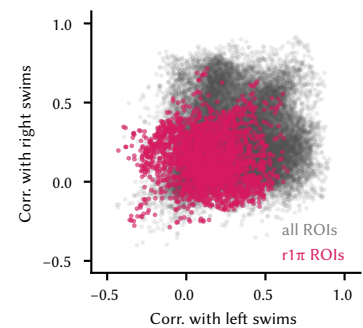


Figure 5.20: Correlations of all ROIs and r1$\pi$ ROIs with left and right swims regressors.



Figure 5.21: Horizontal, sagittal and frontal view showing all ROIs that have a correlation > 0.7 with a regressor for swims in one direction and < 0.7 with the regressor for swims to the opposite side (blue: left swims; golden: right swims), and their relative position with respect to r1$\pi$ neurons, in purple.

## 5.4    The aHB r1$\pi$ network is modulated by eye movements

Subpopulations of cells in the aHB are known to represent eye-related variables such as eye position and saccade timing[8]. We therefore decided to understand whether eye motion could also modulate the phase of the network.

To this end, we freed the eyes of the larvae in a subset of experiments

[8] Ramirez and Aksay, "Ramp-to-threshold dynamics in a hindbrain population controls the timing of spontaneous saccades".
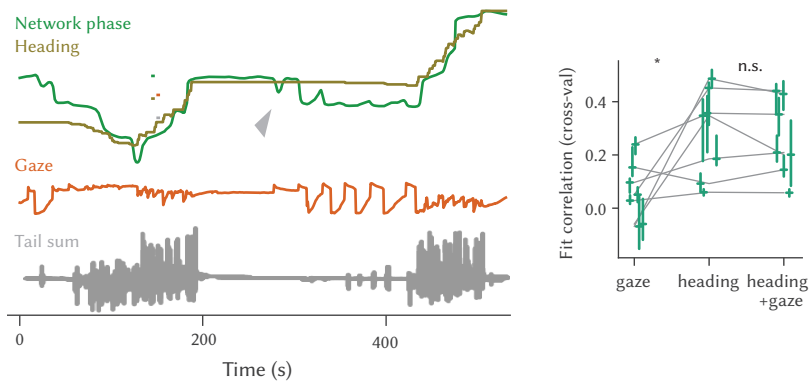
Figure 5.22: *Left*, Network phase (green) represented with (flipped) heading direction (golden) and gaze direction (orange). The arrow highlights a period of low swimming and large saccades. *Right*, Correlation of the reconstructed test phase and the actual phase when the prediction was performed using only the gaze information, using only the heading information, or a combination of both (gaze: median = 0.0507, $Q_1 = -0.0155$, $Q_3 = 0.125$, n = 7 fish); (heading: median = 0.348, $Q_1 = 0.139$, $Q_3 = 0.404$, n = 7 fish); (gaze + heading: median = 0.209, $Q_1 = 0.173$, $Q_3 = 0.391$, n = 7 fish). Comparisons: Wilcoxon test, n = 7 fish.

and tracked their motion together with that of the tail. In periods where swimming was absent, we observed that eye motion could explain some low amplitude modulation in the network phase, although eye motion on its own did poorly compared to heading direction when swimming did occur (Figure 5.22).

However, overall r1π neurons were not the most eye-modulated neurons in the network. Instead, a more caudal population appears to be more correlated with clockwise and counterclockwise rotations of the eyes (Figure 5.23).
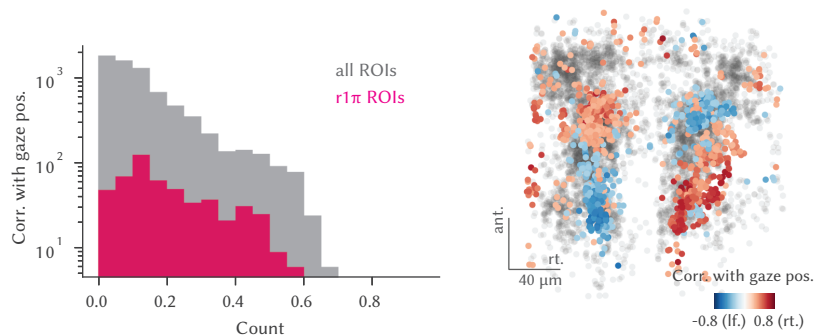


Figure 5.23: *Left*, Histogram of the correlation of r1π neurons with a gaze position regressor, compared with the distribution obtained from all ROIs. *Right*, Anatomical view (horizontal projection) of the correlation values of neurons with a gaze position regressor.
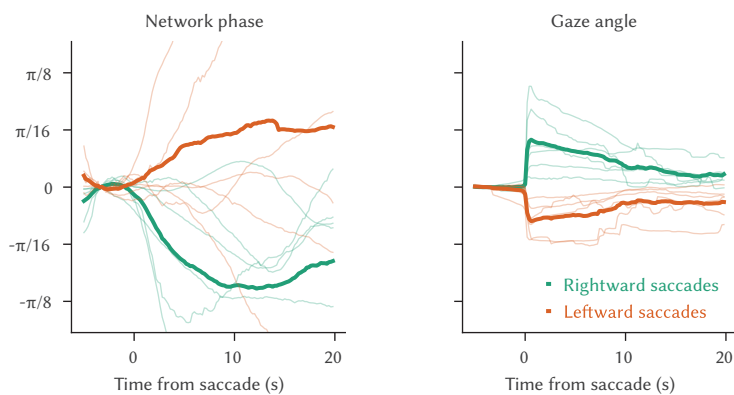


Figure 5.24: *Left*, Saccade-triggered phase changes in the network, and *right*, gaze deflections for rightward (green) and leftward (orange) saccades.

Interestingly, the sign of the modulation was consistent with the heading changes. Leftward saccades increased the network phase as leftward swims do, and rightward saccades decreasing it as rightward swims do (Fig-

ure 5.24). This raises the intriguing possibility that gaze-related inputs refine the representation of the heading direction.

## 5.5    aHB neurons arborize in the dorsal IPN

As discussed in the first part of the thesis, a population of neurons with the soma in the aHB was found to send axons and dentrites toward the IPN. To understand whether those neurons might be the same from which we were recording heading-related activity, we proceeded to investigate the anatomy of neurons in the fish line we were using for targeting cells in the aHB. Anatomical stacks of the GABAergic line we used show a prominent, bilaterally-paired, tract of fibers that extended ventro-medially from the GABAergic nuclei of rhombomere 1 towards the interpeduncular nucleus (IPN) (Figure 5.25 - red arrow).
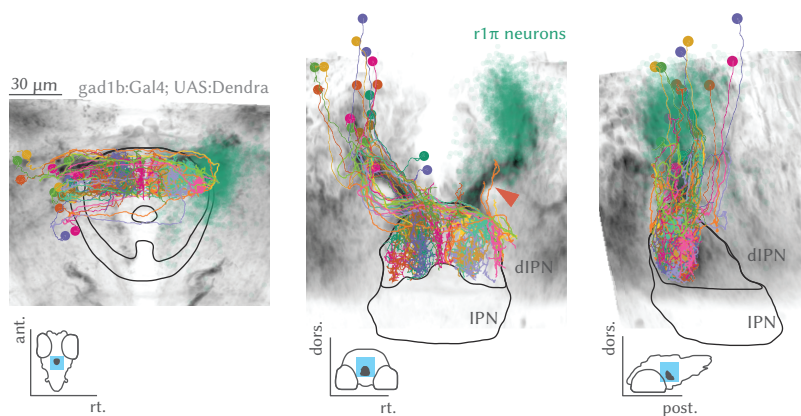


Figure 5.25: Anatomical projections of a stack from the *Tg(gad1b:Gal4)* line used in the experiments. The lines mark the IPN and dIPN boundaries, and the insets show the position in the brain of the IPN mask and the views. The red arrow highlights the tract of fibers that extend from the aHB to the IPN. The r1π neurons from the imaging experiments are shown in the same coordinate space in green on the right, together with the morphology of all neurons reconstructed from the SBEM data on the left.

When we presented the reconstructions of individual neurons at high resolution from the SBEM dataset, we reported a class of neurons with the somata in the aHB that extended a single projection that bifurcated into a dendrite and axon which ended in the dIPN (Figure 5.25, Movie 3). Those neurons were classified in Cluster 4 in the first chapter.

The small dendritic tree covered a localized compartment in the ipsilateral IPN, whereas the axon projected contralaterally with minimal branching that occurred only in the terminal sections (Figure 5.27).

### Two-photon imaging in the IPN show signs of r1π dynamics

To confirm that r1π neurons project to the dIPN, we imaged the same GABAergic line under a two-photon microscope to investigate neuropil activity. Performing the same analysis as for the r1π neurons presented in Figures 5.6, 5.8 and 5.17 uncovered a set of ROIs that were mostly restricted to the dIPN. Those ROIs showed stable circular dynamics and displayed the same relationship to heading direction (Figure 5.28). Interestingly, a region caudal from the dIPN also seemed to contain ROIs somehow related to the anticorrelated dynamics of r1π ROIs. This area roughly correspond to where aHB neurons of Cluster 3 described in the first part send their axons, suggesting that this region could also be implicated in the direction integration circuit.



Movie 3: https://doi.org/10.6084/m9.figshare.19608204
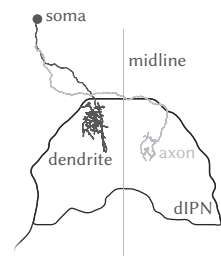


Figure 5.26: One of the neurons from Figure 5.25 singled out to show the cell morphology with a process splitting in an ipsilateral dendrite and a contralateral axon.
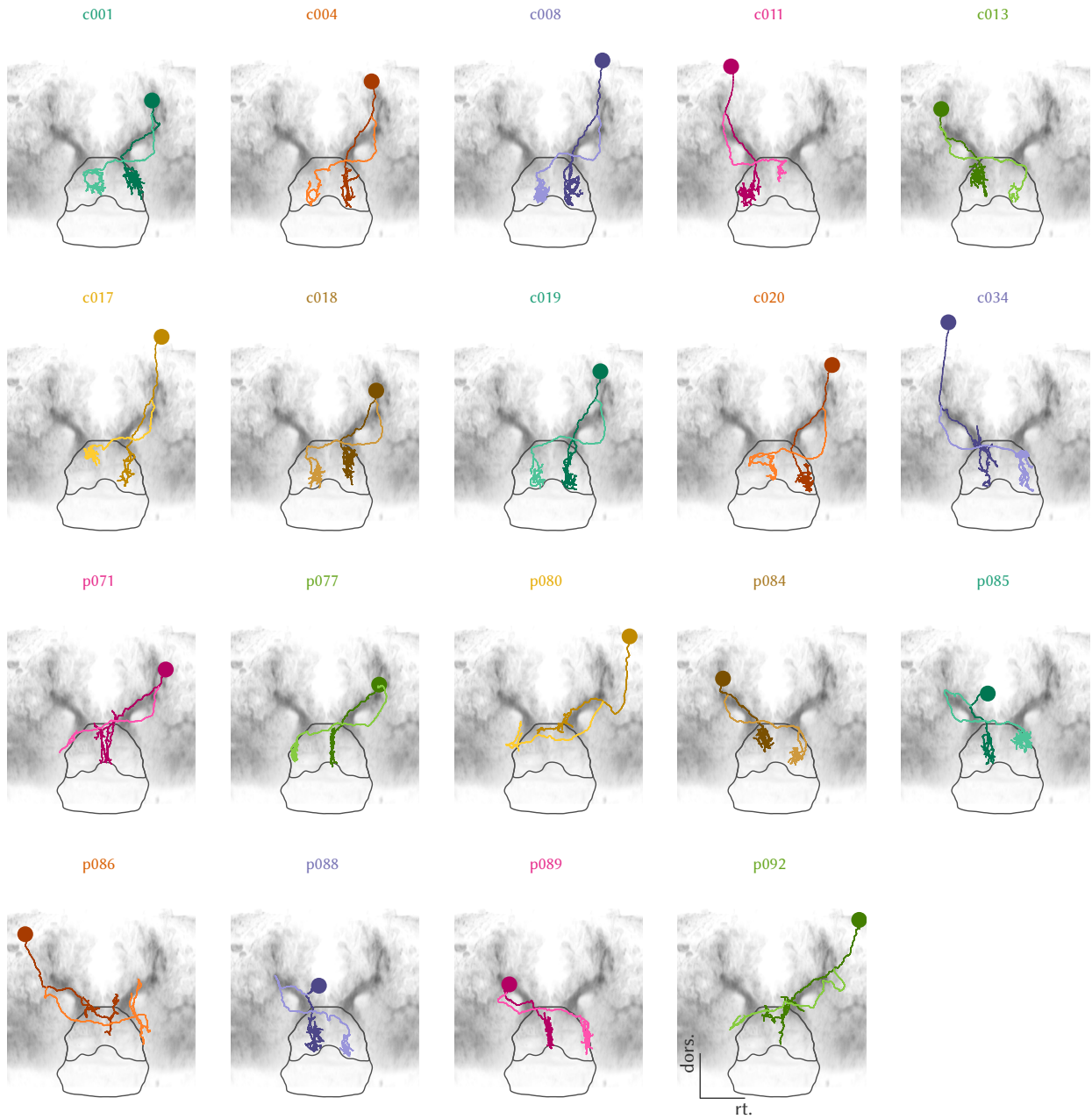
Figure 5.27: Individual plots of SBEM reconstructed neurons. Frontal view for all neurons presented in Figure 5.25.
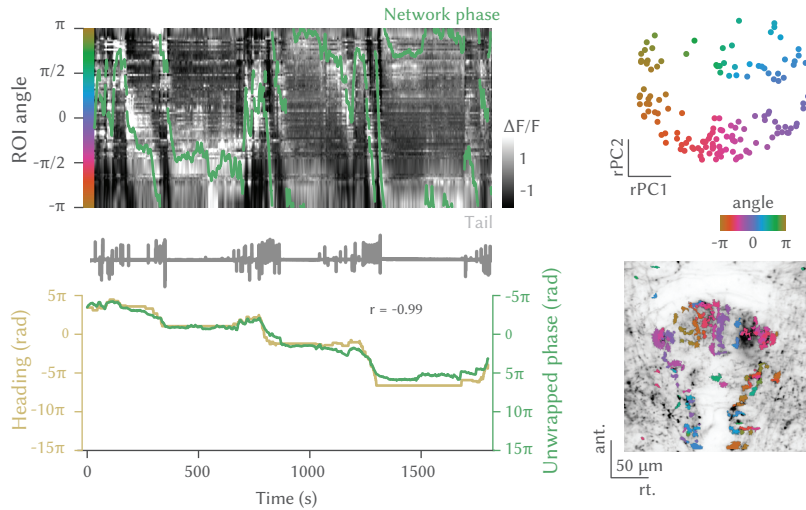
Figure 5.28: *Left, top*, Traces of ROIs in the dIPN showing r1π-like dynamics, sorted by angle in PC space, and phase of the network (green line). The tail trace is shown in gray on top. *Left, bottom*, Estimated heading direction (gold) and network phase (green) are highly correlated. *Right, top*, projection over the first 2 PCs in time of all the ROIs showing r1π-like activity, color-coded by angle around the circle. *Right, bottom*, Anatomical distribution of the same neurons, color-coded by angle in PC space. The anatomy of the recorded plane is shown in the background. Data from Hagar Lavian.

## 5.6   aHB projections map linearly the functional topology of r1π neurons in the dIPN

As I have described in the previous chapter, heading directions systems considered to be neuronal implementations of ring-attractor networks. In a ring attractor network, excitatory activity between neighboring cells is stabilized and localized by long-range inhibitory connections. We therefore wanted to investigate whether there is any evidence that the morphology and projections of the GABAergic r1π neurons could implement such a structure.

### Principles of connectivity in the aHB projections to dIPN

To this end, we turned back to the SBEM reconstructions. We wanted to investigate whether there was any principle in their projection patterns to the dIPN. We observed that the projections of different neurons occupy different locations in the medio-lateral axis and appear to cover the whole dIPN (Figure 5.29, Movie 3 and Figure 5.27). As observed when presenting the morphological reconstructions, some of the dendrites of those neurons were extremely planar, and occupy a very contained space along the frontal axis; many of those planar neurons are then stacked along the frontal axis, tiling the dIPN.

The striking observation was that, when we looked at the position of the axon targeting the contralateral dIPN, the distance of the dendrite from the midline anticorrelated with the distance of the axon from the midline (r = −0.9, n = 19 neurons). This means that a neuron with a lateral dendrite would extend a medial axon and vice-versa (Figure 5.29).

In our imaging data we observed a pseudo-circular arrangment of similarity between the activity of pairs of neurons: a neuron on the left would have a high probability of been correlated with a neuron on the left, and anticorrelated with a neuron on the left; and a rostral neuron would have a high probability of been correlated with a rostral neuron (both on the left and on the right), and anticorrelated with a caudal neuron. We speculated that if proximity in dendrite positions correlates with proximity in cellular

Frontal view    Horizontal view

Figure 5.29: *Left*, Frontal view of IPN-projecting aHB neurons, color-coded by position of the dendrite on the coronal axis (lateral-medial). Inset: scatterplot of the distance from the midline of dendrite and axon for each neuron (R = −0.90, n = n = 19 neurons). *Right*, Horizontal view IPN-projecting aHB neurons, color-coded by position of the dendrite on the coronal axis (lateral-medial). Inset: scatterplot of the distance from the midline of dendrite and position of the soma of the antero-posterior axis for each neuron (r = −0.65, n = 19 neurons).

activity, we would expect an antero-caudal gradient where rostral neurons and caudal neurons would have a higher probability of having the dendrite in the same location. Intriguingly, we observed exacly this correlation between the antero-posterior position of a cell's soma and the distance of its dendrites from the midline (r = −0.65, n = 19 neurons) (Figure 5.29 right).

### Structure of correlations in imaging data predicts the observed neuronal morphologies

In the two-photon experiments signal in the dIPN comes from very sparsely labelled patches of neuropil. When firing, most neurons present calcium transients that invest both their dendrites and their axons. Therefore, the anatomical organization we describe would predict that in the activity recorded from the sparsely expressing dIPN, pixels that are the most correlated with each other are at a fixed distance on the medio-lateral axis, as their signal comes from the dendrites and axons of the same neurons. Therefore, we computed correlation maps were we display the correlation of each pixel of the image with a focal pixel as a function of distance from that focal pixel. We found the expected pattern when examining data from individual fish (Figure 5.30) and across all fish (Figure 5.31).

As we hypothesise that the side lobes in the correlation map in Figure 5.30 comes from the presence in the imaging data of dendritic and axonal processes of the same neuron, we can predict that the distance of the lobes matches the average distance between dendrite and axon in the SBEM reconstructions. Indeed when computing a map of average distance of a neuron's processes from a focal process, the distribution that we obtained was very similar to the distribution of correlations, with sidelobes appearing at almost exactly the same distance (Figure 5.31, bottom).

These observations suggest that a circular functional structure in the aHB, corresponding to angles from −π to π, is coupled to a linear structure in the dIPN. Given Figure 5.29, we expect to find neurons with paired dendritic and axonal projections. Remarkably, we found such pairs of neurons that had their somata on opposite sides of the aHB and which projected axons towards each other's dendrites (Figure 5.32). In this way, a neuron is



Figure 5.30: *Left*, Anatomy of *Tg(gad1b:Gal4, UAS:GCaMP6s)* from a two photon experiment with a focal bin highlighted by the red arrow and *right*, maps of correlations of bins with the focal bin. Each row corresponds to a different focal point. Analysis by You Wu.
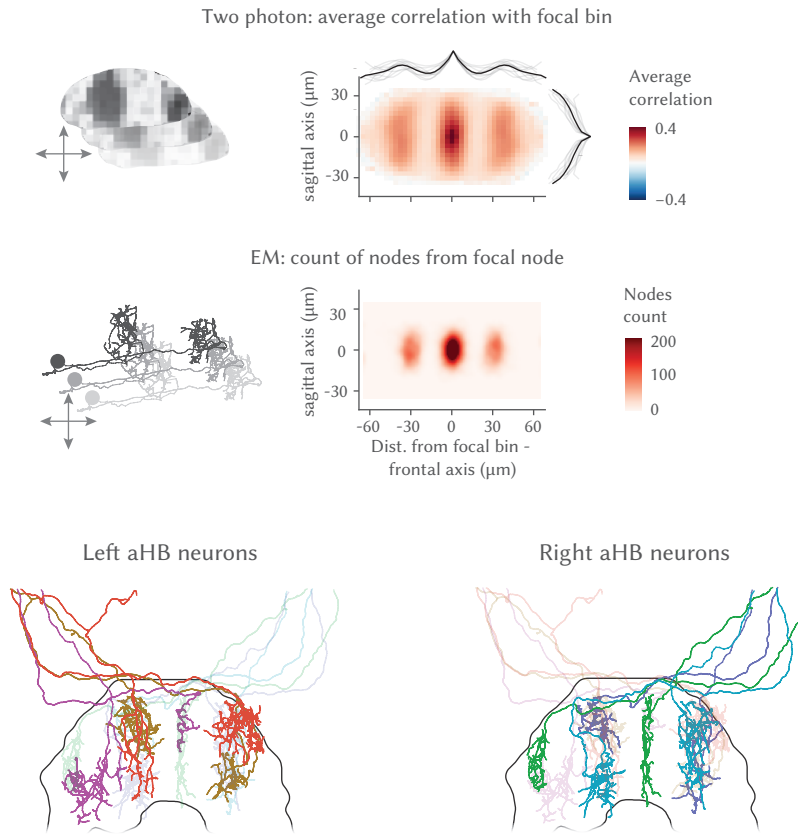
Figure 5.32: Neurons on the left and on the right of the brain (top and bottom views).

ideally placed to inhibit its corresponding out-of-phase neurons. This projection pattern could stabilize and localize the heading direction activity we observed in the aHB network by providing long range inhibition (Figure 5.33).

## 5.7   Discussion

IN OUR STUDY WE DESCRIBE a network of GABAergic neurons in rhombomere 1 of the larval zebrafish hindbrain, just next to the midbrain hindbrain boundary, that encodes the heading direction of the fish in external (allocentric) coordinates. This integration of internally generated neural activity proves the existence of an internal model of turning behavior to complement the internal models of forward swimming that have been recently described[9].

[9] Markov et al., "A cerebellar internal model calibrates a feedback controller involved in sensorimotor control".

### A heading-direction network in the fish aHB

The dynamics of the r1π neurons network fullfills several of the criteria that define a head-direction network (see *Circuits for heading direction*). First, there is a sustained (present at every point in time) and unique (always localized in a specific part of the circuit) bump of activity that translates across the network. Second, this activity shifts in opposite directions across the network when the animal perform leftward and rightward movements

(integration). Finally, the activation of the network is stable over tens of seconds even in the absence of motion (persistence).

## A preliminary model for an attractor network circuit in the larval zebrafish

The reconstruction of neuron morphologies suggests a provisional model for the organization of the r1π network. GABAergic cells from the aHB send dendrites in a portion of the dIPN, and the axon in the contralateral side. The distance between the axon and the dendrite is constant, so that cells with medial dendrites have lateral (contralateral) axons, and viceversa. Moreover, this linear organization in the dIPN corresponds to a rostrocaudal gradient in the position of the cell somas, so that rostral cells have medial dendrites, and caudal cells more lateral ones.

From this morphological data, a model for the stabilization of a ring attractor network arises quite naturally if we make two assumptions:

- all r1π neurons are inhibitory
- all r1π neurons receive a tonic excitatory drive, that balances their reciprocal inhibition

When a part of the r1π network is active, the inhibitory r1π neurons will provide out-of-phase inhibition to the neurons that are on the opposite side. This opponency holds both for left/right neurons, and for rostral/caudal ones. Indeed, rostral neurons will have a dendrite close to the dIPN midline, both on the left and on the right side of it, and will therefore provide inhibition to the two lateral extremes of the dIPN, both on the left and on the right side. In turn, neurons with the dendrite on both the left and the right extrema of the dIPN will send an axon close to the midline.

If we assume that there is either a constant tonic drive impinging on all r1π neurons, or local recurrent mechanisms that can provide excitation of the neuron's dendrites, the network could generate a sustained bump of activity whose localization and uniqueness are ensured by out-of-phase inhibition provided by the axons of r1π neurons. In this way, a bump propagating in a circular fashion at the level of the r1π neurons somas would correspond to a linear propagation across the dIPN along the frontal axis.
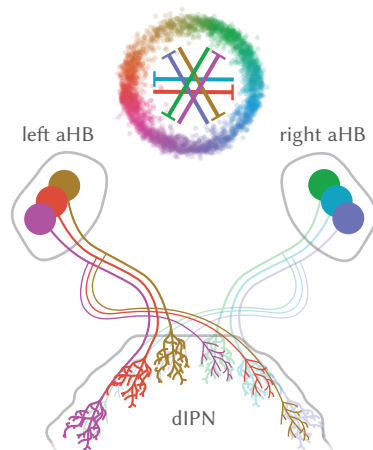


Figure 5.33: Summary illustration of the relationship between the functional experiments (PCA circle above) in the anterior hindbrain and the anatomical reconstructions (neuron cartoons below).

*Updating activity in the network*

As the representation can be observed in the dark, in the absence of external landmarks and visual sensory feedback, it is likely generated by the integration of efference copies. Although integration of proprioceptive feedback cannot be ruled out, motor-related activity has already been recorded in this region in paralyzed fish[10], and it is the most parsimonious explanation for explaining the motor-related signals we observe in rhombomeres 2/3. How this activity might drive shifts in the network activity is still an open question.

*The role of interpeduncular afferents*

The role of interpeduncular afferents is likely to be central to the network function, as they represent a large fraction of all synaptic terminals found in the IPN. Moreover, the reticular nature of their arborization in the dIPN suggest a highly specialized function. One possibility is that their role in the heading direction network is just to provide a widespread tonic activation, that is subsequently sculpted by the activity of inhibitory r1$\pi$ neurons.

Another intriguing possibility is that inputs from the habenula might exhibit forms of local plasticity similar to what happens in the terminals of r1$\pi$ neurons in the drosophila central complex that associate visual landmarks with heading representations. Since habenular neurons are activated by various sensory queues, this mechanism might potentially lead to the association of a given sensory input and the localization of the activity bump in one position of the topological r1$\pi$, and represent a possible way of associate sensory inputs with heading representations in the network.

*Possible analogy between the DTN and the zebrafish aHB*

Several features of the GABAergic cells of the larval zebrafish suggest a possible homology with what in mammals is defined as DTN.

- Both structures originate from the hindbrain in rhombomere 1, and are located aroun the floor of the third ventricle

- Both nuclei are GABAergic

- Both structures are functionally integrated in the IPN, *i.e.* they send and receive projections from the IPN. Importantly, in zebrafish GABAergic neurons of the aHB send an axon and a dendrite in the IPN, and are effectively to be considered IPN interneurons; such morphologies have never been reported in mammals so far

- Both structures are implicated in the heading direction integration, and display loosely tuned activity with neurons active for a broad range of (fictive or real) heading orientations.

The evidence for a correspondence between those two areas is obviously very preliminary and circumstantial. More careful developmental studies addressing more precisely the molecular identity of r1$\pi$ neurons of the zebrafish aHB will be required to really understand them in the contex of the comparative anatomy of the vertebrate hindbrain.

[10] X. Chen, Mu, et al., "Brainwide Organization of Neuronal Activity and Convergent Sensorimotor Transformations in Larval Zebrafish"; Dunn et al., "Brain-wide mapping of neural activity controlling zebrafish exploratory locomotion".

*Navigation in zebrafish*

A number of studies has described a region of the larval zebrafish brain termed hindbrain oscillator, whose activity correlates with the instantaneous turning state[11]. The r1π neurons we describe are anatomically and functionally distinct from these. Activity in the r1π network does not correlate with current turning direction. In addition, oculomotor integrators and saccade generating neurons have been described in the larval zebrafish hindbrain[12]. Even though the activity of the neurons we describe may reflect, in small measure, gaze direction, the neurons which better report eye direction are located more caudally, consistent with the location of oculomotor integrator neurons[13].

Recent experiments in adult zebrafish have shown that the habenula to dorsal-IPN pathway is required for fish to associate a reward based on self-referenced turning but not when the turning is based on external sensory cues[14]. In addition, recent work has also highlighted the representation of turning behavior in the IPN activity of zebrafish larvae[15]. Although assays that probe global navigation have not been successfully established in larval zebrafish, there is indication that they can perform optimal turns to return to a light environment in the absence of any active sensory cue[16]. These studies suggest that zebrafish can use information about their heading in allocentric space. In this context, it is important to note that the zero of the angular heading direction conveyed by r1π neurons may point in a special direction in space with respect to the fish, for example in terms of behavioral relevance, although future work is needed to corroborate this hypothesis.

In this context it is also interesting to note how the profile of activation of the r1π network is surprisingly precise, and can be fit very well by a sinusoidal function. Although the functional meaning of this activity is still unknown, and the mechanisms proposed to generate it are still entirely speculative, one might wonder if this particular activation profile has some functional role. As we described in the previous chapter, sinusoidal representations of heading could be crucial to perform vector operations in the fly heading direction system[17]. As the anterior hindbrain is an area of high convergence of sensory cues, in particular of signals related to directional motion of a visual stimulus, we can ponder the intriguing hypothesis that the sinusoidal activity across the r1π network can constitute an optimal representation to perform downstream integrations of current heading estimation with experienced sensory optic flow.

*Heading direction systems in other animals*

Several elegant studies have described networks that encode heading direction in the insect central complex (discussed in *The* Drosophila *heading direction circuit*). The activity and anatomy of this system constitutes a neuronal implementation of a ring attractor network and the level of detail being uncovered allows for a mechanistic understanding of how the circuit works. The integration of external and internal sensory cues, efference copies and various coordinate transformations all play an important role in the activity of the network and the behavior of the animals. The r1π network we observe bears intriguing similarities with this system and

[11] Ahrens et al., "Whole-brain functional imaging at cellular resolution using light-sheet microscopy"; Dunn et al., "Brain-wide mapping of neural activity controlling zebrafish exploratory locomotion"; Wolf et al., "Sensorimotor computation underlying phototaxis in zebrafish".

[12] Ramirez and Aksay, "Ramp-to-threshold dynamics in a hindbrain population controls the timing of spontaneous saccades"; Miri et al., "Spatial gradients and multidimensional dynamics in a neural integrator circuit".

[13] Miri et al., "Spatial gradients and multidimensional dynamics in a neural integrator circuit"; Pastor, De La Cruz, and Baker, "Eye position and eye velocity integrators reside in separate brainstem nuclei"; Aksay et al., "Anatomy and discharge properties of pre-motor neurons in the goldfish medulla that have eye-position signals during fixations."

[14] Cherng et al., "The Dorsal Lateral Habenula-Interpeduncular Nucleus Pathway Is Essential for Left-Right-Dependent Decision Making in Zebrafish".

[15] Dragomir, Štih, and Portugues, "Evidence accumulation during a sensorimotor decision task revealed by whole-brain imaging".

[16] X. Chen and Engert, "Navigational strategies underlying phototaxis in larval zebrafish".

[17] Lyu, Abbott, and Maimon, "Building an allocentric travelling direction signal via vector computation".

a detailed comparative analysis of both may uncover important theoretical insights into persistent neuronal representations in general and head-direction systems and ring attractors in particular[18].

The heading direction network we describe is GABAergic and projects prominently to the IPN. As I discussed in the previous chapter (see *Head direction signals in mammals*) mammals, head direction neurons have been described in the DTN, a GABAergic structure derived from rhombomere 1 that is reciprocally connected to the IPN. From the DTN, this spatial information is known to flow via the mammillary bodies into regions such as the retrosplenial cortex and the hippocampal-entorhinal formation (see[19] for a review), where they play an important role in spatial navigation. The heading direction neurons that have been observed in the DTN seem to be broadly tuned, and they might rely on motor efference copies more than on visual and vestibular inputs, similarly to the neurons we report in the fish aHB.

Theoretical studies proposed the notion of ring attractor networks as a mechanism to encode heading direction information. The (topologically) circular manifold that is predicted by those models has been observed in the phase space trajectory of heading directional neurons recorded from the anterodorsal thalamic nucleus of mice[20]. However, this data comes from extracellular recordings of anatomically unidentified neurons, and the challenges of the mammalian anatomy have hindered the progress of a mechanistic understanding for the vertebrate heading direction circuit.

Compartmentalized projections from neurons of the tegmental region (aHB) to the IPN that have been described before[21] bear similarity with the ones we describe in this study, although the function of those neurons is largely unknown. Here, we provide evidence that these projections organize in a precise way within the IPN, and we hypothesize that the architecture of their arborizations within the IPN is paramount in the organization of the reciprocal inhibition required for the network dynamics we observed. Although previously overlooked, the aHB-IPN circuit could in the future provide an inroad to understanding the mechanisms underpinning cognitive maps in vertebrates.

[18] Hulse and Jayaraman, "Mechanisms Underlying the Neural Computation of Head Direction".

[19] Jeffrey S. Taube, "The head direction signal: Origins and sensory-motor integration".

[20] Chaudhuri et al., "The intrinsic attractor manifold and population dynamics of a canonical cognitive circuit across waking and sleep".

[21] Herrick, "Interpeduncular Nucleus"; Iwahori et al., "Terminal patterns of the tegmental afferents in the interpeduncular nucleus: a Golgi study in the mouse".

# Materials and methods

6

## 6.1 Zebrafish husbandry

All procedures related to animal handling were conducted following protocols approved by the Technische Universität München and the Regierung von Oberbayern. Adult zebrafish (*Danio rerio*) from Tüpfel long fin (TL) strain were kept at 27.5 °C to 28 °C on a 14/10 light cycle, and hosted in a fish facility that provided full re-circulation of water with carbon-, bio- and UV filtering and a daily exchange of 12% of water. Water pH was kept at 7.0 to 7.5 and conductivity at 750 μSv to 800 μSv. Fish were hosted in 3.5 L tanks in groups of 10 to 17 animals. Adults were fed with Gemma micron 300 (Skretting) and live food (*Artemia salina*) twice per day and the larvae were fed with Sera micron Nature (Sera) and ST-1 (Aquaschwarz) three times a day. All experiments were conducted on 6 dpf to 9 dpf larvae of yet undetermined sex. The week before the experiment, one male and one female or three male and three female animals were left breeding overnight in a Sloping Breeding Tank or breeding tank (Tecniplast). The day after, eggs were collected in the morning, rinsed with water from the facility water system, and then kept in groups of 20 to 40 in 90 cm Petri dishes filled with 0.3× Danieau's solution (17.4 mM NaCl, 0.21 mM KCl, 0.12 mM MgSO4, 0.18 mM Ca(NO3)2, 1.5 mM HEPES, reagents from Sigma-Aldrich) until hatching and in water from the fish facility afterwards. Larvae were kept in an incubator that maintained temperature at 28.5 °C and a 14/10 hour light/dark cycle, and their solution was changed daily. At 4 dpf to 5 dpf, animals were lightly anesthetized with Tricaine mesylate (Sigma-Aldrich) and screened for fluorescence under an epifluorescence microscope. Animals positive for GCaMP6s/Dendra/mCherry fluorescence were selected for the imaging experiments.

### Transgenic animals

The *Tg(gad1b/GAD67:Gal4-VP16)mpn155* (referred to as *Tg(gad1b:Gal4)*) was used for all experiments, which drives expression in a subpopulation of GABAergic cells under *gad1b* regulatory elements [1]. The animals for functional imaging and anatomical experiments were double transgenic with *Tg(UAS:GCaMP6s)mpn101* [2] and *Tg(UAS:Dendra-kras)s1998t* [3], respectively. In some anatomical experiments, the animals also had *Tg(elavl3:H2B-mCherry)* which was generated by Tol2 transposon-mediated transgenesis. All the transgenic animals were also *mitfa-/-* and thus lacked melanophores [4].

[1] Förster et al., "An optogenetic toolbox for unbiased discovery of functionally connected cells in neural circuits".
[2] Thiele, Donovan, and Baier, "Descending Control of Swim Posture by a Midbrain Nucleus in Zebrafish".
[3] Arrenberg, Del Bene, and Baier, "Optical control of zebrafish behavior with halorhodopsin".
[4] Lister et al., "nacre encodes a zebrafish microphthalmia-related protein that regulatesneural-crest-derived pigment cell fate".

## 6.2    Lightsheet experiments

### Preparation

For lightsheet experiments, animals were embedded in 2.2% low-melting point agarose (Thermofisher) in a custom lightsheet chamber. The chamber consisted of a 3D printed frame(seethe `.stl` file) with a glass coverslip sealed on the side in the position where the lateral beam of the lightsheet enters the chamber, and a square of transparent acrylic on the bottom, for behavioral tracking (see *Lightsheet microscope*).

The chamber was filled with water from the fish facility system and agarose was removed along the optic path of the lateral laser beam (to prevent scattering), and around the tail of the animal, to enable movements of the tail (Figure 6.1). In some larvae, the eyes were also freed from the agarose. After embedding, fish were left recovering 1 h to 6 h before the imaging session. Before starting the imaging, light tapping on the side of the chamber was used to select the most active fish for the experiment.
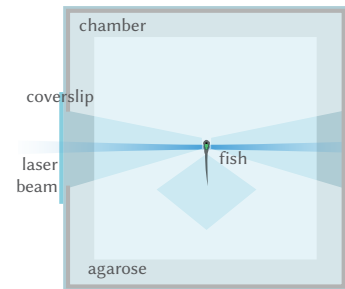


Figure 6.1: Schema of the preparation for the lightsheet, with a fish head-restrained in agarose in the chamber.

### Lightsheet microscope

Imaging experiments were performed using a custom-built lightsheet microscope. A 473 nm wavelength laser source (modulated laser diodes, Cobolt) was used to produce a ~1.5 mm laser beam that was conveyed on the excitation scanning arm. The arm consisted in a pair of galvanometric mirrors that scanned vertically and horizontally; a line diffuser (Edmund Optics) to minimize stripe artifacts [5], a 2× telescope composed by a 75 mm and a 150 mm focal distance lens (Thorlabs) that expanded the beam before it entered a low numerical aperture air objective (Olympus) that focused it through the lateral glass coverslip of the lightsheet chamber on the fish.

[5] Taylor et al., "Diffuse light-sheet microscopy for stripe-free calcium imaging of neural populations".



Figure 6.2: Schema of the lightsheet microscope described in the text. Software is indicated in italics, and gray lines indicate the parts of the setup controlled by each program.

The excitation light sheet was generated by scanning at 800 Hz the beam on the horizontal plane. A paper screen was positioned in the image conjugate plane within the telescope lens pair to protect the eyes of the fish from the lateral scanning of the laser beam. The emitted fluorescence was collected with a 20× water-immersion objective (Olympus), filtered with a 525/50 band-pass filter (AHF Analysentechnik) and focused on a CMOS cam-

era (Hamamatsu Photonics) with a tube lens (Thorlabs).

The imaging acquisition was run using `sashimi`, a custom Python-based software [6] to coordinate the laser scanning, the camera triggering and the piezo movement. The objective was moved with a saw tooth profile with a frequency of 5 Hz in most experiments (frequency was adjusted to 3 Hz in experiments where a larger vertical span was scanned). TTL pulses locked with the scanning profile of the piezo were sent to the camera to trigger the acquisition of each plane at a fixed vertical position during the scanning. No pulse was sent during the descending phase of the scanning, when the objective would cover a large vertical span in a short time. In most experiments a total of 8 planes were acquired over a range of approximately 80 μm to 100 μm, slightly adjusted for every fish. The resulting imaging data had a voxel size of ~10 μm × 0.6 μm × 0.6 μm, and a temporal resolution of 3 Hz to 5 Hz.

### Tail/eyes tracking and stimulus presentation

To monitor tail movements during the imaging session, an infrared LED source (RS Components) was used to illuminate the larvae from above. A camera (Ximea) with a macro objective (Navitar) was aimed at the animal through the transparent bottom of the lightsheet chamber with the help of a mirror placed at 45° below the imaging stage. A long-pass filter (Thorlabs) was placed in front of the camera. A projector (Optoma) with a red long-pass filter (Kodak Wratten No.25) was used to display visual stimuli; light from the projector was conveyed to the stage through a cold mirror that reflected the projected image on the 45° mirror placed below the stage. The stimuli were projected on a white paper screen positioned below the fish, with a triangular hole that kept the fish visible from the camera. The behavior tracking part of the rig was very similar to the setup for restrained fish tracking described in [7].

Frames from the behavioral camera were acquired at 400 Hz and tail movements were tracked online using `Stytra` [8] with Stytra's default algorithm to fit to the tail 9 linear segments. The *tail angle* quantity used for controlling the closed-loop was computed online during the experiment in the Stytra application as the difference between the average angle of the first two and last two segments of the tail and saved with the rest of the log from Stytra. For eye tracking, a video of the entire acquisition was saved to be analyzed offline (see below).

The stimulus presentation and the behavior tracking were synchronized with the imaging acquisition with a ZMQ-based trigger signal supported natively by `Stytra`.

### 6.3    Two photon experiments

Two photon experiments were performed in a custom-built microscope as describe in [9]. Full frames were acquired every 334.51 ms in four, 0.83 μm-spaced interlaced scans, which resulted in a pixel size of 0.3 μm to 0.6 μm (varying resolutions here depending on field of view covered). After acquisition from one plane was done, the focal plane was shifted ventrally by

0.5 µm to 4 µm and the process was repeated.

For two photon experiments, animals were embedded in 2% low-melting point agarose (Thermofisher) in 30 mm Petri dishes. The agarose around the tail, caudal to the pectoral fins, was cut away with a fine scalpel to allow for tail movement. The dish was placed onto an acrylic support with a light-diffusing screen and imaged on a custom-built two-photon microscope as previously described in [10]. The custom Python package `brunoise` was used to control the microscope hardware [11].

### Two photon functional experiments

Visual stimuli (see below) were generated using a custom written Python script with the `Stytra` package, and were projected at 60 Hz using an Asus P2E microprojector and a red long-pass filter (Kodak Wratten No.25) to allow for simultaneous imaging and visual stimulation. Fish were illuminated using infrared light-emitting diodes (850 nm wavelength) and imaged from below at up to 200 Hz using an infrared- sensitive charge-coupled device camera (Pike F032b, Allied Vision Technologies). Tail movements were tracked online using Stytra as described for the lightsheet experiments.

### Two photon anatomical experiments

High resolution 0.5 µm × 0.5 µm × 0.5 µm two-photon stacks of the aHB and IPN were acquired from fish expressing *gad1b:Gal4* and *UAS:Dendra-kras* transgenes (n = 7 fish, 6 dpf to 7 dpf). The stacks were registered to one another using the `CMTK` [12]. The transformed stacks were then averaged to generate an average brain stack showing the projections of GABAergic aHB neurons to the IPN.

## 6.4    Confocal experiments

For confocal experiments, larvae were embedded in 1.5% agarose and anesthetized with Tricaine. Whole brain stacks of three 7 dpf fish expressing *gad1b:Gal4, UAS:Dendra-kras* and *elavl3:H2B-mCherry* transgenes were acquired using a 20× water immersion objective (NA = 1.0) with a voxel resolution of 1 µm × 0.6 µm × 0.6 µm (LSM 880, Carl Zeiss). The stacks were registered to one another using `CMTK` [13]. The transformed stacks were then averaged to generate an average brain stack showing the expression pattern of the *gad1b:Gal4* on top of pan-neuronal H2B-mCherry expression.

## 6.5    Electron microscopy experiments

### serial block-face electron microscopy dataset acquisition

Details of the SBEM dataset acquisition will be published elsewhere (Svara et al., in preparation). Briefly, a 5 dpf larval *Tg(elavl3:GCaMP5G)a4598* transgenic zebrafish was fixed with extracellular space preservation and stained as described previously [14]. The sample was embedded in an epoxy mixture containing 2.5% Carbon Black [15]. The brain was imaged at a resolution of 14 nm × 14 nm and sections were cut at a thickness of 25 nm. The long (y)

[10] Dragomir, Štih, and Portugues, "Evidence accumulation during a sensorimotor decision task revealed by whole-brain imaging".

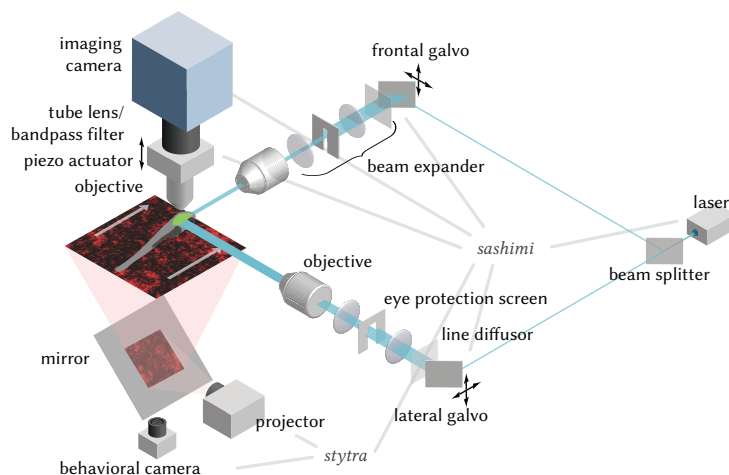[11] Štih, EmanPaoli, and AC, *portugues-lab/brunoise: Alpha.*
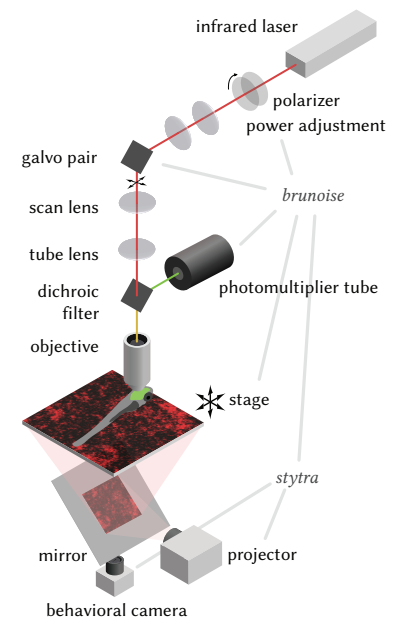


Figure 6.3: Schema of the two photon microscope described in the text. Software is indicated in italics, and gray lines indicate the parts of the setup controlled by each program.

[12] Rohlfing and Maurer, "Nonrigid image registration in shared-memory multiprocessor environments with application to brains, breasts, and bees".

[13] Rohlfing and Maurer, "Nonrigid image registration in shared-memory multiprocessor environments with application to brains, breasts, and bees".

[14] Svara et al., "Volume EM Reconstruction of Spinal Cord Reveals Wiring Specificity in Speed-Related Motor Circuits"; Briggman, Helmstaedter, and Denk, "Wiring specificity in the direction-selectivity circuit of the retina".

[15] Nguyen et al., "Conductive resins improve charging and resolution of acquired images in electron microscopic volume imaging".

axis of each image tile was scanned by gradually moving the stage, while the short axis (x) was scanned with the electron beam. The shape of the tile pattern was determined based on a 4 μm voxel size X-Ray microCT scan (SCANCO Medical AG, Brütisellen) of the embedded sample.

## 6.6 Visual stimuli

The observations reported in the paper were performed in experiments where different visual stimuli were presented to the fish:

- Darkness: in those experiments, no visual stimuli were presented, the projector was on and a static black frame was displayed;

- Open loop: in open loop epochs, a pink noise pattern was projected and moved in x and theta with a path that was computed from the trajectory of a freely swimming fish taken from a previous experiment in the lab. The stimulus moved backward according to velocity of the fish, and rotated according to changes in its direction. As a result, the fish was presented with the optic flow that it would have perceived moving over a static pink noise pattern with that trajectory.

- Closed loop: a pink noise pattern was projected below the fish; the pattern was static if the animal was not moved, and it translated backward and rotated when the fish performed spontaneous movements. The stimulus moved backward according to an estimate of the velocity of the fish computed using vigor, and rotated according to changes in its direction estimated using the swim bias, so that right turns, i.e, clockwise rotations of the fish, would be matched with clockwise rotations of the stimulus. The gain factor that transformed a given swim bias into an angular velocity was modulated with factors 0.5, 1 and 2 to observe if the slope of the aHB network and the estimated heading would be altered by visual feedback. An additional control gain of −1, where fish would receive a visual feedback opposite to the performed movements, was also included.

- Directional motion: in some experiments (n = 2 fish), the animal was also shown a pink noise pattern moving in 8 equally spaced directions on the plane, presented one after the other first in clockwise sequence (starting from forward) and then in counter-clockwise sequence.

As the activity we describe was not modulated by the presented visual stimuli in those experiments, we pooled together observations from different experimental conditions for all the analyses that quantified the property of the r1π neurons network.

The paradigm to investigate the role of visual feedback (Figure 5.19) consisted of an alternation of 5 min of the closed loop and 5 min of the open loop condition. The paradigm addressing the effect of changing gains (Figure 5.19) consisted in 5 min blocks of each gain condition, with two repetitions for each condition, in the following sequence of gains: [1, 0.5, 2, 1, 0.5, 2, −1, −1]. The Stytra scripts for the control of the experimental stimuli

will be shared together with the rest of the code in the publication that will accompany this thesis.

## 6.7    Data analysis and statistics

All parts of the data analysis were performed using Python 3.7, and Python libraries for scientific computing, in particular numpy[16], scipy[17] and scikit-learn[18]. The Python environment required to replicate the analysis in the paper can be found in the paper code repository. All figures were produced using matplotlib [19]. All statistical tests used were non-parametric, either Mann-Whitney U test for unpaired comparisons (mannwhitneyu() from scipy) or Wilcoxon signed-rank test for paired comparisons (wilcoxon() from scipy).

### Lightsheet imaging data preprocessing

The imaging stacks were saved in `hdf5` files and then directly fed into suite2p, a Python package for calcium imaging data registration and ROI extraction [20]. We did not use suite2p algorithms for spike deconvolution. As the planes were spaced by roughly 10 µm, we ran the detection on individual planes and did not merge ROIs across planes. Parameters used for registration and source extraction in suite2p can be found in the shared analysis code. The parameter that specifies the threshold over noise that is used to detect ROIs (threshold_scaling) was adjusted differently from acquisition to acquisition to compensate for the variability in brightness that we observed from fish to fish. From the raw F traces saved from suite2p (`F.npy` file), $\Delta F/F$ was calculated using as baseline the average fluorescence in a rolling window of 900 s, to compensate for some small amount of bleaching that was observed in some acquisition. The signal then was smoothed with a median filter (medfilt() from scipy), and Z-scored so that all traces were centered on 0 and normalized to a standard deviation of 1. The coordinate of each ROI was taken as the centroid of its voxels. To register all lightsheet experiments to a common coordinate system, we defined manually for each experiment the location over the three axes of a point corresponding on the mid-line of the fish on the anterior-inferior limit of the aHB, and translate all coordinates so that such point was set to 0.

### Behavior data preprocessing

The behavioral data was pre-processed to detect swims and extract their properties using the bouter package [21]. First, the tail trace was processed with a function to reconstruct terminal tail segments that were miss-tracked during the online tracking using an interpolation based on an extrapolation from the reconstructed segments angles and the tail angles at previous time points. Then, tail angle was re-computed, and vigor was calculated as the standard deviation of the tail angle trace in a rolling window of 50 ms. Swims were defined as episodes when the vigor crossed a threshold of 0.1 for all fish. For all swims, we then computed the laterality index as the average angle of the tail during the first 70 ms of the swim. This value has

[16] Harris et al., "Array programming with NumPy".

[17] Virtanen et al., "SciPy 1.0: fundamental algorithms for scientific computing in Python".

[18] Pedregosa et al., "Scikit-learn: Machine Learning in Python".

[19] Hunter, "Matplotlib: A 2D graphics environment".

[20] Pachitariu et al., "Suite2p: beyond 10,000 neurons with standard two-photon microscopy".

[21] Štih, Petrucco, Prat, et al., Bouter.

been shown to correlate well with the angle turned by a fish when swimming freely [22]. To classify right, left, and forward swims, we fit a trimodal Gaussian distribution to the histogram of swim laterality indexes, enforcing the two side curves to be symmetric. Then, we used the intercept of the central and lateral Gaussians to determine the threshold used for the swim classification (±0.239 rad).

For eye tracking, the video recording of the entire experiment was processed using the `deeplabcut 2.0` package [23], a Python pose estimation package based on DeeperCut [24] to detect in every frame four points evenly spaced on each eye. Eye angle was defined as the median angle of the segments that connected the rostral-most point of the eye with all the others. *Gaze direction* was defined as the average of the angles obtained for the two eyes.

### Detecting r1π neurons

r1π ROIs were first observed to be the ones with the highest anticorrelation with other ROIs in the dataset. Therefore, to detect them, for every experiment we computed the correlation matrix of all traces and selected ROIs that had a correlation below a given threshold with at least another ROI in the dataset. The threshold was manually adjusted for every fish, in order to include as many ROIs that were part of the network as possible, while keeping out other signals. For all fish, the threshold was between $-0.75$ and $-0.5$ for both the lightsheet and the two photon experiments. To check that the selected ROIs were convincingly part of the ring and that we were including enough cells from it, we performed PCA over time using only traces from the selected ROIs and we then looked at the projection of all ROIs onto the first two principal components. When a satisfactory threshold was chosen, most included neurons formed a circular pattern in PC space (see Figure 5.6).[25]

As sometimes some additional ROIs were included, an additional manual step of selection was performed on the correlation matrix of the cells. An optimal sorting of the traces based on their angle in PC space was computed, and the correlation matrix plotted with the same sorting. Then, some traces were excluded based on the amount of discontinuity they would produce in the matrix.

With our strategy, we could detect a r1π network in approximately 20% to 30% of the imaged animals. In the rest of the fish, sometimes behavior was just very sparse (a few swims over the entire experiment), or not very directional (only forward swims performed). In other fish, even if behavior was good the anti-correlation criterion could find only a handful of strongly anti-correlated neurons. Although those neurons were likely to be of the described network, as their activity state changed with the occurrence of directional swims, the low number of ROIs made it impossible to properly characterize their population dynamics. Finally, in some fish the rotatory dynamics was observable only in a small temporal interval of the experiment, and they were not included in the dataset.

[22] Huang et al., "Spinal projection neurons control turning behaviors in zebrafish"; Dragomir, Štih, and Portugues, "Evidence accumulation during a sensorimotor decision task revealed by whole-brain imaging".

[23] Mathis et al., "DeepLabCut: markerless pose estimation of user-defined body parts with deep learning"; Nath et al., "Using DeepLabCut for 3D markerless pose estimation across species and behaviors".

[24] Insafutdinov et al., "DeeperCut: A Deeper, Stronger and Faster Multi-person Pose Estimation Model".

[25] We note that other approaches could be used to parse out those cells, such as restricting the anatomical location where to find them, or including them based on the proximity to some ring fit in PC space. We used just the anti-correlation and exclusion from the correlation matrix to avoid circular reasoning in the observations reported. Future investigations on this system might develop more principled procedures to isolate the r1π neuron population from the rest of the network by the features of their highly constrained dynamics.

## Rotated principal component calculation

We developed a way of registering PC projections from one fish to the other in a way that was consistent with the anatomical distribution of the cells. After computing principal components over time for the r1π neurons, we fit a circle to the projection of the activity of all individual r1π neurons to the first two PCs using the hyper_fit from the `circle_fit` package, a Python implementation of the hyper least square algorithm [26], and rescale and translate the PCs to have a unit radius circle centered on $(0, 0)$.

[26] Kanatani and Rangarajan, "Hyper least squares fitting of circles and ellipses".



Figure 6.4: Co-registration of PC projections. *Left*, Projection over the first two PCs calculated over time, color-coded by left-right location of the ROI or anterior-posterior location. The anatomical axes vectors computed by vector average of the ROI projections weighted by their anatomical location are also displayed. *Right*, The projections in rPC space, where the angular distances $\theta_1$ and $\theta_2$ between the anatomical axes and the rPC axes were minimized. The schematics of the fish illustrates the orientation of the rPC projections after the registration.

Then, we computed a weighted average across all the vectors representing ROIs in this two-dimensional space, weighted by their location in the rostro-caudal and the left-right anatomical axes (Figure 6.4). As a result, we got two vectors, one pointing in the direction of the most rostral ROIs, and the other in the direction of the rightmost ROIs; we then rotated and flipped each fish's projection so that those two axes matched across fish, *i.e.* the sum of the two angular distances $abs(\theta_1) + abs(\theta_2)$ was minimized (see Figure 6.4 for the definition of $\theta_1$ and $\theta_2$). We call the axes of this space *rotated principal components (rPCs)*.

After having calculated rPCs for an experiment, all ROIs were assigned an angle $\alpha_i$ based on their position over the circle in rPCs space. The convention used for the angle was that:

- $\alpha \in (-\pi, \pi]$
- Caudal neurons had $\alpha = 0$
- $\alpha$ increased when moving clockwise in the anatomical location of the neurons

Therefore, looking from above the horizontal plane, leftmost ROIs had $\alpha = \pi/2$, and rightmost ROIs $\alpha = -\pi/2$.

To test the hypothesis that the network is anatomically organized, we used the circular correlation coefficient as defined in Fisher and Lee, "A Correlation Coefficient for Circular Data". We also fit a sinusoidal curve to the distribution of ROIs left-right and anterior-posterior coordinates over the ROIs angle in rPCs space, and compared the fit residuals to the residuals computed over a shuffle computed by reassigning randomly ROI coordinates (Figure 6.6).



Figure 6.5: Illustration of the convention used for defining angles in the paper. *Top*: ROIs in rPC space, with labeled $\alpha$ and corresponding anatomical position of the ROIs. *Bottom*: the anatomy for the same ROIs, color-coded by $\alpha$ in rPC space.

## Network phase calculation

To recapitulate at every point in time the state of activation of the network, we derived the phase ($\phi(t)$) quantity to describe which part of the circle in
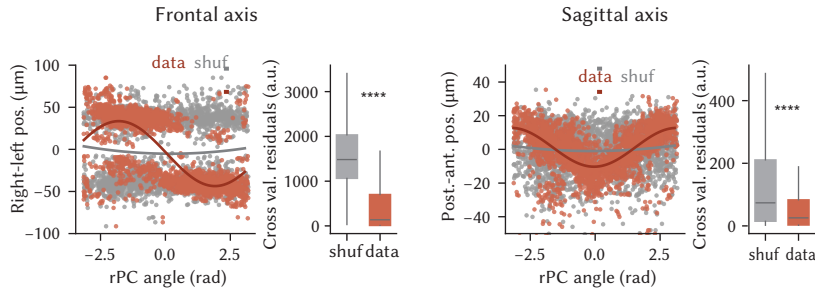
Figure 6.6: *Left*, Fit of a sinusoidal wave to the anterior posterior or the right-left position, as a function of the ROI phase in rPC space, and distribution of square distances of ROIs from the fit ($p < 0.001$, Mann-Whitney U test, n = 1330 ROIs from n = 31 fish). The fit was computed over 50% of the ROIs, and the residuals calculation over the left-out 50%. *Right*, The same, for the antero-posterior axis ($p < 0.001$, Mann-Whitney U test, n = 1330 ROIs from n = 31 fish).

rPCs space was the most active at every time point (Figure 6.7, Movie 2). For every frame, we computed a vector average **v** of all the $n$ ROI vectors **rPC$_i$** in the two-dimensional rPCs space, weighted by the state of activation of each ROI $f_i(t)$ (the $\Delta F/F$ at time $t$):

$$\mathbf{v}(t) = \frac{1}{n} \sum_{i=1}^{n} f_i(t)\,\mathbf{rPC_i}$$

Note that for this vector averaging, the $\Delta F/F$ of all ROIs at time $t$ were clipped to their 2% and 98% percentiles and normalized to have mean 0 across ROIs at every time point:

$$\frac{1}{n} \sum_{i=1}^{n} f_i(t) = 0$$

Where **rPC$_i$** is the 2-dimensional vector of rPC scores for the $i^{th}$ neuron, and $f_i(t)$ its (normalized) $\Delta F/F$ at time $t$.
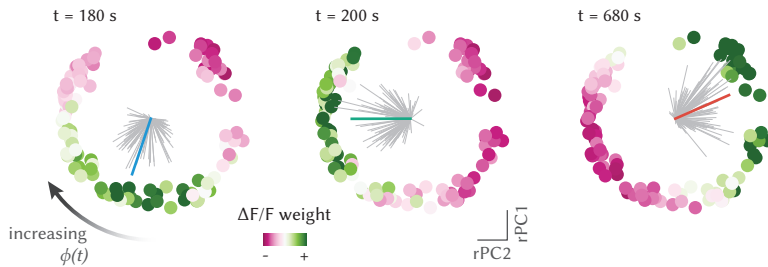


Figure 6.7: Network phase was computed as the angle of the vector average over all neuron projections in rPC space weighted by their (normalized) activation. In the plot, left, center, and right panels show the rPC projections color-coded by the state of activation of neurons at three different time points. Gray lines show the weighted vector of each neuron, and the thick line their average, color-coded by their angle. Note how the angle definition and the colors match the legend defined in Figure 6.5.

The *network phase* $\phi(t)$ is then defined as the angle $\phi(t)$ subtended by this vector **v**$(t)$ subject to the same conventions as the $\alpha_i$s defined above Figure 6.5:

- $\phi = 0$ corresponds to caudal neurons being active
- increments in $\phi$ correspond to activity rotating clockwise, and decrements of $\phi$ to activity rotating counterclockwise

Therefore, $\phi = 0$ corresponded to the activation of the network in the rostral part, $\phi = \pi/2$ to activation of the left part, $\phi = \pm\pi$ to activation in the rostral part, and $\phi = 2$ to activation in the right part (Figure 6.5). For all further analyses, the *unwrapped* or cumulative phase was used (unwrap function from numpy), *i.e.* every discontinuity at $\pi$/-$\pi$ was removed adding to parts of the trace an offset $2k\pi$ for some integer $k$.

## Calculation of average activity profile

To estimate the average activation profile of the network across the ring of neurons, we started by interpolating the neuron's traces to a matrix spanning the interval $-\pi$ to $\pi$ in 100 bins (Figure 6.8).
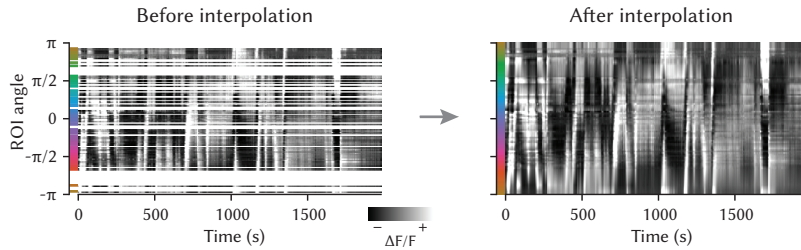


Figure 6.8: Interpolation of network activity from neuron angles. *Left*, Traces of individual neurons sorted and spaced in $y$ using their angle $\alpha_i$. The colors on the left map neuron angles. *Right*, The same activity, after interpolating the activation between $-\pi$ and $\pi$.

Then, we circularly shifted each column of the matrix so that the phase, and hence the network activation peak, was always positioned at the center of the matrix (Figure 6.9). Finally, we calculated the average and standard deviation of the matrix across the time axis. To make sure the result was not the consequence of the resampling procedure, we also performed the circular shift of the raw matrix of traces, sorted according to neurons' $\alpha_i$, and we got consistent results (Figure 5.10).
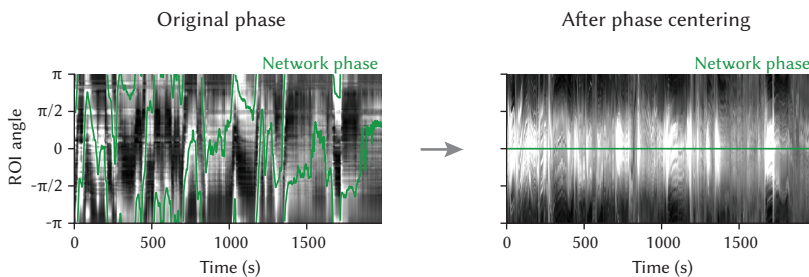


Figure 6.9: Phase-zeroing process: for every time point, a circular permutation of the (interpolated) activity matrix was computed so that the peak of activation, mapped by the phase (*left*), was always in the center of the matrix. *Right*, The matrix of traces, after the interpolation.

## Estimated heading calculation and correlation with phase

To compute estimated heading for the analysis reported in Figures 5.17 and 5.18, we estimated the instantaneous angular velocity as the laterality index value for each individual swim (see *Behavior data preprocessing*), and we integrated it over time to obtain an estimated heading direction for the head-restrained fish.

We note that although the relationship between the laterality index and the fish orientation change in freely swimming animals is highly linear, the slope of the linearity is not necessarily one; moreover, the precise extent of the tail that is tracked, the embedding procedure, and the fact that the head is immobilized in agarose for our head-restrained imaging experiments are all parameters that can impact on the precise kinematic of the tail movements and make a precise numerical comparison between head-restrained and freely swimming experiments difficult. Therefore, we did not aim at reconstructing a fully realistic estimated heading direction, and relied on quantifications that were either aimed at just capturing the correlation between estimated heading changes and network phase changes, or
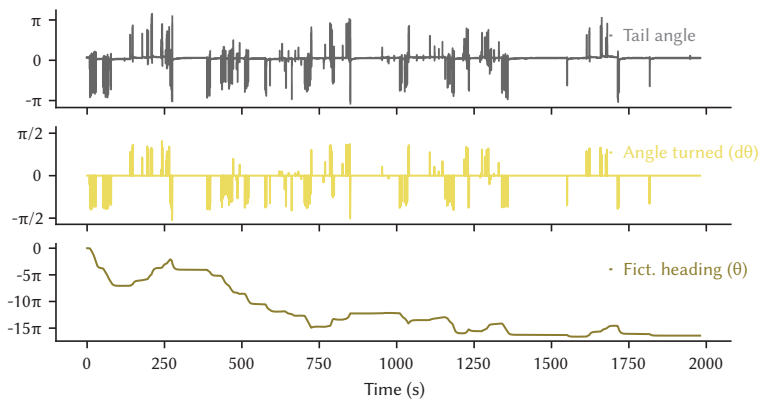
Figure 6.10: Calculation of the fish heading estimate. *Top*, Raw tail trace. *Middle*, Laterality index for each swim. *bottom*, Cumulative sum of laterality indexes of swims.

quantified the slope coefficient between the two quantities in relative comparisons within one experiment (for the visual feedback and gain change experiments).

For the results reported in Figure 5.18, we calculated for each fish the correlation between heading and phase in a rolling window of 300 s (10 overlaps for each window), and the same correlation but using a non-overlapping 5 min epoch of the heading trace for the shuffle distribution. The moments reported in Figure 5.18 refer to this population of intervals and shuffle intervals for each fish.

For the directional swim-triggered and saccade triggered analysis of Figure 5.14, we cropped for each fish the phase around each event, we computed a fish average for all curves with at least 3 cropped samples, and we subtracted the mean of the 10 s interval before the event.

### Heading/phase slope fitting for visual feedback experiments

In the experiments reported in *The aHB ring attractor network is not affected by visual inputs*, we wanted to quantify whether the presence of closed-loop visual feedback or the effect of different gain parameters of the closed loop visual feedback had an effect on the relationship between the change in heading and the phase of the network. As swims often happen in sequences and the average network phase change seems to plateau after approx. 5 s from the focal swim, we decided to look at the relationship between the amount of phase changed in a window between 15 s to 20 s after the swim, and the amount of estimated heading change in the same interval (which will potentially accumulate also the effect of other swims in the sequence).

The choice of the window was arbitrary, and all the results hold with other intervals in the 5 s to 20 s range. To quantify this relationship, we performed linear regression on the ($\Delta_{heading}$, $\Delta_{phase}$ phase) points for all swims in each experimental condition (Figure 6.11 shows this calculation for all fish), and we compared the values of the regression slope across conditions (Figure 5.19).

## Left and right swim and gaze angle regression

To understand whether in the region there was activity related to left and right swims, we performed a regressor-based analysis. A set of regressors was built by convolving with an exponential decay function an array that was zero everywhere and 1 in correspondence of either left or right swims (for Figure 5.20) or with the gaze direction array (for Figure 5.23).
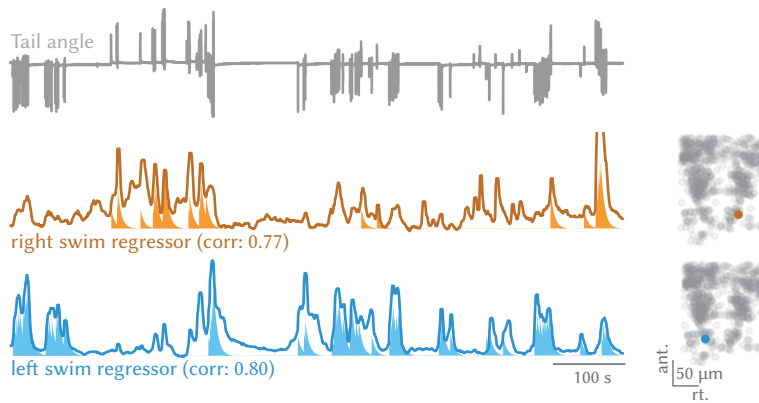


Figure 6.12: *Left*, Example traces for right and left swims-selective neurons together with the fish tail trace, and *right*, their anatomical location, shown on top of a scatter plot of all ROIs from the same fish. The regressors are shaded below the traces, and the correlations of the traces with the regressors are reported in the plot.

The time constant used was 3 s; the value was higher than the GCaMP6s time constant, but was chosen as it matched more closely the experimentally observed curves. The exact value of the time constant was not critical for the reported results. Each cell's fluorescence trace was then correlated with both regressors, and the correlation values were used for the analysis and visualizations in Figure 5.20, Figure 5.21 and Figure 5.23. In the maps of Figure 5.20 and Figure 5.21 left- and right- swim related cells were defined by including in the category cells with a correlation with left- or right-swim regressor > 0.7, and correlation with the other regressor < 0.7.

## Multilinear regression of eye and tail to network phase

For addressing the relationship between network phase and eye motion, we used the gaze direction, computed as the average between the two eyes angles. For the regression analysis, we used the gaze velocity or the instantaneous fish angular velocity estimated from the swim laterality indexes (both convolved using the same tau as in *Left and right swim regression*), either alone or in combination to fit the temporal derivative of the (unwrapped)

network phase.
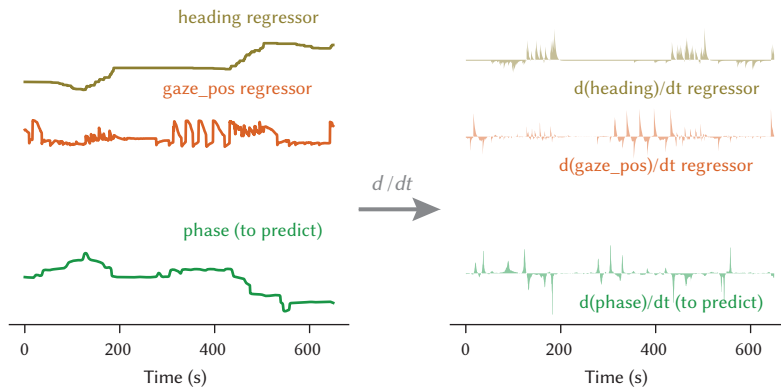


Figure 6.13: Illustration of the procedure for fitting the phase. We performed either linear regression or multiple linear regression to fit the network phase from heading and/or gaze. *Right*, For the fit we used the time derivatives of those quantities.

As a multilinear regression is likely to outperform the regression using only one of the two regressors just by overfitting, we cross-validated the analysis by first calculating the regression values on a randomly drawn epoch of 5 min of the experiment, and calculated the correlation of the phase derivative and the predicted phase derivative in a test 5 min epoch, drawn randomly by making sure it did not overlap with the fit window. The random sampling was repeated 500 times, and the plot in Figure 5.22 reports for each fish the moments of the population of these draws.

### serial block-face electron microscopy data skeletonization

The first reconstructions of cells in the aHB with processes in the IPN were observed by seeding for reconstruction dendrites or axons in the IPN and reaching from there somas in the aHB, in the context of a (still unpublished) broader reconstruction effort. The IPN location in the SBEM stack was firstly inferred by the recognizable organization of the neuropil and cell somata in the rhombomere 1 ventral region. Then, it was confirmed by the tracing of axons that could be reconstructed back to the habenulae through a long bundle of fibers unambiguously identifiable as the fasciculus retroflexus by its course (unpublished data). After those first observations, additional cells with the soma in the aHB were seeded based on the similarity of their processes with already reconstructed cells.

Skeletonization was performed manually by a team of annotators at ariadne.ai ag (Buchrain, Switzerland). Annotators were instructed to flag difficult locations without extending the skeleton at those locations, and to stop tracing after a total time of 2 h was reached. At that point, or when a cell was completed, a quality check was performed by an expert annotator. Difficult locations were then decided by the expert, and sent back to the annotator team for additional tracing if necessary. This procedure was iterated until all cells were fully traced. The skeletons were then annotated to distinguish the dendrite and the axon by their morphological features (processes thickness and presence of presynaptic boutons) independently by Ariadne expert annotators or the authors, with convergent results. All further analyses and quantification of the reconstructions were performed using Python. To calculate the centroid position of dendrite and axon for

the analyses in Figure 5.29, we took the average coordinate of the coordinates (in IPN reference space) of all the branching points of dendrites and axons. To generate the distance plot in Figure 5.31, bottom we calculated for every branching point of every neuron the distance along the frontal and sagittal axis of all the other branching points (of both axons and dendrites) and show the distribution of such distances.

subsectionAnatomical registrations

To work with the anatomical spaces and their annotations, we used the BrainGlobe `bg-atlasapi` package [27] and either the larval zebrafish brain reference MapZeBrain [28], or a custom lab reference of the aHB and IPN region that will be published together with the data, created by morphing together stacks from different lines using either `dipy` [29] or `CMTK` [30]. To visualize functional data in the references, an average anatomy computed after centering all stacks with the centering point described in (*Lightsheet imaging data preprocessing*), and then a manual affine registration was performed to the IPN reference. A similar procedure was used to map the electron microscopy data. From the skeletons, a density stack was computed in which the shape and features of the IPN were prominently visible. An affine matrix transformation was found to match this stack on the IPN reference, and used for transforming the neuron's coordinates. The masks delimiting the IPN and the dIPN were drawn in the IPN reference atlas looking at the localization of habenular axons afferents to the region.

### 2D auto-correlation of the neuronal activity

For the plots reported in Figures 5.30 and 5.31, two-photon microscopy images from a single plane in the IPN were aligned to the frontal and sagittal axes of the brain. The dorsal IPN in the images were masked by manual drawing. The area inside of the mask was divided into $3.5\,\mu m \times 3.5\,\mu m$ square bins. The average fluorescence signal at each bin was z-scored. For each bin, Pearson correlation of the signal traces between the focal bin and all other bins were computed (as shown in Figure 5.30), and sorted in two dimensions by the distances between two bins in the frontal and sagittal axes (for Figure 5.31). The correlation coefficients at the same distance were averaged across bins for each animal, and then averaged across animals.

[27] Claudi, Petrucco, et al., "BrainGlobe Atlas API: a common interface for neuroanatomical atlases".

[28] Kunst et al., "A Cellular-Resolution Atlas of the Larval Zebrafish Brain".

[29] Garyfallidis et al., "Dipy, a library for the analysis of diffusion MRI data".

[30] Rohlfing and Maurer, "Nonrigid image registration in shared-memory multiprocessor environments with application to brains, breasts, and bees".

# III

## Appendix

# *Software contributions* A

A crucial requirement for the experimental work reported in this thesis has been the collaborative development of many of the (open source) software resources upon which it builds. In this appendix, I provide a brief overview of such resources. Since the very first days in the lab, I have been exposed to the importance of writing code that can be easily reused, tested, and understood and tested by fellow researchers. Python is an extremely powerful language in this sense[1], and has been used in all parts of this work. Python provides scientists with a high level language that can be extended in its usage with tens of thousands of packages that make it suitable for countless applications, from high level statistics to heavy numerical computations, from hardware control to data visualization.

[1] E. Muller et al., "Python in neuroscience".

In the day-to-day writing and usage of Python-based software, scientists face an important trade off. On the one hand, there are the requirements for specificity that running a particular setup (with some given camera, configuration, *etc.*) or analysis (requirements for input data formatting, definition of a pipeline, emphetc.). On the other, there is the need to reuse as much as possible of the code that we write, not to reinvent the wheel every time. However, using again code from the past is hard, as it has to be:

- accessible: one should not be wasting time looking for old code in forgotten locations
- reliable: one of the highest barriers for using old code is trusting its correctness when we are using it as a black box
- general: it has to be written in a way that can cover our present needs

Python offers a very suitable framework for creating code that satisfies those requirements. When the opportunity for reusing code presents itself, for example at the first steps of the analysis of imaging or behavior data which are always the same independently of the experiment, functions and classes can be easily collected in a Python package. The package is version-controlled (in our lab using GitHub), and it is always accessible from any machine at the repository location. Moreover, it can be uploaded to the Python Package Index (PyPI), and, once there, be made available in any machine after a simple installation: `pip install package_name`.

Over the years we have been creating an ecosystem of packages that are reciprocally integrated, and cover all the experimental flow of the lab. There are packages for controlling the tracking of the animal and the presentation of multimodal stimuli in open- and closed-loop (`Stytra`) and for running the hardware of a lightsheet microscope (`Sashimi`) or a two-photon

microscope (`Brunoise`); packages to help with the preprocessing of imaging data (`fimpy`) and behavior data (`bouter`); and packages that help with the organization and the visualization of processed data. In this last category, I have launched the BrainGlobe initiative together with collaborators at the Sainsbury Wellcome Centre for Neural Circuits and Behaviour, for the development of tools for computational (neuro)anatomy that share a standard format for brain atlases and coordinate systems.

In this appendix I provide a brief overview of the main Python packages that I contributed to develop. For `Stytra`, `Sashimi`, `fimpy` and `bouter` the development effort has been lead by Vilim Štih, a former graduate student who structured most of the software infrastructure of the lab.

## A.1   Stytra

`Stytra` is a flexible, open-source software package, designed to cover all the general requirements involved in larval zebrafish behavioral experiments. It provides timed stimulus presentation, interfacing with external devices and simultaneous real-time tracking of behavioral parameters such as position, orientation, tail and eye motion in both freely-swimming and head-restrained preparations. `Stytra` logs all recorded quantities, metadata, and code version in standardized formats to allow full provenance tracking, from data acquisition through analysis to publication. The package is modular and expandable for different experimental protocols and setups. Current releases can be found at https://github.com/portugueslab/stytra, and the package is uploaded to PyPI and `pip`-installable. We have also written an thorough documentation with examples for extending the package to new stimuli and hardware, as well as a schema and parts list for behavioral setups.

When generating a new experimental protocol in `Stytra`, the developer can just focus on the features of the stimuli that are presented (`Stytra` comes with a library of implemented visual stimuli, and additional stimuli can be generated in Python and executed). Once the experimental protocol is scripted, it can be run over multiple setups with different configurations and camera models. `Stytra` handles the stimulus presentation and behavioral tracking in the backend, and offers a graphical user interface that can be used to enter experiment metadata, preview the tracking, and adjust experimental parameters.

In the lab, `Stytra` has proven crucial to allow people to autonomously prototype and deploy on the setups their experimental protocols. Not only it lowers the expertise required to start running autonomously an experiment, but it also strengthens reproducibility by decoupling the flow of the experiment, that can be shared between laboratories and setups, and the hardware control. Since `Stytra` has been introduced in the lab, sharing the code that generated an experimental protocol with the rest of the analysis code has been very easy (for an example, see Markov et al., "A cerebellar internal model calibrates a feedback controller involved in sensorimotor control").

We have also received support requests from many other laboratories, mainly from the zebrafish community but also from researchers doing neu-

roscientific experiments in rats and flies. `Stytra` can serve as a platform to design behavioral experiments involving tracking or visual stimulation with other animals - for example, we provided an example integration with the DeepLabCut neural network-based tracking method Štih, Petrucco, Kist, et al., "Stytra: An open-source, integrated system for stimulation, tracking and closed-loop behavioral experiments". Our aim is to enable more laboratories to easily implement behavioral experiments, as well as to provide a platform for sharing stimulus protocols that permits easy reproduction of experiments and straightforward validation.

`Stytra` is constantly undergoing improvements and further development, and we have been awarded a grant from the Kavli foundation to support the export of Neurodata Without Borders ( `.nwb` ) files to share experimental data collected using `Stytra` using this format, that has been adopted by an increasing number of neuroscientists.

## A.2   Sashimi

`Sashimi` is a user-friendly software for efficient control of digital scanned light sheet microscopes. While built for a particular microscope configuration, the modular architecture allows for easy replacement of hardware by other vendors to support other cameras, boards and light sources. A version of the software to control a camera in a Light Field Microscope setup is currently being developed. In the backend, `Sashimi` leverages th `nidaqmx` package, which provides an API (Application Programming Interface) for interacting with the NI-DAQmx driver, to control the scanning of the objective and the laser beams (see *Lightsheet microscope*). In the frontend, `Sashimi` relies on the fast, multidimensional Napari viewer to stream live, during the experiment, a preview of the data that is being collected. `Sashimi` saves files in a custom format that allows for data chunking and parallel processing in downstream analyses, supported by the `splitdataset` package (see A.3).

## A.3   `bouter` *and* `fimpy`

For analysing behavioral data from zebrafish larvae, there are some very general quantities that always need to be estracted, such as the time of occurrence of the discrete swims of the larvae (bouts), and their properties (duration, maximum tail amplitude, directionality index...). Moreover, some additional filtering that enforces spatial and temporal continuity for the fish position and the angles of the tail segments have to be applied. To perform those preprocessing steps, and to provide a simple interface for data loading, we created the `bouter` package ([2]). In bouter we provide users with a `Experiment` class to easily load data from a `Stytra` experiment, and functions to perform the required pre-processing steps from the behavior data.

For the analysis of calcium imaging data, we have written `fimpy`. This package contains functions for all the preliminary steps required to extract fluorescent traces from raw imaging stacks, from alignment of the source data to anatomy-based or voxel correlation-based procedures for ROI detection and fluorescence signal extraction. As mentioned above, imaging

[2] Štih, Petrucco, Prat, et al., *Bouter*.

data are saved in `splitdataset` format, chunked over multiple files on the disk. `fimpy` functions can be run in parallel over those chunks, which is important for two reasons. First, raw data, which can be up to hundreds of gigabytes, does not have to be entirely loaded in memory to be processed. Second, operations can be run in parallel over different data chunks by different cores of the CPU, resulting in a significant speed-up of the data processing. Thanks to further optimization of the key functions, which are compiled from Python to optimized machine code at runtime using `numba`. Overall, `fimpy` can align and segment ROIs from one hour of volumetric whole-brain imaging in two to three hours.

## A.4    The BrainGlobe initiative

The BrainGlobe Initiative exists to facilitate the development of interoperable Python-based tools for computational neuroanatomy. BrainGlobe goals are the development of a core infrastructure to facilitate others to build interoperable tools in Python, the development of specialist software for specific analysis and visualisation needs, and the creation of community of neuroscientists and developers who share knowledge, build software and engage with the scientific and open-source community.

BrainGlobe was born from the realization that many of the useful tools that are being developed for computational neuroanatomy (the analysis and visualization of neuroanatomical data in standard coordinate systems) were limited to a single brain atlas in one species, and they weren't compatible or interoperable with any other software. To solve this problem, we developed the BrainGlobe Atlas API. This API provides a common interface for programmers to download and process brain atlas data from multiple sources. All BrainGlobe software is built around this API, which means that all the software is compatible, and can be used with different atlases, in different species.

Many tools are being developed using the BrainGlobe Atlas API as a backend to the atlas of choice. Below, I will present `brainrender`, whose development I have contributed to after the launch of BrainGlobe. By developing it under the BrainGlobe initiative, this tool, originally based on the Allen Brain Atlas mouse brain, can now be used with all the animal species that have an atlas in BrainGlobe, including the larval zebrafish.

### bg-atlasapi

Many excellent brain atlases exist for different species. Some of them have an API (application programming interface) to allow users to interact with the data programmatically (e.g. the excellent Allen Mouse Brain Atlas), but many do not, and there is no consistent way to process data from multiple sources. The brainglobe atlas API (`bg-atlasapi`) deals with this problem by providing a common interface for programmers to download and process data from multiple sources.

Each atlas consists of data files in a common format:

- A *reference* image of a brain ( `.tiff` )

- An *annotation* image, with each brain region defined by a unique pixel value ( `.tiff` )
- A structure hierarchy with numbering consistent with the *annotation* ( `.json` )
- Metadata defining the shape, orientation etc. of the data, and other info such as animal species and authors ( `.json` )
- Meshes defining the surface of each brain region ( `.obj` )

When queried for an atlas, `bg-atlasapi` will check if it is available in a dedicated local folder, and if it is not, it will automatically download it from a repository of atlases served through the G-Node initiative GIN servers.

A number of atlases are in development, but those available currently are listed in table A.1.

Table A.1: List of atlases available in BrainGlobe.

| Atlas name | Species | Resolution |
|---|---|---|
| Max Planck Zebrafish Brain Atlas | Danio rerio | 1 µm |
| Adult Zebrafish Brain Atlas | *Danio rerio* | 4 µm |
| Allen Mouse Brain Atlas | *Mus musculus* | 10, 25, 50, 100 and 500 µm |
| Enhanced and Unified Mouse Brain Atlas | *Mus musculus* | 10, 25, 50 and 100 µm |
| Osten Mouse Atlas | *Mus musculus* | 10, 25, 50 and 100 µm |
| Waxholm Space Atlas for the Rat Brain | *Rattus norvegicus* | 39 µm |
| Allen Human Brain Atlas | *Homo sapiens* | 500 µm |

More atlases for other species such as birds, bats and macaque, are being developed thanks to the work of external collaborators, showcasing the importance of opening such open-source initiatives to the contributions of the community.

## brainrender

`brainrender` is a package for the visualization of three dimensional neuro-anatomical data. It can be used to render data in the coordinate spaces of any of the atlases available in the BrainGlobe common format. The goal of `brainrender` is to facilitate the analysis and description of neuro-anatomical data by easily generating high-quality 3D renderings. In `brainrender`, neuroanatomical visualizations outlining the brain profile and the borders of any brain structure of interest can easily be achieved by specifying which brain regions to include in the rendering with a few lines of code. `bg-atlasapi` is used to load the 3D data and subsequently renders them (Figure 1B). Moreover, points representing the location of cells detected in whole-brain experiments as well as fiber tracts or probe locations can be easily added to the visualization. The anatomical visualizations in *Results and discussion* have all been created using `brainrender`.

# Historical notes

In this appendix we discuss the first known description of the habenulo-interpeduncular circuit by Forel. After a brief introduction on the figure of Forel, we report a trascription from the sections of the publication that concern the description of the habenula, the interpeduncular nucleus and the fasciculus retroflexus, and the relative illustrations.

## B.1  Auguste Henri Forel

Auguste Henri Forel (1848-1931) was a Swiss myrmecologist, neuroanatomist, and psychiatrist.

After having studied medicine in Zurich while dedicating summers to the study of myrmecology, Forel earned a doctorate in Vienna in 1872 under the supervision of the Austrian anatomist and psychiatrist Theodor Meynert(1833-1892). He later moved to Munich, where he worked as Assistant Physician under the supervision of Bernhard von Gudden (1824-1886), the director of Munich's asylum in Kreis-Irrenanstalt. Under Gudden supervision, he improved the so called *Gudden's microtome*, a device that allowed him to conduct histological studies in slices of entire brains from humans and other mammals.

The results of his four-year long work were presented in an extensive publication: Forel, "Untersuchungen über die Haubenregion und ihre oberen Verknüpfungen im Gehirne des Menschen und einiger Säugethiere, mit Beiträgen zu den Methoden der Gehirnuntersuchung" (*Studies on the tegmental region and its ascending connections in the brain of man and various mammals*). This paper proved to be a cornerstone in our understanding of the organization of the tegmental region of vertebrates. There, among a plethora of other beautiful observations, the organization of the habenulo-interpeduncular tract and its related nuclei was laid out in full for the first time.

When describing it, Forel observes that it *"is extremely intensely stained with carmine"* and that it *"contains masses of round or ribbon-shaped, dark-appearing, more or less sharply defined small nests"* which *"do not look very dissimilar to the glomeruli of the olfactory bulb of the rabbit"*. The phrasing that Forel uses is fasciating, as it describes the presence of structures resembling *glomeruli* in the interpeduncular nucleus. We are left with the impression that those structures, largely overlooked in the most recent literature (see *Glomeruli in the IPN*), might very well have been known by the first descriptor of this region.

Another prominent pupil of Meynert was Sigmund Freud, who moved some if his first steps in the clinical psychiatry in his clinic in 1883.

von Gudden was another prominent figure in the history of neuroanatomy and psychiatry. While serving as the Kreis-Irrenanstalt asylum director he was also providing care for the Bavarian royal family. In 1886 he was assigned the delicate task of assessing the mental equilibrium of King Ludwig II (1845-1886), who was considered mad and unfit to reign for his extravagant behavior. Both Ludwig II and Bernhard von Gudden were found dead two days after the deposition and confinement of the King in the Starnberg Lake close to the castle of Berg. Although they were reported as having drowned either by accident or as the consequence of a suicidal move by the king, the details surrounding their deaths remain unclear.

Regular bike rides to the beautiful areas close to Starnberg Lake were essential part of this thesis author's life in Munich long before the historical connection with the thesis subject came out.

## B.2    Untersuchungen über die Haubenregion *by Forel*

Here we report an excerpt (pp.465-468) from of the original article, *Untersuchungen über die Haubenregion und ihre oberen Verknüpfungen im Gehirne des Menschen und einiger Säugethiere, mit Beiträgen zu den Methoden der Gehirnuntersuchung* (Investigations on the tegmental region and its upper connections in the brain of man and some mammals, with contributions to the methods of examination of the brain.), published by Auguste Forel in 1877 in the *Archiv für Psychiatrie und Nervenkrankheiten*, together with a digitalization of the original figures that refer to his description. The text was obtained with the help of Prof. Adrian Danek, who also provided useful historical background. Translation from German was possible thanks to the help of Katharina Kötter and Prof. Mario Wullimann.

[...]

13. Meynert'sches Bündel.

Es bleibt uns endlich das paarige von Meynert zuerst beim Menschen entdeckte und von ihm, "Haubenbündel des Ganglion Habenula" genannte runde Faserbündel mit seinen Verbindungen zu besprechen. Da dasselbe nicht in die Haube übergeht, und somit sein Name unhaltbar ist, erlaube ich mir, es Meynert'sches Bündel zu nennen. Nach Flechsig wird es erst beim 44 cm. langen Fötus des Menschen markweiss. Früher (a. a. O.) habe ich dasselbe als obere Begrenzung der Haube angegeben, eine freilich etwas willkürliche, doch in Ermangelung einer besseren Grenze hier beizubehaltende Annahme. Ich habe damals die Mächtigkeit dieses Bündels beim Meerschwein und bei der Fledermaus hervorgehoben. Seine Fasern sind sehr rein, zerfallen nicht wie diejenige der Radix (Columna) anterior Fornicis in secundäre Bündel, sondern bilden einen gleichmässigen Strang. Auch bleibt es bei niederen Säugern nicht so schön markweiss wie die Gewölbwurzel, sondern färbt sich rosa mit Carmin, besonders im Querschnitt. Dass es beim Menschen gebogen am medialen Rand des RK verlauft und daselbst oft dessen Substanz eine kurze Strecke durchbohrt, was Luys einen Hilus des RK vorgetäuscht hat, haben wir oben (Bindearm und RK) gesehen. Bei niederen Säugethieren berührt dieses Bündel den hier schon weiter unten aufhörenden kleineren RK gar nicht, liegt direct oberhalb desselben und wird daher auch nicht von ihm verschoben, so dass es compact und ganz scharf begrenzt schnurgerade vom Ganglion Habenulae zum Ganglion interpedunculare verläuft (Fig. 27 Hbd). Beim Menschen und schon beim Affen muss es seinen Weg, wie Meynert

[...]

13. Meynert's bundle.

It finally remains for us to discuss the paired bundles of fibers that Meynert first discovered in humans and his connections, called the *tegmental bundle of the habenula ganglion*. Since the paired bundle does not go into the tegmentum, and thus its name is untenable, I take the liberty of calling it *Meynert's bundle* (called *fasciculus retroflexus* nowadays, NdT). According to Flechsig, it only becomes white matter (literally, *marrow*) in the 44 cm long human fetus. I stated the same as the upper limit of the tegmentum in an earlier publication (op. cit. (?)), an assumption that is admittedly somewhat arbitrary, but should be retained here in the absence of a better one. There, I emphasized the thickness of this bundle in Guinea pigs and in bats. Its fibers are very pure, do not disintegrate into secondary bundles like those of the radix (columns) of the anterior fornicis, but form an even cord. In lower mammals, too, it does not remain as beautifully marrow-white (see above) as the vault root, but it looks pink when stained with carmine, especially in cross-section. We have seen above that in humans it is curved and runs along the medial edge of the red nucleus (RK: roter Kern) and there often pierces its substance a short distance, which appeared as a hilus of the red nucleus to Luys ... (*untranslatable*). In lower mammals this bundle does not even touch the smaller red nucleus: it lies directly above it and is therefore not displaced by it, so that it runs, compact and very sharply delimited, as a straight line from the ganglion habenulae to the ganglion interpedunculare (labelled as *Hbd* in Fig. 27). In humans and even in monkeys, as Meynert showed, it has to find its way through

Figure B.1: The original illustrations by Forel of the sections of the midbrain that contain elements of the habenulo-interpeduncular circuit. *Top* Selection of slices from a series of frontal cross sections cut through a human brain and stained with carmine. *Bottom, left.* Left half of a cross-section of the brainstem of a dog, stained with carmine. *Bottom, right* Stem parts of a sagittal section of the rabbit brain, stained with carmine. G.L.p.p.: *Ganglion interpedunculare*, G.hab.: *Ganglion habenula*, RK: *roter Kern*, Hbd.: *Meynert's bundle (fasciculus retroflexus)*

zeigte, durch eine S-förmige Schlängelung finden (Fig. 4-9 Hbd). Dieses Bündel stellt eine der am Klarsten daliegenden Faserbahnen des Gehirnes dar. Unzweideutig ist sein Verlauf sowohl in Quer- als in Sagittal- und anderen Schnittreihen aller Säugethiere, die ich untersuchte. Das von Stieda (Wirbelth. S. 113; Fig. 45 u. 46 ft.) bei der Maus ohne Bezeichnung beschriebene und abgebildete Bündel kann kaum etwas anderes sein als das Meynert'sche Bündel. Stieda lässt es richtig in seiner Substantia cinerea media (= Ganglion interpedunculare) entstehen, irrtümlich aber dorsalwärts sieh in den Thalamus ausbreiten. Meynert dagegen hat seine dorsale Verbindung richtig erkannt, lässt es aber ventral- und abwärts als sagittal verlaufendes Hauben- bündel sich fortsetzen, was durchaus unrichtig ist; ebenfalls irrig ist die Angabe Meynert's, es sei beim Menschen ein mätchtiges Bündel. Die Endigung bei- der Meynert'schen Bündel in das unpaarige Ganglion interpedunculare kennt Prof. Gudden schon seit vielen Jahren (lange vor dem Erseheinen von Stieda's Arbeit). Dieselbe ist an der Sagittalschnittreihe vom Kan- inchengehirn (Fig. 27 Hbd. G. L. pp.) so unzweideutig und schön zu sehen, dass jeder Zweifel fallen muss. Wir müssen nun beide Ursprungsganglien dieses Bün- dels näher betrachten. Dieselben sind bei niederen Säugethieren weitaus am schönsten ausgebildet.

14. Lamina perforata posterior und Ganglion interpedunculare. Die Lamina perforata posterior des Menschen, Substantia perforata posterior, Sub- stantia perforata media von Vicq d'Azyr, Pons Tarini, Spatium interpedunculare Cruveilhier (nach Henle) ist eine Lage grauer Substanz, welche, von vielen Gefassen durchlöchert, den concaven medialen Theil der ventralen Oberfläche der Haube, zwischen Pons, Corpora mammillaria und beiden Hirnschenkelfüssen bildet. Diese graue Substanz setzt sich in die Raphe dorsalwärts fort und bildet somit, wie Henle es be- merkt, im Querschnitt ein umgekehrtes T (⊥). Ihr medialer ventraler Theil, also die Verbindungsstelle beider Schenkel des ⊥ ist beim Menschen nicht auf- fallend von der übrigen Substanz differenzirt. Bei niederen Säugethieren dagegen, schon beim Hund, sehr schon aber bei den Nagern, beim Maulwurf, bei der Fledermaus, sondert sieh an dieser Stelle im unteren Abschnitt der Lamina perf. post. ein ganz scharf begrenztes unpaariges, im Querschnitt stumpf dreieckiges (mit dem Scheitel dorsal gerichtet), im Sagittalschnitt längliches, ziemlich mächtiges Gan-

an S-shaped winding (*Hbd* in Fig. 4-9). This bundle represents one of the most obvious fiber tracts of the brain. Its course is unambiguous, both in transverse and in sagittal and other sectional series of all mam- mals which I have examined. The bundle described and depicted by Stieda in the mouse without a desig- nation (Wirbelth. P. 113; Figs. 45 and 46 ft.) can hardly be anything other than Meynert's bundle. Stieda cor- rectly lets it arise in his substantia cinerea media (= ganglion interpedunculare), but describes it mistak- enly as extending dorsally into the thalamus. Meynert, on the other hand, has correctly recognized its dorsal connection, but describe it as extending ventrally and downwards as a sagittal tegmental bundle, which is completely incorrect. Meynert's statement that it is a heavy bundle in humans is also erroneous. Prof. Gudden has known the termination of both Meynert's bundles in the unpaired ganglion interpedunculare for many years (long before Stieda's work began). This can be seen so clearly and beautifully in the sagittal series of sections of the rabbit brain (*Hbd* and *G. L. pp.* in Fig. 27) that it is settled now beyond doubt. We now have to take a closer look at both ganglia of origin of this bundle. These are by far the most beautifully developed in the lower mammals.

14. Lamina perforata posterior and ganglion interpedunculare. The *human lamina perforata posterior*, *substantia perforata posterior*, *substantia perforata media of Vicq d'Azyr*, *Pons Tarini*, *Spatium interpedunculare Cruveilhier* (after Henle) is a layer of gray matter which is perforated by many vessels, and forms the concave medial part of the ventral surface the tegmentum, between the pons, corpora mammil- laria and both cerebral peduncles. This gray matter continues dorsally in the raphe and thus, as Henle notes, forms an inverted T in the transverse section (⊥). Its medial ventral part, that is, the junction of the two legs of the ⊥, is not noticeably differentiated from the rest of the substance in humans. In the case of lower mammals (in the dog, but even more promi- nently in rodents, in the mole and in the bat), on the other hand, we can observe in the lower section of the Lamina perforata posterior an unpaired ganglion quite prominent and very sharply demarcated, shaped as an obtuse triangle (with the apex directed dorsally) in cross section and elongated in the sagittal section. This ganglion is called *ganglion of the lamina perforata*

glion ab, das man Ganglion der Lamina perforata posterior, oder besser nach dem Vorsehlag von Prof. Gudden Ganglion interpedunculare (* Alte, aber noch nicht veröffentlichte Benennung von ihm) nennen kann (Fig. 27 G. L. pp.). Dieses Ganglion wird von Meynert ( Stricker , Fig. 230 und 231 Lp) bei Vespertilio abgebildet und als Lamina perforata posterior bezeichnet, was also nur zum Theil richtig ist. Die Substantia cinerea posterior media von Stieda (a. a. O.) scheint dem Ganglion interpeduncoulare zu entsprechen.

Es besteht dieses Ganglion beim Kaninchen aus einer sieh ungemein intensiv mit Carmin färbenden Grundsubstanz, welche an Durchschnitten massenhafte rundliche oder bandförmige, dunkel erscheinende, mehr oder weniger scharf ausgeprägte kleine Nester enthält, die den Glomeruli des Bulbus olfactoriuns vom Kaninchen nicht ganz unähnlich sehen, jedoch aus mir unklaren Elementen bestehen. Ausserdem ist das Ganglion von dicht angehäuften, meist sehr kleinen rundlichen oder spindelförmigen Ganglienzellen ausgefüllt, deren kleinste von den „Körnern" der Grundsubstanz kaum mehr zu unterscheiden sind. In dieses unpaare Ganglion nun strahlen, sich pinselförmig in ihm ausbreitend und verlierend, die unteren Enden der beiden Meynert'schen Bündel ein, das eine rechts, das andere links, nachdem sie vorher rasch nach unten sich umgebogen hatten (Fig. 27 Hbd., G. L. pp.). Beim Hund sind die Verhältnisse gleich, nur enthält das Ganglion weniger dunkle Nester, wobei die kleinen Nervenzellen um so deutlicher hervortreten. Beim Menschen lässt sich kein deutliches Ganglion von den übrigen Theilen der Lamina perforata posterior abgrenzen. Doch scheint das hier kleinere Meynert'sche Bündel in denselben, dem Ganglion interpeduncolare der niederen Säugethieren entsprechenden medial-ventralen Theil der Lam. perfor. post. einzustrahlen. Jedenfalls sind die Verhältnisse ungleich verwickelter als bei niederen Säugethieren, und es ist leicht begreiflich, wie Meynert eine Fortsetzung des Bündels in die Haubenfaserung annehmen konnte, indem er dasselbe beim Menschen studirte. Beim Affen (Macacus) sind die Verhältnisse nahezu wie beim Menschen.

15. Ganglion habenulae. Das paarige Ganglion habenulae, von Meynert so genannt, wurde auch von Stieda (Vögel und Säugethiere S. 80; Wirbelthiere S. 113) ohne Benennung bei der Maus beschrieben. Es

posterior, or better, after the suggestion of Prof. Gudden, *ganglion interpedunculare* (the denomination is not new, but this term has not yet been published) (*G. L. pp.* in Fig. 27). This ganglion is depicted by Meynert (Stricker, Figs. 230 and 231 Lp) in *Vespertilio* (a bat, t.n.) and called the *lamina perforata posterior*, which is only partially correct. The *substantia cinerea posterior media* of Stieda (op. cit.) seems to correspond to the ganglion interpedunculare.

In rabbits, this ganglion consists of a ground substance which is extremely intensely stained with carmine and which, in cross-section, contains masses of round or ribbon-shaped, dark-appearing, more or less sharply defined small nests which, however, do not look very dissimilar to the glomeruli of the olfactory bulb of the rabbit, but consist of elements that are unclear to me. In addition, the ganglion is filled with densely clustered, mostly very small, rounded or spindle-shaped ganglion cells, which can hardly be distinguished from the smallest "grains" of the background staining. The lower ends of the two Meynert's bundles then radiate into this unpaired ganglion, spreading out in the shape of a brush and fading out, one on the right, the other on the left, after they had previously bent down quickly (*Hbd.* and *G. L. pp.* in Fig. 27). In the dog the proportions are the same, only that the ganglion includes less dark nests, whereby the small nerve cells stand out much more clearly. In humans no clear ganglion can be delimited from the other parts of the lamina perforata posterior. But the Meynert bundle, which in humans is smaller, seems to radiate in the same medial-ventral part of the lamina Perforata Posterior" that corresponds to the ganglion interpedunculare of the lower mammals. In any case, the organization of the are is incomparably more complicated than in the lower mammals, and it is easy to understand how Meynert could believe there was a continuation of the bundle into the fibers of the tegmentum when studying it in humans. In the monkey (*Macacus*) the organization is similar to that in human.

15. Ganglion habenulae. The paired ganglion habenulae, thus named by Meynert, was also described by Stieda (birds and mammals p. 80; vertebrates p. 113) in the mouse without naming it. As

ist, wie Meynert angiebt, bei Säugethieren stärker als beim Menschen, und durch dichte Zellenanhäufung charakterisirt. Es liegt beiderseits von der hinteren Commissur und vom unteren Ende der dorsalen Abtheilung des III. Ventrikels, wo es eine deutliche Erhabenheit der dorsalen Oberfläche des centralen Höhlengraues medial vom Thalamus bildet. Jedes der beiden Ganglien wird von der entsprechenden Habena der Zirbel überzogen und vielleicht zum Theil durchdrungen. Das G. habenulae unterscheidet sich vom G. interpedunculare dadurch, dass es paarig ist, dann durch den Mangel der dunkeln Nester, und endlich durch die nicht so intensiv sich mit Carmin färbende Grundsubstanz; die Nervenzellen sind dagegen ziemlich ähnlich dicht angehäuft, fast so klein, doch etwas eckiger als im genannten Ganglion. Durch diese dichte Anhäufung kleiner Zellen ist es scharf vom übrigen centralen Höhlengrau sowie vom Thalamus abgegrenzt. Diese Verhältnisse sind beim Menschen weniger deutlich ausgesprochen als bei niederen Säugethieren; doch ist das Ganglion habenulae gut ausgebildet. Das Ganglion habenulae bildet so zu sagen den Knotenpunkt von drei Faserzügen, die theils ihn umgürten, theils in ihm sich zu zerstreuen scheinen. Es sind dies: 1) das eben besprochene Meynert'sche Bündel; 2) die paarige Markleiste am medial-dorsalen Rande des Thalamus Opticus, welche vom Haller lineae albae, von den Gebr. Wenzel (nach Burdach) und von Henle (a. a. O. S. 128, Fig. 70) Taenia Thalami optici, von Burdach Sehstreifen besonders genannt, von Meynert als dem Stratum zonale des Thalamus zugehörig angesehen, von den meisten, aber nicht von allen älteren Autoren einfach als Fortsetzung des folgenden Faserzuges betrachtet wurde; 3) das paarige Markbündel aus der Zirbel, welches Habena, Habenula, Zirbelstiel, Pedunculus Conarii genannt wird. Wie diese drei Faserbündel mit dem Ganglion habenulae zusammenhängen, in wie fern die Fasern derselben sich hier mit Zellen verbinden, odereinfach durchgehen und sich direct von einem Faserbündel in das andere fortsetzen, ist nicht genau zu eruiren. Ziemlich sicher scheint es nur bei Nagern zu sein, dass ein Theil der Taenia Thalami optici, direct über die dorsale Oberfläche des Ganglion habenulae hinweg laufeud, sich in den Pedunculus conarii fortsetzt, und dass ein anderer Theil derselben, dicht ventral vom Ganglion habenulae hinunterschlüpfend, in das Meynert'sche Bündel direct übergeht (Fig. 27). Letzteres habe ich schon früher (a. a. O. Sep. S. 15)

Meynert states, it is stronger in mammals than in humans, and is characterized by a dense accumulation of cells. It lies on either side of the posterior commissure and the lower end of the dorsal division of the third ventricle, where there is a distinct protrusion of the dorsal surface of the central gray cave medial to the thalamus. Each of the two ganglia is covered by the corresponding stone pine shaped habena perhaps partially penetrated. The ganglion habenulae differs from the ganglion interpedunculare by the fact that it is paired, the lack of dark nests, and finally by the base substance, which is not so intensely colored with carmine; the nerve cells, on the other hand, are clustered in a fairly similar density, almost as small, but somewhat more angular than in the ganglion interpedunculare. This dense accumulation of small cells distinguishes it is sharply from the rest of the central gray cavity and from the thalamus. These distinctions are less clearly visible in humans than in lower mammals; but the ganglion habenulae is well developed. The ganglion habenulae forms, so to speak, the junction of three strands of fibers, which partly encircles it, partly seem to disperse in it. They are: 1) the Meynert bundle just discussed; 2) the paired medullary ridge on the medial-dorsal edge of the optic thalamus, which is called *lineae albae* by Haller, *Taenia thalami optici* by the Wenzel brothers (after Burdach) and by Henle (op. cit. p. 128, Fig. 70), and in particular *eye stripes* by Burdach, and is viewed by Meynert as belonging to the stratum zonale of the thalamus, and considered by most, but not all older authors, simply as a continuation of the following fiber strand; 3) the paired medullary bundle from the stone pine, which is called *habena, habenula, Zirbelstiel, Pedunculus Conarii.* How these three fiber bundles are connected with the ganglion habenulae, and how much the fibers of those bundles connect with cells in the ganglion habenulae or simply go through and continue directly from one bundle into the other, cannot be precisely determined. It seems to be fairly certain only in rodents that a part of the Taenia Thalami optici, running directly over the dorsal surface of the ganglion habenulae, continues into the pedunculus conarii, and that another part of it, slipping down ventrally from the ganglion habenulae, passes directly into Meynert's bundle (Fig. 27). I have already described the latter earlier (op. cit. Sep. p. 15). In any case, however, a good part of Meynert's bundle really dissipates into the ganglion and appears to end there.

angegeben. Jedenfalls aber zerstreut sich ein guter
Theil des Meynert'schen Bündels wirklich in das
Ganglion und scheint daselbst zu endigen.

# Bibliography

Ables, Jessica L., Beatriz Antolin-Fontes, and Ines Ibañez-Tallon. "Habenular synapses and nicotine". In: 2019, pp. 71–78. ISBN: 9780128130353. DOI: 10.1016/B978-0-12-813035-3.00010-1 (cit. on p. 9).

Agetsuma, Masakazu et al. "The habenula is crucial for experience-dependent modification of fear responses in zebrafish". In: *Nature Neuroscience* 13.11 (2010), pp. 1354–1356. ISSN: 10976256. DOI: 10.1038/nn.2654 (cit. on pp. 12, 31).

Ahrens, Misha B. et al. "Whole-brain functional imaging at cellular resolution using light-sheet microscopy". In: *Nature Methods* 10.5 (May 2013), pp. 413–420. ISSN: 1548-7091. DOI: 10.1038/nmeth.2434. URL: https://www.nature.com/articles/nmeth.2434 (cit. on p. 69).

Aizawa, Hidenori, Ryunosuke Amo, and Hitoshi Okamoto. "Phylogeny and ontogeny of the habenular structure". In: *Frontiers in Neuroscience* 5.DEC (2011), pp. 1–7. ISSN: 16624548. DOI: 10.3389/fnins.2011.00138 (cit. on pp. 3, 4).

Aksay, Emre R.F. et al. "Anatomy and discharge properties of pre-motor neurons in the goldfish medulla that have eye-position signals during fixations." In: *Journal of Neurophysiology* 84.2 (Aug. 2000), pp. 1035–1049. ISSN: 00223077. DOI: 10.1152/jn.2000.84.2.1035. URL: http://www.physiology.org/doi/10.1152/jn.2000.84.2.1035 (cit. on p. 69).

Angelaki, Dora E and Jean Laurens. "The head direction cell network: Attractor dynamics, integration within the navigation system, and three-dimensional properties". In: *Current opinion in neurobiology* 60 (2020), pp. 136–144 (cit. on p. 40).

Antolin-Fontes, Beatriz et al. "The habenulo-interpeduncular pathway in nicotine aversion and withdrawal". In: *Neuropharmacology* 96.PB (2015), pp. 213–222. ISSN: 18737064. DOI: 10.1016/j.neuropharm.2014.11.019 (cit. on p. 9).

Arrenberg, Aristides B., Filippo Del Bene, and Herwig Baier. "Optical control of zebrafish behavior with halorhodopsin". In: *Proceedings of the National Academy of Sciences of the United States of America* 106.42 (2009), pp. 17968–17973. ISSN: 00278424. DOI: 10.1073/pnas.0906252106 (cit. on p. 71).

Bahl, Armin and Florian Engert. "Neural circuits for evidence accumulation and decision making in larval zebrafish." In: *Nature neuroscience* 23.1 (Jan. 2020), pp. 94–102. ISSN: 1546-1726. DOI: 10.1038/s41593-019-0534-9 (cit. on pp. 27, 30, 49).

Baratti, Greta, Davide Potrich, and Valeria Anna Sovrano. "The Environmental Geometry in Spatial Learning by Zebrafish (Danio rerio)". In: *Zebrafish* 17.2 (2020), pp. 131–138. ISSN: 15458547. DOI: 10.1089/zeb.2019.1845 (cit. on p. 47).

Beetz, M. Jerome et al. "Flight-induced compass representation in the monarch butterfly heading network". In: *Current Biology* 32.2 (2022), 338–349.e5. ISSN: 18790445. DOI: 10.1016/j.cub.2021.11.009 (cit. on p. 40).

Bianco, Isaac H., Matthias Carl, et al. "Brain asymmetry is encoded at the level of axon terminal morphology". In: *Neural Development* 3.1 (2008). ISSN: 17498104. DOI: 10.1186/1749-8104-3-9 (cit. on pp. 18, 20).

Bianco, Isaac H. and Stephen W. Wilson. "The habenular nuclei: A conserved asymmetric relay station in the vertebrate brain". In: *Philosophical Transactions of the Royal Society B: Biological Sciences* 364.1519 (2009), pp. 1005–1020. ISSN: 14712970. DOI: 10.1098/rstb.2008.0213 (cit. on p. 4).

Briggman, Kevin L., Moritz Helmstaedter, and Winfried Denk. "Wiring specificity in the direction-selectivity circuit of the retina". In: *Nature* 471.7337 (Mar. 2011), pp. 183–188. ISSN: 0028-0836. DOI: 10.1038/nature09818. URL: http://www.nature.com/articles/nature09818 (cit. on pp. 34, 74).

Cajal, Santiago Ramón. *Histologie du systeme nerveux de l'Homme et des vertebres.* Vol. 2. 1911, pp. 222–225 (cit. on pp. 6, 7, 10).

Chaudhuri, Rishidev et al. "The intrinsic attractor manifold and population dynamics of a canonical cognitive circuit across waking and sleep". In: *Nature Neuroscience* 22.9 (2019), pp. 1512–1520. ISSN: 15461726. DOI: 10.1038/s41593-019-0460-x. URL: https://doi.org/10.1038/s41593-019-0460-x (cit. on pp. 40, 43, 70).

Chen, Wei-yu et al. "Role of Olfactorily Responsive Neurons in the Right Dorsal Habenula–Ventral Interpeduncular Nucleus Pathway in Food-Seeking Behaviors of Larval Zebrafish". In: *Neuroscience* 404 (2019), pp. 259–267. ISSN: 18737544. DOI: 10.1016/j.neuroscience.2019.01.057. URL: https://doi.org/10.1016/j.neuroscience.2019.01.057 (cit. on pp. 5, 25, 28).

Chen, Xiuye and Florian Engert. "Navigational strategies underlying phototaxis in larval zebrafish". In: *Frontiers in Systems Neuroscience* 8.MAR (2014). ISSN: 16625137. DOI: 10.3389/fnsys.2014.00039. URL: http://www.ncbi.nlm.nih.gov/pmc/articles/PMC3971168/%20file:///Frontiers%20in%20systems%20neuroscience/Navigational%20strategies%20underlying%20phototaxis%20in%20larval%20zebrafish%20-%202014.pdf%20papers3://publication/doi/10.3389/fnsys.2014.00039 (cit. on pp. 47, 69).

Chen, Xiuye, Yu Mu, et al. "Brainwide Organization of Neuronal Activity and Convergent Sensorimotor Transformations in Larval Zebrafish". In: *Neuron* 100.4 (2018), 876–890.e5. ISSN: 10974199. DOI: 10.1016/j.neuron.2018.09.042 (cit. on pp. 27, 30, 49, 68).

Cherng, Bor Wei et al. "The Dorsal Lateral Habenula-Interpeduncular Nucleus Pathway Is Essential for Left-Right-Dependent Decision Making in Zebrafish". In: *Cell Reports* 32.11 (Sept. 2020), p. 108143. ISSN: 22111247. DOI: 10.1016/j.celrep.2020.108143 (cit. on pp. 14, 47, 69).

Chou, Ming Yi et al. "Social conflict resolution regulated by two dorsal habenular subregions in zebrafish". In: *Science* 352.6281 (2016), pp. 87–90. ISSN: 10959203. DOI: `10.1126/science.aac9508` (cit. on pp. 9, 13).

Chu, D. C.M. et al. "Distribution and kinetics of GABAB binding sites in rat central nervous system: A quantitative autoradiographic study". In: *Neuroscience* 34.2 (1990), pp. 341–357. ISSN: 03064522. DOI: `10.1016/0306-4522(90)90144-S` (cit. on p. 9).

Clark, Benjamin J., Asha Sarma, and Jeffrey S. Taube. "Head direction cell instability in the anterior dorsal thalamus after lesions of the interpeduncular nucleus". In: *Journal of Neuroscience* 29.2 (2009), pp. 493–507. ISSN: 02706474. DOI: `10.1523/JNEUROSCI.2811-08.2009` (cit. on p. 13).

Clark, Benjamin J. and Jeffrey S. Taube. "Deficits in Landmark Navigation and Path Integration After Lesions of the Interpeduncular Nucleus". In: *Behavioral Neuroscience* 123.3 (2009), pp. 490–503. ISSN: 07357044. DOI: `10.1037/a0015477` (cit. on pp. 13, 43).

–   "Vestibular and attractor network basis of the head direction cell signal in subcortical circuits". In: *Frontiers in Neural Circuits* 6.FEBRUARY (2012), pp. 1–12. ISSN: 16625110. DOI: `10.3389/fncir.2012.00007` (cit. on p. 43).

Claudi, Federico, Luigi Petrucco, et al. "BrainGlobe Atlas API: a common interface for neuroanatomical atlases". In: *Journal of Open Source Software* 5.54 (Oct. 2020), p. 2668. ISSN: 2475-9066. DOI: `10.21105/joss.02668` (cit. on pp. 35, 84).

Claudi, Federico, Adam L. Tyson, et al. "Visualizing anatomically registered data with brainrender". In: *eLife* 10 (2021), pp. 1–16. ISSN: 2050084X. DOI: `10.7554/eLife.65751` (cit. on p. 35).

Contestabile, A and B A Flumerfelt. "Afferent Connections of the Interpeduncular Nucleus and the Topographic Organization of the Habenu lo-lnterpeduncu lar Pathway: An HRP Study in the Rat". In: *The Journal of Comparative Neurology* 196 (1981), pp. 253–270 (cit. on p. 7).

Costa, Marta et al. "NBLAST: Rapid, Sensitive Comparison of Neuronal Structure and Construction of Neuron Family Databases". In: *Neuron* 91.2 (2016), pp. 293–311. ISSN: 10974199. DOI: `10.1016/j.neuron.2016.06.012`. URL: `http://dx.doi.org/10.1016/j.neuron.2016.06.012` (cit. on p. 34).

Cullen, Kathleen E. and Jeffrey S. Taube. "Our sense of direction: Progress, controversies and challenges". In: *Nature Neuroscience* 20.11 (2017), pp. 1465–1473. ISSN: 15461726. DOI: `10.1038/nn.4658` (cit. on p. 43).

Dragomir, Elena I., Vilim Štih, and Ruben Portugues. "Evidence accumulation during a sensorimotor decision task revealed by whole-brain imaging". In: *Nature Neuroscience* 23.1 (2020), pp. 85–93. ISSN: 15461726. DOI: `10.1038/s41593-019-0535-8`. URL: `http://dx.doi.org/10.1038/s41593-019-0535-8` (cit. on pp. 14, 25, 27, 28, 30, 49, 69, 73, 74, 77).

Dreosti, Elena et al. "Left-Right Asymmetry Is Required for the Habenulae to Respond to Both Visual and Olfactory Stimuli". In: *Current Biology* 24.4 (2014), pp. 440–445. ISSN: 09609822. DOI: `10.1016/j.cub.2014.01.016`. URL: `http://dx.doi.org/10.1016/j.cub.2014.01.016` (cit. on p. 5).

Dunn, Timothy W. et al. "Brain-wide mapping of neural activity controlling zebrafish exploratory locomotion". In: *eLife* 5.MARCH2016 (2016), pp. 1–29. ISSN: 2050084X. DOI: 10.7554/eLife.12741 (cit. on pp. 27, 68, 69).

Fisher, N I and A J Lee. "A Correlation Coefficient for Circular Data". In: *Biometrika* 70.2 (1983), pp. 327–332 (cit. on p. 78).

Forel, August. "Untersuchungen über die Haubenregion und ihre oberen Verknüpfungen im Gehirne des Menschen und einiger Säugethiere, mit Beiträgen zu den Methoden der Gehirnuntersuchung". In: *Archiv für Psychiatrie und Nervenkrankheiten* 7.3 (1877), pp. 393–495 (cit. on pp. 3, 10, 93).

Förster, Dominique et al. "An optogenetic toolbox for unbiased discovery of functionally connected cells in neural circuits". In: *Nature Communications* 8.1 (2017). ISSN: 20411723. DOI: 10.1038/s41467-017-00160-z. URL: http://dx.doi.org/10.1038/s41467-017-00160-z (cit. on p. 71).

Fowler, Christie D. et al. "Habenular $\alpha 5$ nicotinic receptor subunit signalling controls nicotine intake". In: *Nature* 471.7340 (2011), pp. 597–601. ISSN: 00280836. DOI: 10.1038/nature09797. URL: http://dx.doi.org/10.1038/nature09797 (cit. on p. 12).

Frahm, Silke et al. "Aversion to Nicotine Is Regulated by the Balanced Activity of $\beta 4$ and $\alpha 5$ Nicotinic Receptor Subunits in the Medial Habenula". In: *Neuron* 70.3 (2011), pp. 522–535. ISSN: 08966273. DOI: 10.1016/j.neuron.2011.04.013 (cit. on p. 12).

Freudenmacher, Lars, Arndt von Twickel, and Wolfgang Walkowiak. "The habenula as an evolutionary conserved link between basal ganglia, limbic, and sensory systems—A phylogenetic comparison based on anuran amphibians". In: *Journal of Comparative Neurology* 528.5 (2020), pp. 705–728. ISSN: 10969861. DOI: 10.1002/cne.24777 (cit. on p. 4).

Garyfallidis, Eleftherios et al. "Dipy, a library for the analysis of diffusion MRI data". In: *Frontiers in Neuroinformatics* 8.FEB (Feb. 2014). ISSN: 16625196. DOI: 10.3389/fninf.2014.00008 (cit. on pp. 34, 35, 84).

Green, Jonathan and Gaby Maimon. "Building a heading signal from anatomically defined neuron types in the Drosophila central complex". In: *Current Opinion in Neurobiology* 52 (2018), pp. 156–164. ISSN: 18736882. DOI: 10.1016/j.conb.2018.06.010. URL: https://doi.org/10.1016/j.conb.2018.06.010 (cit. on pp. 40, 44).

Groenewegen, H J et al. "Cytoarchitecture, Fiber Connections, and Some Histochemical Aspects of the Interpeduncular Nucleus in the Rat". In: *The Journal of Comparative Neurology* (1986), pp. 249–65 (cit. on pp. 7, 8).

Harris, Charles R. et al. "Array programming with NumPy". In: *Nature* 585.7825 (Sept. 2020), pp. 357–362. ISSN: 14764687. DOI: 10.1038/s41586-020-2649-2. arXiv: 2006.10256 (cit. on p. 76).

Heinze, Stanley and Uwe Homberg. "Maplike Representation of". In: *Science* 431.February (2007), pp. 2004–2006 (cit. on p. 44).

Heinze, Stanley and Steven M. Reppert. "Sun compass integration of skylight cues in migratory monarch butterflies". In: *Neuron* 69.2 (2011), pp. 345–358. ISSN: 08966273. DOI: 10.1016/j.neuron.2010.12.025. URL: http://dx.doi.org/10.1016/j.neuron.2010.12.025 (cit. on p. 44).

Herrick, C Judson. "Interpeduncular Nucleus". In: *The Brain of the Tiger Salamander*. University of Chicago Press, 1948. Chap. 14, pp. 191–211 (cit. on pp. 3, 7, 10, 11, 24, 70).

Hong, Elim et al. "Cholinergic left-right asymmetry in the habenulo-interpeduncular pathway". In: *Proceedings of the National Academy of Sciences of the United States of America* 110.52 (2013), pp. 21171–21176. ISSN: 00278424. DOI: `10.1073/pnas.1319566110` (cit. on pp. 6, 9).

Huang, Kuo Hua et al. "Spinal projection neurons control turning behaviors in zebrafish". In: *Current Biology* 23.16 (Aug. 2013), pp. 1566–1573. ISSN: 09609822. DOI: `10.1016/j.cub.2013.06.044` (cit. on pp. 58, 77).

Hulse, Brad K., Hannah Haberkern, et al. "A connectome of the drosophila central complex reveals network motifs suitable for flexible navigation and context-dependent action selection". In: *eLife* 10 (2021). ISSN: 2050084X. DOI: `10.7554/eLife.66039` (cit. on p. 44).

Hulse, Brad K. and Vivek Jayaraman. "Mechanisms Underlying the Neural Computation of Head Direction". In: *Annual Review of Neuroscience* 43 (July 2020), pp. 31–54. ISSN: 15454126. DOI: `10.1146/annurev-neuro-072116-031516`. URL: `https://www.annualreviews.org/doi/abs/10.1146/annurev-neuro-072116-031516` (cit. on pp. 39–44, 70).

Hunter, John D. "Matplotlib: A 2D graphics environment". In: *Computing in Science and Engineering* 9.3 (2007), pp. 90–95. ISSN: 15219615. DOI: `10.1109/MCSE.2007.55` (cit. on pp. 35, 76).

Insafutdinov, Eldar et al. "DeeperCut: A Deeper, Stronger and Faster Multi-person Pose Estimation Model". In: *Lecture Notes in Computer Science (including subseries Lecture Notes in Artificial Intelligence and Lecture Notes in Bioinformatics)* 9906 LNCS (2016), pp. VII–IX. ISSN: 16113349. DOI: `10.1007/978-3-319-46466-4` (cit. on p. 77).

Iwahori, Nobuharu et al. "Terminal patterns of the tegmental afferents in the interpeduncular nucleus: a Golgi study in the mouse". In: *Anatomy and Embryology* 188.6 (1993), pp. 593–599. ISSN: 03402061. DOI: `10.1007/BF00187015` (cit. on pp. 5, 7, 11, 70).

Kanatani, Kenichi and Prasanna Rangarajan. "Hyper least squares fitting of circles and ellipses". In: *Computational Statistics and Data Analysis* 55.6 (June 2011), pp. 2197–2208. ISSN: 01679473. DOI: `10.1016/j.csda.2010.12.012` (cit. on p. 78).

Koppensteiner, Peter, Riccardo Melani, and Ipe Ninan. "A Cooperative Mechanism Involving Ca2+-Permeable AMPA Receptors and Retrograde Activation of GABAB Receptors in Interpeduncular Nucleus Plasticity". In: *Cell Reports* 20.5 (2017), pp. 1111–1122. ISSN: 22111247. DOI: `10.1016/j.celrep.2017.07.013`. URL: `http://dx.doi.org/10.1016/j.celrep.2017.07.013` (cit. on p. 10).

Kunst, Michael et al. "A Cellular-Resolution Atlas of the Larval Zebrafish Brain". In: *Neuron* 103.1 (2019), 21–38.e5. ISSN: 10974199. DOI: `10.1016/j.neuron.2019.04.034` (cit. on pp. 15, 27, 35, 84).

Lecourtier, Lucas, Hans C. Neijt, and Peter H. Kelly. "Habenula lesions cause impaired cognitive performance in rats: Implications for schizophrenia". In: *European Journal of Neuroscience* 19.9 (2004), pp. 2551–2560. ISSN: 0953816X. DOI: `10.1111/j.0953-816X.2004.03356.x` (cit. on p. 13).

Lenn, N. J., V. Wong, and G. S. Hamill. "Left-right pairing at the crest synapses of rat interpeduncular nucleus". In: *Neuroscience* 9.2 (1983). ISSN: 03064522. DOI: 10.1016/0306-4522(83)90301-9 (cit. on pp. 8, 10).

Lenn, Nicholas J. "Synapses in the interpeduncular nucleus: Electron microscopy of normal and habenula lesioned rats". In: *Journal of Comparative Neurology* 166.1 (1976), pp. 73–99. ISSN: 10969861. DOI: 10.1002/cne.901660106 (cit. on pp. 8, 10).

Lima, Leandro B. et al. "Afferent and efferent connections of the interpeduncular nucleus with special reference to circuits involving the habenula and raphe nuclei". In: *Journal of Comparative Neurology* 525.10 (2017), pp. 2411–2442. ISSN: 10969861. DOI: 10.1002/cne.24217 (cit. on p. 4).

Lister, James A. et al. "nacre encodes a zebrafish microphthalmia-related protein that regulatesneural-crest-derived pigment cell fate". In: *Development* 126.17 (1999), pp. 3757–3767. DOI: https://doi.org/10.1242/dev.126.17.3757 (cit. on p. 71).

Lyu, Cheng, L. F. Abbott, and Gaby Maimon. "Building an allocentric travelling direction signal via vector computation". In: *Nature* 601.7891 (Jan. 2022), pp. 92–97. ISSN: 0028-0836. DOI: 10.1038/s41586-021-04067-0. URL: https://www.nature.com/articles/s41586-021-04067-0 (cit. on pp. 46, 69).

Margeta-mitrovic, Marta et al. "of GABA B Receptors in the Rat Central Nervous System". In: *Journal of Comparative Neurology* 321.November 1998 (1999), pp. 299–321 (cit. on p. 9).

Markov, Daniil A. et al. "A cerebellar internal model calibrates a feedback controller involved in sensorimotor control". In: *Nature Communications* 12.1 (2021), pp. 1–21. ISSN: 2041-1723. DOI: 10.1038/s41467-021-26988-0 (cit. on pp. 66, 88).

Mathis, Alexander et al. "DeepLabCut: markerless pose estimation of user-defined body parts with deep learning". In: *Nature Neuroscience* 21.9 (Sept. 2018), pp. 1281–1289. ISSN: 15461726. DOI: 10.1038/s41593-018-0209-y (cit. on p. 77).

Miri, Andrew et al. "Spatial gradients and multidimensional dynamics in a neural integrator circuit". In: *Nature Neuroscience* 14.9 (Sept. 2011), pp. 1150–1161. ISSN: 10976256. DOI: 10.1038/nn.2888. arXiv: NIHMS150003. URL: http://www.nature.com/articles/nn.2888 (cit. on p. 69).

Molas, Susanna et al. "A circuit-based mechanism underlying familiarity signaling and the preference for novelty". In: *Nature Neuroscience* 20.9 (2017), pp. 1260–1268. ISSN: 15461726. DOI: 10.1038/nn.4607 (cit. on p. 12).

Morley, Barbara J. "The Interpeduncular Nucleus". In: *International Review of Neurobiology* 28 (1986), pp. 157–182 (cit. on pp. 5, 9).

Muller, Eilif et al. "Python in neuroscience". In: *Frontiers in neuroinformatics* 9 (2015), p. 11 (cit. on p. 87).

Namboodiri, Vijay Mohan K., Jose Rodriguez-Romaguera, and Garret D. Stuber. "The habenula". In: *Current Biology* 26.19 (2016), R873–R877. ISSN: 09609822. DOI: 10.1016/j.cub.2016.08.051 (cit. on pp. 4, 5).

Nath, Tanmay et al. "Using DeepLabCut for 3D markerless pose estimation across species and behaviors". In: *Nature Protocols* 14.7 (July 2019),

pp. 2152–2176. ISSN: 17502799. DOI: 10.1038/s41596-019-0176-0 (cit. on p. 77).

Nguyen, Huy Bang et al. "Conductive resins improve charging and resolution of acquired images in electron microscopic volume imaging". In: *Scientific Reports* 6.1 (July 2016), p. 23721. ISSN: 2045-2322. DOI: 10.1038/srep23721. URL: http://www.nature.com/articles/srep23721 (cit. on pp. 34, 74).

Orger, Michael B. and Gonzalo G. De Polavieja. "Zebrafish Behavior: Opportunities and Challenges". In: *Annual Review of Neuroscience* 40 (2017), pp. 125–147. ISSN: 15454126. DOI: 10.1146/annurev-neuro-071714-033857 (cit. on p. 47).

Otsu, Yo et al. "Functional Principles of Posterior Septal Inputs to the Medial Habenula". In: *Cell Reports* 22.3 (2018), pp. 693–705. ISSN: 22111247. DOI: 10.1016/j.celrep.2017.12.064 (cit. on p. 4).

Pachitariu, Marius et al. "Suite2p: beyond 10,000 neurons with standard two-photon microscopy". In: *bioRxiv* (2016), p. 061507. DOI: 10.1101/061507 (cit. on p. 76).

Pang, Xueyan et al. "Habenula cholinergic neurons regulate anxiety during nicotine withdrawal via nicotinic acetylcholine receptors". In: *Neuropharmacology* 107.12 (2016), pp. 294–304. ISSN: 18737064. DOI: 10.1016/j.neuropharm.2016.03.039 (cit. on p. 13).

Parajuli, Laxmi Kumar et al. "Unique synaptic topography of crest-type synapses in the interpeduncular nucleus". In: *Biochemical and Biophysical Research Communications* 530.1 (2020), pp. 130–135. ISSN: 10902104. DOI: 10.1016/j.bbrc.2020.06.046. URL: https://doi.org/10.1016/j.bbrc.2020.06.046 (cit. on p. 11).

Pastor, Angel M., Rosa R. De La Cruz, and Robert Baker. "Eye position and eye velocity integrators reside in separate brainstem nuclei". In: *Proceedings of the National Academy of Sciences of the United States of America* 91.2 (Jan. 1994), pp. 807–811. ISSN: 00278424. DOI: 10.1073/pnas.91.2.807. URL: https://www.pnas.org/content/91/2/807%20https://www.pnas.org/content/91/2/807.abstract (cit. on p. 69).

Pedregosa, Fabian et al. "Scikit-learn: Machine Learning in Python". In: *Journal of Machine Learning Research* 12 (2011), pp. 2825–2830. ISSN: 15324435. arXiv: 1201.0490. URL: http://scikit-learn.sourceforge.net.%20http://jmlr.csail.mit.edu/papers/v12/pedregosa11a.html%5C%5Cnhttp://arxiv.org/abs/1201.0490 (cit. on p. 76).

Puelles, Luis. "Comments on the limits and internal structure of the mammalian midbrain". In: *Anatomy* 10.1 (2016), pp. 60–70. ISSN: 13078798. DOI: 10.2399/ana.15.045 (cit. on pp. 43, 49).

Quina, Lely A. et al. "Specific connections of the interpeduncular subnuclei reveal distinct components of the habenulopeduncular pathway". In: *Journal of Comparative Neurology* 525.12 (2017), pp. 2632–2656. ISSN: 10969861. DOI: 10.1002/cne.24221 (cit. on pp. 5–9, 13).

Ramirez, Alexandro D. and Emre R.F. Aksay. "Ramp-to-threshold dynamics in a hindbrain population controls the timing of spontaneous saccades". In: *Nature Communications* 12.1 (2021), pp. 1–19. ISSN: 20411723. DOI: 10.1038/s41467-021-24336-w. URL: http://dx.doi.org/10.1038/s41467-021-24336-w (cit. on pp. 60, 69).

Ren, Jing et al. "Habenula " Cholinergic" Neurons Corelease Glutamate and Acetylcholine and Activate Postsynaptic Neurons via Distinct Transmission Modes". In: *Neuron* 69.3 (2011), pp. 445–452. ISSN: 08966273. DOI: 10.1016/j.neuron.2010.12.038. URL: http://dx.doi.org/10.1016/j.neuron.2010.12.038 (cit. on p. 9).

Robertson, Robert G. et al. "Head direction cells in the primate pre-subiculum". In: *Hippocampus* 9.3 (1999), pp. 206–219. ISSN: 10509631. DOI: 10.1002/(SICI)1098-1063(1999)9:3<206::AID-HIPO2>3.0.CO;2-H (cit. on p. 40).

Rodríguez, Fernando et al. "Spatial cognition in teleost fish: Strategies and mechanisms". In: *Animals* 11.8 (2021). ISSN: 20762615. DOI: 10.3390/ani11082271 (cit. on p. 47).

Rohlfing, Torsten and Calvin R. Maurer. "Nonrigid image registration in shared-memory multiprocessor environments with application to brains, breasts, and bees". In: *IEEE Transactions on Information Technology in Biomedicine* 7.1 (Mar. 2003), pp. 16–25. ISSN: 10897771. DOI: 10.1109/TITB.2003.808506 (cit. on pp. 35, 74, 84).

Rubin, Alon, Michael M. Yartsev, and Nachum Ulanovsky. "Encoding of head direction by hippocampal place cells in bats". In: *Journal of Neuroscience* 34.3 (2014), pp. 1067–1080. ISSN: 02706474. DOI: 10.1523/JNEUROSCI.5393-12.2014 (cit. on p. 40).

Seelig, Johannes D. and Vivek Jayaraman. "Neural dynamics for landmark orientation and angular path integration". In: *Nature* 521.7551 (May 2015), pp. 186–191. ISSN: 14764687. DOI: 10.1038/nature14446. URL: https://www.nature.com/articles/nature14446 (cit. on pp. 40, 44).

Seigneur, Erica, Jai S. Polepalli, and Thomas C. Südhof. "Cbln2 and Cbln4 are expressed in distinct medial habenula-interpeduncular projections and contribute to different behavioral outputs". In: *Proceedings of the National Academy of Sciences of the United States of America* 115.43 (2018), E10235–E10244. ISSN: 10916490. DOI: 10.1073/pnas.1811086115 (cit. on pp. 5, 6, 13).

Sharp, Patricia E., Amanda Tinkelman, and Jeiwon Cho. "Angular velocity and head direction signals recorded from the dorsal tegmental nucleus of gudden in the rat: Implications for path integration in the head direction cell circuit." In: *Behavioral Neuroscience* 115.3 (2001), pp. 571–588. ISSN: 0735-7044. DOI: 10.1037//0735-7044.115.3.571 (cit. on pp. 43, 49).

Sharp, Patricia E., Shawnda Turner-Williams, and Sarah Tuttle. "Movement-related correlates of single cell activity in the interpeduncular nucleus and habenula of the rat during a pellet-chasing task". In: *Behavioural Brain Research* 166.1 (2006), pp. 55–70. ISSN: 01664328. DOI: 10.1016/j.bbr.2005.07.004 (cit. on p. 14).

Skaggs, William E et al. "A model of the neural basis of the rat's sense of direction." In: *Advances in neural information processing systems* 7 (1995), pp. 173–180. ISSN: 10495258 (cit. on p. 49).

Stackman, Robert W. and Jeffrey S. Taube. "Firing properties of head direction cells in the rat anterior thalamic nucleus: Dependence on vestibular input". In: *Journal of Neuroscience* 17.11 (1997), pp. 4349–4358. ISSN: 02706474. DOI: 10.1523/jneurosci.17-11-04349.1997 (cit. on p. 42).

Stephenson-Jones, Marcus et al. "Evolutionary conservation of the habenular nuclei and their circuitry controlling the dopamine and 5-hydroxytryptophan (5-HT) systems". In: *Proceedings of the National Academy of Sciences of the United States of America* 109.3 (2012). ISSN: 00278424. DOI: 10.1073/pnas.1119348109 (cit. on p. 3).

Štih, Vilim. "Signatures of motion processing and decisions in the larval zebrafsh brain". PhD thesis. 2020 (cit. on p. 25).

Štih, Vilim, Diego Asua, et al. *Sashimi*. Version v0.2.1. Jan. 2022. DOI: 10.5281/zenodo.5932227. URL: https://doi.org/10.5281/zenodo.5932227 (cit. on p. 73).

Štih, Vilim, EmanPaoli, and Diego AC. *portugueslab/brunoise: Alpha*. Version 0.1. Oct. 2020. DOI: 10.5281/zenodo.4122064. URL: https://doi.org/10.5281/zenodo.4122064 (cit. on p. 74).

Štih, Vilim, Luigi Petrucco, Andreas M. Kist, et al. "Stytra: An open-source, integrated system for stimulation, tracking and closed-loop behavioral experiments". In: *PLoS Computational Biology* 15.4 (2019). ISSN: 15537358. DOI: 10.1371/journal.pcbi.1006699 (cit. on pp. 73, 89).

Štih, Vilim, Luigi Petrucco, Ot Prat, et al. *Bouter*. Version v0.2.0. Jan. 2022. DOI: 10.5281/zenodo.5931684. URL: https://doi.org/10.5281/zenodo.5931684 (cit. on pp. 76, 89).

Svara, Fabian N. et al. "Volume EM Reconstruction of Spinal Cord Reveals Wiring Specificity in Speed-Related Motor Circuits". In: *Cell Reports* 23.10 (June 2018), pp. 2942–2954. ISSN: 22111247. DOI: 10.1016/j.celrep.2018.05.023. URL: https://linkinghub.elsevier.com/retrieve/pii/S2211124718307563 (cit. on pp. 34, 74).

Taube, J. S., R. U. Muller, and J. B. Ranck. "Head-direction cells recorded from the postsubiculum in freely moving rats. I. Description and quantitative analysis". In: *Journal of Neuroscience* 10.2 (1990), pp. 420–435. ISSN: 02706474. DOI: 10.1523/jneurosci.10-02-00420.1990 (cit. on pp. 13, 40).

Taube, Jeffrey S. "Head direction cells recorded in the anterior thalamic nuclei of freely moving rats". In: *Journal of Neuroscience* 15.1 I (1995), pp. 70–86. ISSN: 02706474. DOI: 10.1523/jneurosci.15-01-00070.1995 (cit. on p. 42).

– "The head direction signal: Origins and sensory-motor integration". In: *Annual Review of Neuroscience* 30 (2007), pp. 181–207. ISSN: 0147006X. DOI: 10.1146/annurev.neuro.29.051605.112854 (cit. on pp. 39, 40, 42, 43, 45, 49, 70).

Taylor, Michael A. et al. "Diffuse light-sheet microscopy for stripe-free calcium imaging of neural populations". In: *Journal of Biophotonics* 11.12 (2018). ISSN: 18640648. DOI: 10.1002/jbio.201800088 (cit. on p. 72).

Thiele, Tod R., Joseph C. Donovan, and Herwig Baier. "Descending Control of Swim Posture by a Midbrain Nucleus in Zebrafish". In: *Neuron* 83.3 (Aug. 2014), pp. 679–691. ISSN: 10974199. DOI: 10.1016/j.neuron.2014.04.018 (cit. on p. 71).

Thompson, Robert. "Interpeduncular nucleus and avoidance conditioning in the rat". In: *Science* 132.3439 (1960), pp. 1551–1553. ISSN: 00368075. DOI: 10.1126/science.132.3439.1551 (cit. on p. 12).

Thornton, Everard W. and Claire Davies. "A water-maze discrimination learning deficit in the rat following lesion of the habenula". In: *Physiology and Behavior* 49.4 (1991), pp. 819–822. ISSN: 00319384. DOI: 10.1016/0031-9384(91)90324-H (cit. on pp. 13, 43).

Vargas, Juan Pedro et al. "Encoding of geometric and featural spatial information by goldfish (Carassius auratus)". In: *Journal of Comparative Psychology* 118.2 (2004), pp. 206–216. ISSN: 07357036. DOI: 10.1037/0735-7036.118.2.206 (cit. on p. 47).

Virtanen, Pauli et al. "SciPy 1.0: fundamental algorithms for scientific computing in Python". In: *Nature Methods* 17.3 (Mar. 2020), pp. 261–272. ISSN: 15487105. DOI: 10.1038/s41592-019-0686-2. arXiv: 1907.10121 (cit. on pp. 35, 76).

Wilson, J. Roger, James C. Mitchell, and Gary W. Van Hoesen. "Epithalamic and ventral tegmental contributions to avoidance behavior in rats". In: *Journal of Comparative and Physiological Psychology* 78.3 (1972), pp. 442–449. ISSN: 00219940. DOI: 10.1037/h0032371 (cit. on p. 12).

Wirtshafter, David. "The role of interpeduncular connections with the tegmentum in avoidance learning". In: *Physiology and Behavior* 26.6 (1981), pp. 985–989. ISSN: 00319384. DOI: 10.1016/0031-9384(81)90197-9 (cit. on p. 12).

Wolf, Sébastien et al. "Sensorimotor computation underlying phototaxis in zebrafish". In: *Nature Communications* 8.1 (Dec. 2017), p. 651. ISSN: 2041-1723. DOI: 10.1038/s41467-017-00310-3. URL: http://www.nature.com/articles/s41467-017-00310-3 (cit. on p. 69).

Wolff, Tanya and Gerald M. Rubin. "Neuroarchitecture of the Drosophila central complex: A catalog of nodulus and asymmetrical body neurons and a revision of the protocerebral bridge catalog". In: *Journal of Comparative Neurology* 526.16 (2018), pp. 2585–2611. ISSN: 10969861. DOI: 10.1002/cne.24512 (cit. on p. 44).

Wolfman, Shannon L. et al. "Nicotine aversion is mediated by GABAergic interpeduncular nucleus inputs to laterodorsal tegmentum". In: *Nature Communications* 9.1 (2018), pp. 1–11. ISSN: 20411723. DOI: 10.1038/s41467-018-04654-2. URL: http://dx.doi.org/10.1038/s41467-018-04654-2 (cit. on p. 12).

Yamaguchi, Takashi et al. "Distinct roles of segregated transmission of the septo-habenular pathway in anxiety and fear". In: *Neuron* 78.3 (2013), pp. 537–544. ISSN: 08966273. DOI: 10.1016/j.neuron.2013.02.035. URL: http://dx.doi.org/10.1016/j.neuron.2013.02.035 (cit. on p. 13).

Yoder, Ryan M. and Jeffrey S. Taube. "The vestibular contribution to the head direction signal and navigation". In: *Frontiers in Integrative Neuroscience* 8.APR (Apr. 2014). ISSN: 16625145. DOI: 10.3389/fnint.2014.00032 (cit. on p. 59).

Zaupa, Margherita et al. "Trans-inhibition of axon terminals underlies competition in the habenulo-interpeduncular pathway". In: *Current Biology* 31.21 (2021), 4762–4772.e5. ISSN: 18790445. DOI: 10.1016/j.cub.2021.08.051 (cit. on pp. 6, 9).

Zhang, Kechen. "Representation of spatial orientation by the intrinsic dynamics of the head-direction cell ensemble: A theory". In: *Journal of*

*Neuroscience* 16.6 (1996), pp. 2112–2126. ISSN: 02706474. DOI: 10.1523/ jneurosci.16-06-02112.1996 (cit. on pp. 40, 49).

Zhang, Tony et al. "Endotaxis: A Universal Algorithm for Mapping, Goal-Learning, and Navigation". In: *bioRxiv* (2021) (cit. on p. 39).

Zhao-Shea, Rubing et al. "Activation of GABAergic neurons in the interpeduncular nucleus triggers physical nicotine withdrawal symptoms". In: *Current Biology* 23.23 (2013), pp. 2327–2335. ISSN: 09609822. DOI: 10. 1016/j.cub.2013.09.041. URL: http://dx.doi.org/10.1016/j. cub.2013.09.041 (cit. on p. 12).

# *Author Contributions*

The methods and data described in this thesis have been developed, acquired and analysed together with Hagar Lavian, You Kure Wu, and Vilim Štih in the lab of Ruben Portugues, and Fabian Svara (Max Planck Institute for Neurobiology of Behavior — caesar, Bonn, Germany), Federico Claudi and Adam Tyson (Sainsbury Wellcome Centre, University College London, London, U.K.) as external collaborators.

### *Software development*

`stytra` and `bouter` have been co-developed by the author and VŠ, after initial design by VŠ. `fimpy` and `Sashimi` have been developed by VŠ, with contributions from the author on general bug fixing and supporting libraries.

`bg-atlasapi` has been ideated and written by the author, with contributions from FC and AT. `brainrender` has been developed by FC, with contributions from the author on the package organization and support for the zebrafish atlas.

### *Part I*

Most of the observations and figures presented in part II come from analyses performed by the author on data acquired by collaborators. All schemes and visualizations have been produced by the author. Confocal data presented in Figure 2.3 have been acquired by HL. Staining data presented in Figure 2.15 have been acquired by YKW. Figure 2.16 show data from HL analyzed by VŠ. Electron microscopy reconstructions in Figure 2.2, Figure 2.6, Figure 2.7, Figure 2.8, Figure 2.9, Figure 2.10, Figure 2.11, Figure 2.12, Figure 2.13, Figure 2.14, Figure 2.17, Figure 2.18, Figure 2.19, Figure 2.20, Figure 2.21, have been performed by professional annotators coordinated by FS at Ariadne on data acquired by FS. The author selected the neurons to reconstruct, and performed all analyses and visualization of the skeleton data.

### *Part II*

Most of the observations and figures presented in part II come from data and analyses performed by the author. HL acquired the two-photon data and performed the analysis reported in Figure 5.28. YKW acquired the two-photon data and performed the analysis reported in Figure 5.30 and in Figure 5.31. As in part I, the electron microscopy reconstructions presented in Figure 5.25, Figure 5.25, Figure 5.27, Figure 5.29, and Figure 5.31 have been performed by professional annotators coordinated by FS at Ariadne on data

acquired by FS. The author selected the neurons to reconstruct, and performed all analyses and visualization of the skeleton data.

_____

Luigi Petrucco

_____

Hagar Lavian

_____

Ruben Portugues

# *Acknowledgments*

First and foremost, I thank Ruben Portugues, my mentor in those last five years. My approach to any aspect of the scientific enterprise has matured in the course of my PhD thanks to the amazing environment you have made me part of. Thanks for having assembled, maintained, and inspired such a wonderful laboratory. The kindness and humanity you insufflated in it have made it feel like a second home in those years; and the rigor and "clarity of thought" that you have posed as its principles will remain the pillars of any future scientific endeavor of mine. I will always be grateful for the freedom to pursue Science guided by intuition and creativity more than by preconceived models; the insightful discussions and the deeply knowledgeable comments about any experimental and theoretical aspect of a project; the inspiringly open leadership; the support in any other mundane matter.

This exceptional place was made such by the exceptional people who have mentored me, assisted me, endured me, and to whom I am deeply grateful; I will get to you in strictly alphabetical order.

Andreas, first guide in the world of zebrafish neuroscience, for your generous support in my first years in the lab. You taught me the noble art of tinkering, showing me that the first rule for fixing things is not to be scared of messing them up, and you proved me the power of being at the same time a molecular biologist, a programmer, a maker and a neuroscientist (I had to give up on some of those, though...).

Daniil, for the deep love of Science and the constant strive for scientific rigor. Collaborating with you has been truly inspiring, and I learned from you the drive necessary to focus on a project and lead it to an end.

Elena for your culture and your biological insight. You were fundamental in keeping my focus on the fish, and not on the methods, and it is from to your observations that this project could start. Thanks for being one of the few people that can still stand talking with me about the IPN, for the insightful discussions and comment on the project, and for any other conversation about life, literature and art, they have truly enriched the years in the lab.

Ema, fellow student from the "Gimmi school", thank you for your brilliance, your endless knowledgeability in the expanding universe of neuroscientific literature. Thank you for the honesty and the critical mind, your sharp observations are precious for keeping hand-wavy speculation out of an experiment's conclusions (I will make sure to be around when your turn of drawing conclusions will come!).

Hagar, thanks for having shared the adventure of this project, for having stood me and my endless IPN talking, for keeping up the lab morale with screenshots, quotes and banter, and for the exceptional hummus and bread (feat. Barack).

Olga, for your relentless work in the turbulent times of moving the lab to the other side of the city. Thank you for the late hours and the dedication to the health of our little swimming friends and to the functioning of the lab.

Ot, friend and collaborator, and first target of my attempts at passing knowledge to the new generation. Nothing is truly as enjoyable as working with someone smart and with a good sense of humor, but collaborating with you has been a pleasure nonetheless. Thank you for the shared projects, the day together in the office, the chess games, the book recommendations, your own literary productions, and the efforts in bringing my lazy derriére to boulder (I will try harder in Trentino, I promise).

You, for the inspiring patience and perseverance. You are the demonstration that no experiment is too hard, and that quiet obstinacy can overcome even the strongest experimental challenges.

Tugce, for the rare but beautiful conversations in the empty office; I wish we had more time in the lab together.

Vilim, mentor and partner-in-crime in many endeavors, scientific and not, in the lab; you are behind a lot of this thesis. You taught me how far optimist thinking and intransigence for mediocrity can lead you in any pursue; that there is (almost) no such thing as wasted time when learning and beautifying the world. Thank for your friendship, outspokenness and moral rigor; for having thought me everything I know about code, and a fair deal of what I know about many other subjects; your multifaceted interests have always offered endless occasions to learn new things.

Virginia, it is rare and precious to meet a friend so similarly minded; it was a pleasure and an honor growing up in the lab with you (and thanks to you). Thank you for never taking me too seriously in the countless conversations about anything *"whereof one can speak"*, the science and the philosophy, for the laughs, the humor, the frank dialectics, the disenchanted love for the human nature, the shared fascination for any kind of resolute pursue.

Thanks to any other person in the lab and outside with whome I have been sharing laughs, lunches, data, and pull requests. Thank you Laura, Kata, Fede, Younes, Shuhong, Anja, Lisa, Hanyi, Fritz, Amey, Laila, Patricia; to Marco, Joe and Krasimir for the technical support at the Max Planck; to Yan and Tim, Federico and Adam for the variegated collaborations (and to Ruben for having promoted and endorsed them). Thank you to old mentors that made me fall in love with neuroscience in the first place: Gimmi, Marco, Frenki, Pietro, Riccardo and Silvia.


Thanks to the people that have made those years in Munich fly by.

Thank you Kate, for the periodic photosynthetic sessions, the precious friendship born in strides and words, for your intelligence and your unconventional perspectives, the peerless correspondence and the steady feed of intellectual nourishment.

# *Curriculum Vitae*

## Education

- 2017–present: PhD student at Graduate School for Systemic Neurosciences (LMU Munich)/Max-Planck-Institute for Neurobiology, Germany; supervised by Ruben Portugues
- 2016–2017: Preparatory year in Neuroscience at Graduate School for Systemic Neurosciences (LMU Munich), Germany
- 2014–2016: Master's Degree in Biology applied to Biomedicine (at University of Pisa/Scuola Normale Superiore), Italy
- 2011–2014: Bachelor's Degree in Biology (at University of Pisa/Scuola Normale Superiore), Italy
- 2011: High School Diploma at Liceo Scientifico G. Marinelli, Udine, Italy

## Conferences & Meetings

- 2022: Talk at Cosyne (Lisbon, Portugal)
- 2021: Seminar at Italian Institute of Technology (Rovereto, Italy)
- 2020: Poster presentation at FENS (online)
- 2020: Poster presentation at Neuromatch 3.0 (online)
- 2018: Poster presentation at FENS (Berlin, Germany)

## Teaching

- 2021: Teaching assistant for the course *Large-Scale Modeling and Large-Scale Data Analysis*, by Ruben Portugues (TUM Munich)
- 2021: Teaching assistant for *Data Analysis, Modelling and Causality*, by Ruben Portugues and James Fitzgerald (Zebrafish International Training Hub)

## Personal information

- Birthday: 22th November 1992
- Nationality: Italian
- Languages: Italian (native), English (fluent), German (beginner).
- Programming languages: Python, LaTeX (expert); Julia (beginner); matlab (repented).

## Publications List

Claudi, F.,* **Petrucco, L.**,* Tyson, A., Branco,* T., Margrie, T., & Portugues, R. (2020). BrainGlobe Atlas API: a common interface for neuroanatomical atlases. *Journal of Open Source Software*, 5(54), 2668–2668.

Claudi, F., Tyson, A. L., **Petrucco, L.**, Margrie, T. W., Portugues, R., & Branco, T. (2021). Visualizing anatomically registered data with brainrender. *Elife*, 10, e65751.

Markov, D. A., **Petrucco, L.**, Kist, A. M., & Portugues, R. (2021). A cerebellar internal model calibrates a feedback controller involved in sensorimotor control. *Nature Communications*, 12(1), 1–21.

Štih, V.,* **Petrucco, L.**,* Kist, A. M., & Portugues, R. (2019). Stytra: An open-source, integrated system for stimulation, tracking and closed-loop behavioral experiments. *PLoS Computational Biology*, 15(4), e1006699.

Xiao, Y., **Petrucco, L.**, Hoodless, L. J., Portugues, R., & Czopka, T. (2022). Oligodendrocyte precursor cells sculpt the visual system by regulating axonal remodeling. *Nature Neuroscience*, 25, 280–284 (2022).

* equal contribution

# Eidesstattliche Versicherung/Affidavit

Hiermit versichere ich an Eides statt, dass ich die vorliegende Dissertation **A circuit for heading direction estimation in the zebrafish anterior hindbrain** selbstständig angefertigt habe, mich außer der angegebenen keiner weiteren Hilfsmittel bedient und alle Erkenntnisse, die aus dem Schrifttum ganz oder annähernd übernommen sind, als solche kenntlich gemacht und nach ihrer Herkunft unter Bezeichnung der Fundstelle einzeln nachgewiesen habe.

I hereby confirm that the dissertation **A circuit for heading direction estimation in the zebrafish anterior hindbrain** is the result of my own work and that I have only used sources or materials listed and specified in the dissertation.

*München/Munich,*
04/03/2022

_____
Luigi Petrucco